NAS9-14220
DRL Line Item No. 5
FCR-0021
NASA CR-
141854

FINAL REPORT

STUDY OF FUEL CELL POWERPLANT WITH HEAT RECOVERY

by

J. M. King
A. P. Grasso
J. V. Clausi

24 April 1975

Prepared for
National Aeronautics and Space Administration
Lyndon B. Johnson Space Center
Houston, Texas
Mr. Vernon Shields

Power Utility
Division of United Aircraft Corporation

ABSTRACT

The report describes a study of fuel cell powerplants with heat recovery performed during the period 15 August 1974 to 15 February 1975 under NASA Contract NAS9-14220 with the NASA Johnson Space Center Urban Systems Project Office.

The study showed that heat can be recovered from fuel cell powerplants by simply replacing the air cooled heat exchangers in present designs with units which transfer the heat to the integrated utility system. A study of energy availability for a 40 KW powerplant showed that the total usable energy at rated power represents 84 percent of the fuel lower heating value (38 percent as electric energy, 24 percent as heat at temperatures suitable for absorption air conditioning, and 22 percent as usable heat at lower temperatures). Total usable energy increases to 96 percent of the fuel lower heating value for powerplants with ratings in the megawatt class. The study showed that the effects of design variables on heat availability were small.

As part of the effort, design requirements were established for the heat recovery heat exchangers. This activity included measurement of the characteristics of two candidate fuel cell coolants after exposure to fuel cell operating conditions. The tests showed that the coolants are acceptable for use in fuel cell powerplants.

A heat exchanger test program was defined to assess fouling and other characteristics of fuel cell heat exchangers needed to confirm heat exchanger designs for heat recovery. The program would include four tasks – materials selection, definition of fouling considerations, definition of required IUS water loop quality and definition of heat exchanger size and cost differential.

Further effort is recommended to complete the assessment of fuel cell powerplants with heat recovery. This effort should include an evaluation of energy savings in typical integrated utility system applications, implementation of the heat exchanger test program and selection of the most cost effective heat recovery configuration.

TABLE OF CONTENTS

TABLE OF CONTENTS (Cont'd)

ILLUSTRATIONS

ILLUSTRATIONS (CONT'D)

ILLUSTRATIONS (CONT'D)

ILLUSTRATIONS (CONT'D)

TABLES

1.0 SUMMARY

1.1 Background and Objectives

With a view toward more efficient utilization of energy and resource conservation, utility system technologies are being investigated by the NASA Urban Systems Project Office at Johnson Space Center. These systems offer increased energy utilization efficiency and provide freedom from siting restrictions imposed by utility availability.

The characteristics of fuel cell powerplants provide several benefits in integrated utility systems. Simple paralleling and high part load efficiency permit a range of application power demands to be served with a simple catalog. Pollution emissions are insignificant and installation costs are low. Hydrocarbon-air fuel cell powerplants with ratings from 40 KW to 26 MW are being developed at United Aircraft. These powerplants are designed for utility applications and reject excess heat to ambient through air cooled heat exchangers.

The effort described in this report was carried out under NASA contract NAS9-14220 "Study of Fuel Cell Powerplant With Heat Recovery" by The Power Utility Division of United Aircraft Corporation during the period August 15, 1974 through February 15, 1975. The purposes of the contract were:

- identify powerplant changes required to recover heat from fuel cell powerplants and define the availability of useable heat from fuel cell powerplants,
- define the heat transfer properties of fuel cell coolants in the fuel cell powerplant operating range,
- define an experimental program to evaluate heat exchangers for use in recovering heat from fuel cell powerplants.

1.2 Program Results

Study of Heat Recovery Considerations — The recovery of heat from fuel cell powerplants is possible by substituting heat exchangers which reject heat to the integrated utility system (IUS) loops for heat exchangers which reject heat to air (Figure 1). Control of temperatures is achieved through sensors and bypass valves located on the high temperature side of the heat rejection heat exchangers in present designs; these controls are unchanged in powerplants with heat recovery.

At rated power useable heat from natural gas fuel cell powerplants ranges from 46 percent of fuel energy for 40 KW powerplants to 57 percent for multi-megawatt ratings. Approximately half of this heat is available at temperatures greater than 250°F; this "high grade heat" can be used to provide absorption air conditioning, space heating or low pressure process steam. The remaining heat is referred to as "low grade heat" and can be used for heating domestic hot water, for space heating or to preheat process streams. When the useable heat energy is combined with electric energy delivered, the total useable energy from fuel cell powerplants ranges from 84 to 96 percent of the full lower heating valve (Figure 2). The

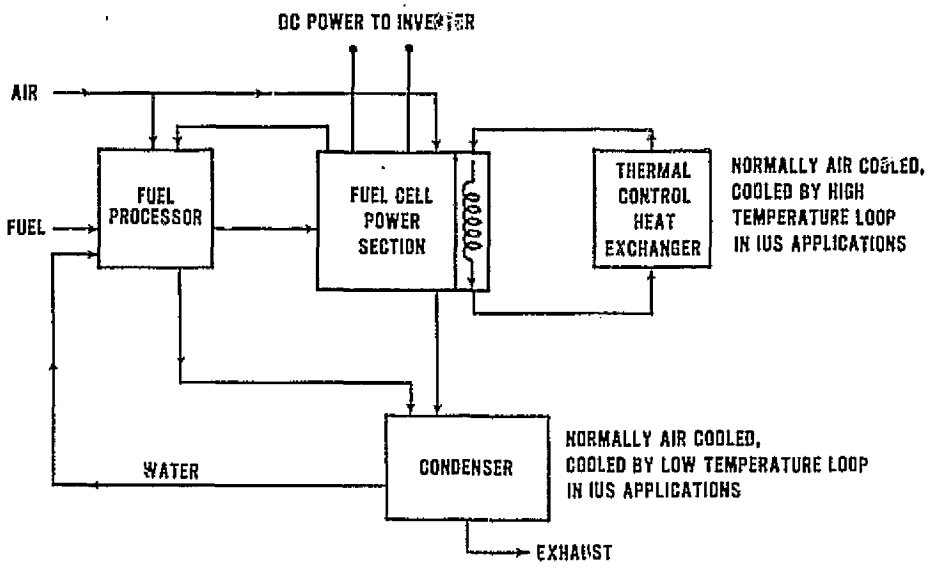

Figure 1 — Fuel Cell Powerplant Schematic

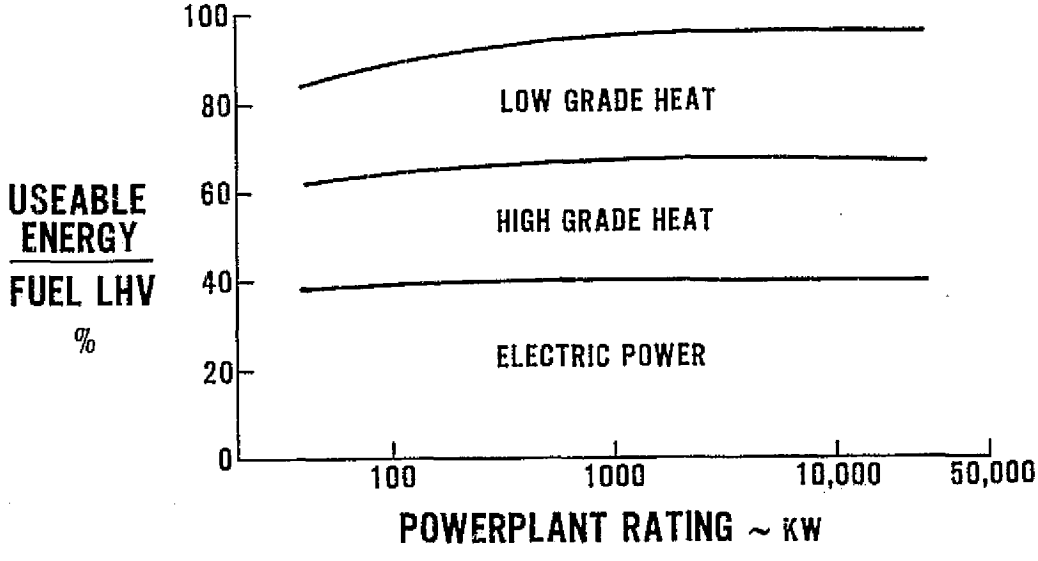

Figure 2—Useable Energy at Rated Power

fraction of the fuel energy available as useable energy decreases slightly at half rated power with electric generation efficiency and low grade heat being a somewhat higher fraction of fuel energy at reduced electrical load demand.

Alternate heat recovery configurations were studied in the contract. Configuration 1 recovers high grade heat only from the cell stack thermal control loop. Configuration 2 recovers additional high grade heat from the powerplant exhaust and is expected to be somewhat more expensive. Figure 3 shows that approximately 15 percent more high grade heat is available for Configuration 2; total useable energy remains the same.

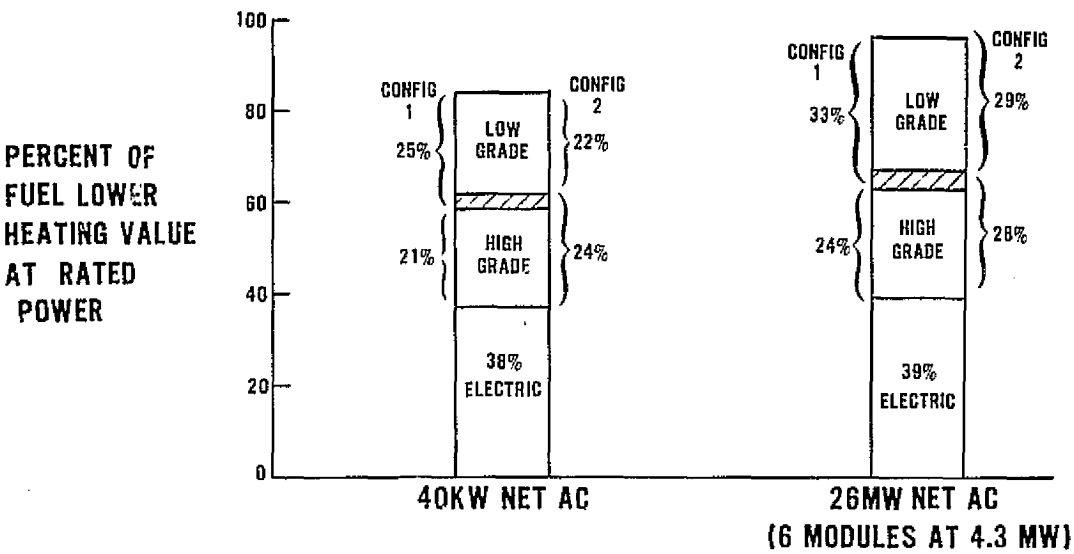

Figure 3 — Effect of Heat Recovery Configuration on Distribution of Useable Energy

The effects of ambient temperature, electric generation efficiency, heat recovery loop temperatures and alternate fuel cell thermal control approaches such as heat pipes or two-phase cooling were also studied. Within the range of interest, these variables were found to have little impact on the availability of useable energy from fuel cell powerplants. As part of this effort, design requirements were established for the heat recovery heat exchangers.

Definition of Coolant Properties — Two silicone oils are being considered for use as fuel cell coolants because they have the high dielectric strength required for fluids contacting the cell stack. The fluids differ in that one fluid (SF-97-50) requires sealed system operation while the other (SF-1093-50) contains an antioxidant to eliminate degradation on exposure to air. Properties of the coolants were measured both initially and after exposure to powerplant operating conditions as part of the contract effort. The initial values of the properties measured are shown in Table 1 at room temperature. Exposure to powerplant conditions

TABLE I

INITIAL COOLANT PROPERTIES AT ROOM TEMPERATURE
(21°C unless noted)

	SF9750	SF1093
Viscosity - centipoise	53	53
Density - grams/cc	0.961	0.961
Specific Heat - cal/gm°C	0.381	0.381
Thermal Conductivity cal/hr-cm-°C	0.99	0.99
Volatility $\frac{\text{grams lost}}{100\ cm^2 - day}$ (75°C)	.01	.01
Flammability		
— Flash Point °C	229	316
— Fire Point °C	343	343
— Auto Ignition °C	421	440
Dielectric Strength kv/m (29.3°C)	11.03	10.24

included simulation of 10 start-stop cycles (representative of 5 years of normal operation in an on-site application) and a 2000-hour endurance test in the presence of coolant loop materials at temperatures somewhat higher than those expected in the powerplant.

In addition, properties of coolant samples from test rigs and experimental powerplants with up to 8000 hours endurance were also measured. The results of the fluid property measurements are summarized in Figure 4. As expected, oxidation caused the viscosity of SF-97-50 to increase gradually during endurance testing. An air-free powerplant environment will be required for this fluid or alternatively, annual replacement will be required. The viscosity of the other candidate fluid, SF-1093-50 remained stable because of the anti-oxidant additive; SF-1093-50 requires exposure to air during powerplant operation to maintain stable properties.

- BOTH FLUIDS ARE COMPATIBLE WITH POWERPLANT MATERIALS AND TEMPERATURES
- SF-97-50 OXIDIZES IF EXPOSED TO AIR DURING POWERPLANT OPERATION
  - REQUIRES AIR-FREE POWERPLANT ENVIRONMENT OR ANNUAL REPLACEMENT
- SF-1093-50 REQUIRES EXPOSURE TO AIR DURING POWERPLANT OPERATION

Figure 4 -- Results of Fluid Property Measurement

Definition of Heat Excahnger Experimental Program — Fuel cell powerplants present unique environments for heat exchangers in the heat recovery loop. The effort under this contract included the definition of an experimental program to obtain the design characteristics of heat exchangers in the heat recovery loop. The program defined encompasses four tasks as shown in Figure 5.

- MATERIALS SELECTION
- DEFINITION OF FOULING CONSIDERATIONS
- DEFINITION OF REQUIRED IUS LOOP WATER QUALITY
- DEFINITION OF HEAT EXCHANGER SIZE AND COST DIFFERENTIAL AND CONFIRMATION

Figure 5 — Recommended Heat Exchanger Test Program Tasks

The four tasks are described below:

Task A - Materials Selection - The materials compatibility problems of heat exchangers interfacing with both fuel cell powerplant fluids and the water in the integrated utility system loop will be investigated and materials will be selected for use in this application. Initial materials selection will be made based upon known constraints. Follow-up testing of primary candidates will confirm these choices.

Task B - Definition of Fouling Considerations - The fouling characteristics experienced with fuel cell heat exchangers will be investigated and design factors and cleaning schedules to eliminate fouling effects on system performance will be established.

Task C - Definition of Required IUS Water Loop Quality - The quality of water in the integrated utility system loop which is required to minimize corrosion and fouling on the system side of the heat exchangers will be identified.

Task D - Definition of Heat Exchanger Size and Cost Differential and Confirmation - Heat exchanger configurations will be selected for 40 KW and 26MW fuel cell powerplants with heat recovery based on characteristics obtained in previous testing. The size of these heat exchangers will be defined and the cost differential between a fuel cell powerplant which rejects heat to air and a fuel cell powerplant which rejects heat to an integrated utility system loop will be determined. If heat exchanger core configurations different from those previously tested are selected, a short test will be conducted to confirm that initial core characteristics and the fouling data are appropriate for the selected configurations.

1.3 Recommendations for Further Effort

It is recommended that further assessment of the use of fuel cell powerplants in integrated utility systems include:

1. Definition of the annual operating efficiency of typical integrated utility system with fuel cell powerplants using the Energy Systems Optimization Computer Program available at NASA USPO.

2. Implementation of the heat exchanger test plan generated in this effort and assessment of the cost impact of alternate heat recovery configurations.

3. Selection of the most cost effective heat recovery configuration based on annual efficiencies defined using the ESOP (Recommendation 1) and the capital cost differential between the configurations (Recommendation 2).

2.0 RESULTS AND CONCLUSIONS

2.1 Program Objectives and Tasks

The objectives of this effort were:

- to identify modifications to present fuel cell powerplant designs to permit recovery of waste heat
- to define the availability of waste heat from fuel cell powerplants
- to define design requirements for heat exchangers to be used in recovering fuel cell powerplant waste heat
- to define the heat transfer properties of fuel cell coolants
- to define an experimental program to assess core characteristics for heat recovery heat exhangers

To meet these objectives, the contract effort was carried out in three tasks: Task 3.2, "Definition of Heat Recovery Considerations in Fuel Cell Powerplants", "Task 3.3, Determination of Heat Transfer Properties of Fuel Cell Coolants", and "Task 3.4, Definition of an Experimental Program for Assessment of Heat Exchanger Core Characteristics". The tasks make use of information and analysis techniques developed in commercial fuel cell programs. Results and Conclusions of each task are described below.

2.2 Task 3.2 — Definition of Heat Recovery Considerations in Fuel Cell Powerplants

The purpose of this task was to define modifications to recover heat from fuel cell powerplants and to define the availability of heat from fuel cell powerplants.

2.2.1 Availability of Heat from Baseline Powerplants

Two fuel cell powerplants were selected for use in these analyses, a 40 KW on-site generator and a 26 MW dispersed utility generator. Both are variations of powerplant designs presently in progress in the commercial fuel cell program at Power Utility Division of United Aircraft. Natural gas was assumed as the fuel for these studies. Results of the studies indicate that only minimal changes to the present designs are necessary for heat recovery. This is due to the high degree of thermal integration incorporated in present fuel cell powerplant design and low exhaust stream temperatures required for water recovery. The only powerplant changes required for heat recovery involve the substitution of heat recovery heat exchangers for the present air-cooled heat rejection units. All controls are located on the fuel cell side of the heat recovery loop and would be the same as in air-cooled designs.

Figures 6 and 7, based on the 40 KW powerplant, show that the total useable energy varies only slightly with the design electric generation efficiency at rated power or at half load.

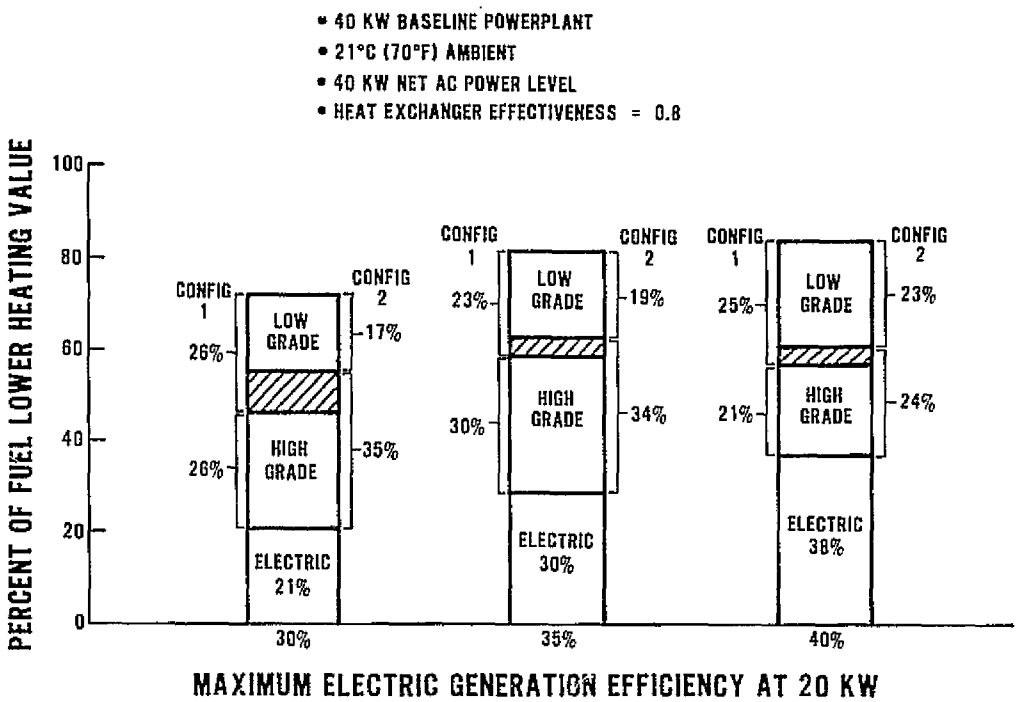

Figure 6 — The Effect of Electric Generation Efficiency On Useable Energy for the 40 KW Baseline Powerplant at Rated Power

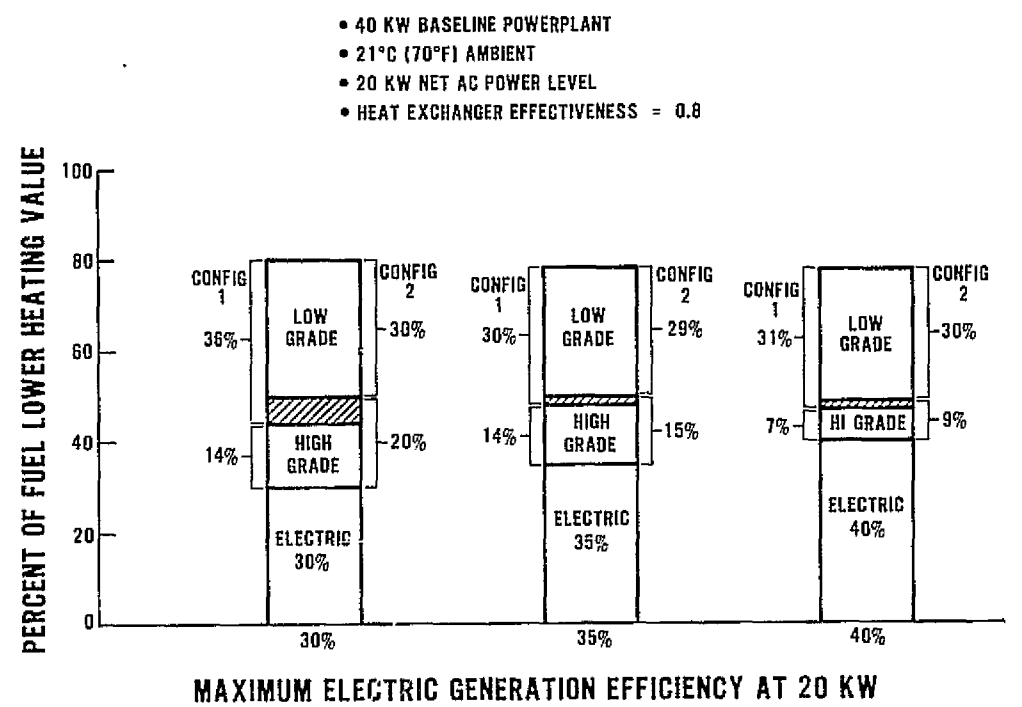

Figure 7 — The Effect of Electric Generation Efficiency On Useable Energy for the 40 KW Baseline Powerplant at Half Load

The percentage of low grade heat remains essentially constant as efficiency varies while the high grade heat decreases with increasing electric generation efficiency. This occurs because the power section design point is the major determinant of electric generation efficiency and also, the major variable in defining high grade heat. Relative quantities of low grade and high grade heat vary slightly with the heat recovery Configuration (1 or 2) but the total useable energy is not affected.

The total useable energy increases substantially at higher powerplant ratings as shown in Figure 8. Figure 8 indicates that the total useable energy is 84 percent of fuel lower heating value at 40 KW with an increase to 96 percent at 26 MW. The change in total useable energy with scale is primarily due to available heat, since the electric generation efficiency is a design input parameter (within limits). The factors which cause available heat to change with power level are: inverter efficiency, component parasite power, and thermal losses. All of these factors are strongly influenced by scale in the region of 40 to 500 KW.

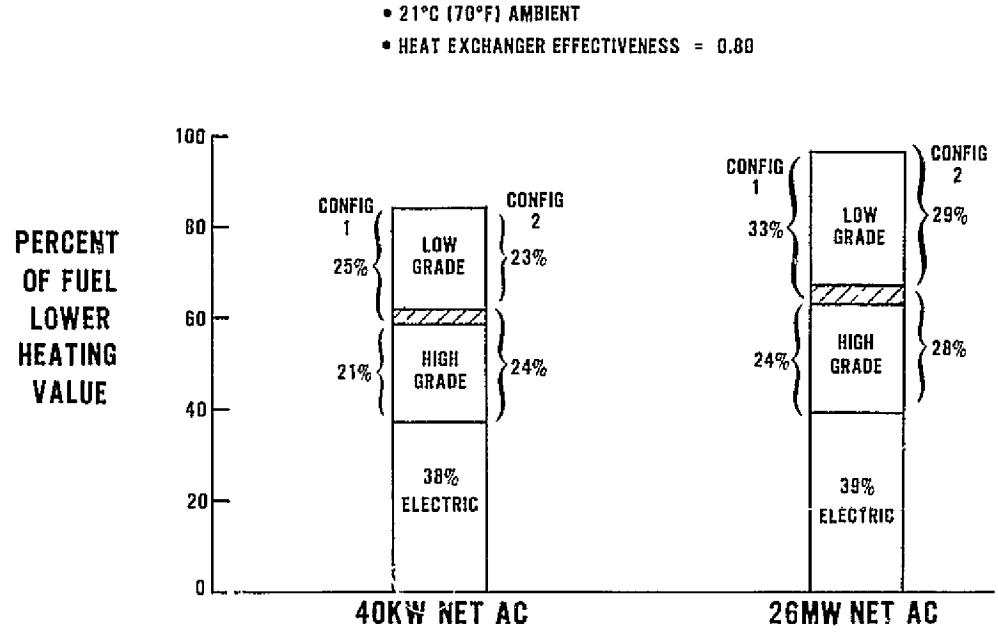

Figure 8 — Total Useable Energy for the 40 KW and 26 MW Powerplants — Configurations 1 and 2

2.2.2 The Impact of Alternate Configurations on Available Heat

Three alternate heat recovery configurations were studied. The first arrangement, Configuration 1, provides a reasonable mix of high grade and low grade heat and is accomplished with a minimum number of heat exchangers. Configuration 2 is a means of obtaining the maximum amount of high grade heat from the powerplant, but at the expense of additional heat exchangers. Figures 9 (35 percent electric generation efficiency) and 10 (40 percent electric generation efficiency) show the amount of high grade heat increasing by about 13

percent for the 40 KW powerplant if Configuration 2 is used. Similarly Figure 11 indicates a 16 percent increase in high grade heat between Configuration 1 and Configuration 2 for the 26 MW powerplant. A third heat recovery arrangement considered for the 40 KW powerplant recovers all thermal energy as low grade heat (Configuration 3). The total available low grade heat increases to the sum of the high grade and low grade heat for the other heat recovery configuration as shown in Figure 9 and 10. Power section heat removal concepts other than the baseline forced convection oil-cooled approach were examined for possible impact on heat recovery. The examination showed that the prime alternate heat removal concept, two-phase water, resulted in the same heat availability as the baseline oil-cooled system. A heat pipe heat removal approach would also show the same heat availability.

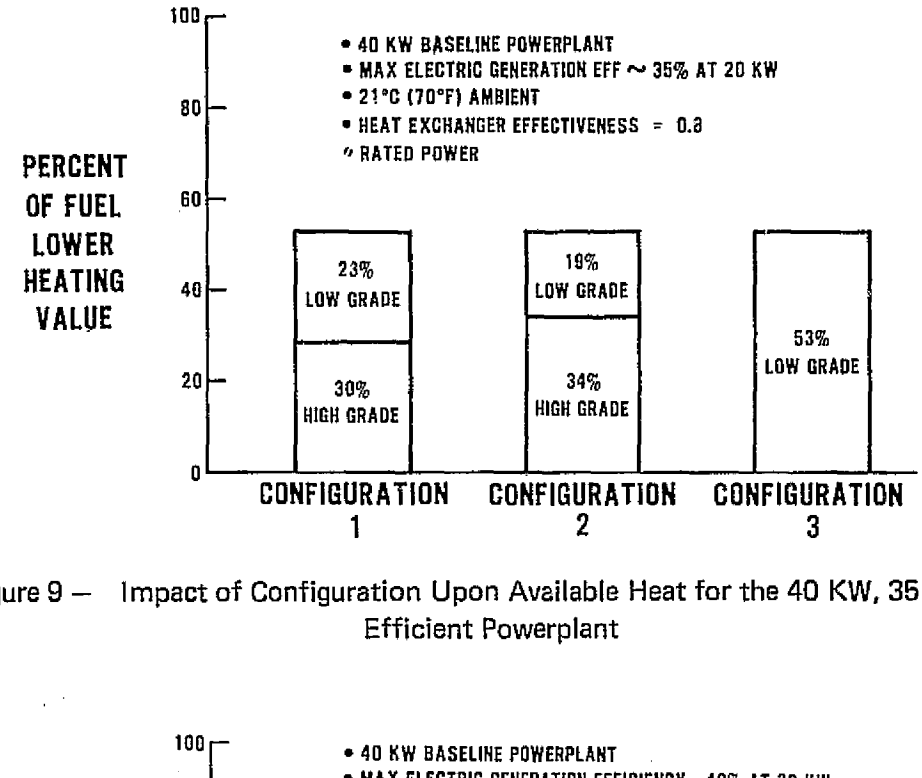

Figure 9 — Impact of Configuration Upon Available Heat for the 40 KW, 35 Percent Efficient Powerplant

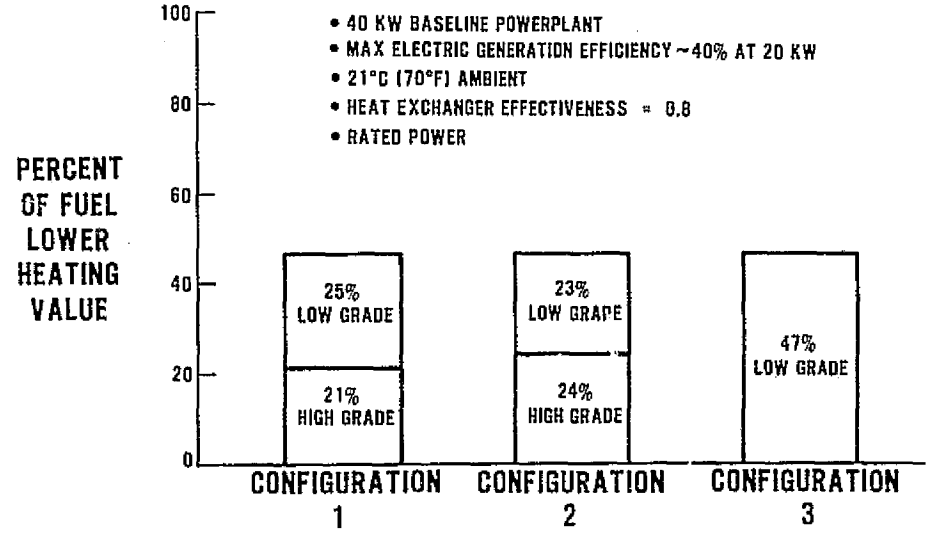

Figure 10 — Impact of Configuration Upon Available Heat for the 40 KW, 40 Percent Efficient Powerplant

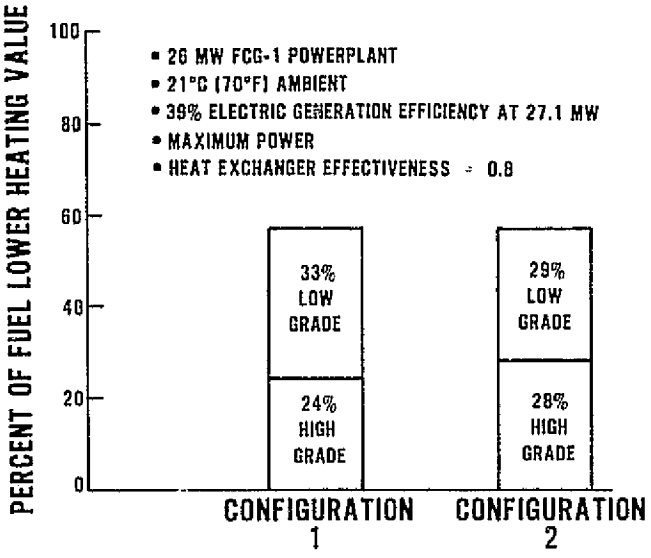

Figure 11 — Impact of Configuration Upon Available Heat for the 26 MW Powerplant

2.2.3 Impact of External Variables on Available Heat

The impact of varying heat recovery loop temperatures was investigated in this study. High grade heat availability remained essentially constant as saturated steam conditions were varied from 10.3 x 10^4 n/m^2 (15 psig) to 62.1 x 10^4 n/m^2 (90 psig) (saturation temperatures of 121°C (250°F) and 166°C (330°F) respectively). In the low grade heat loop the baseline heat recovery loop operates at temperatures between 24°C (75°F) and 71°C (160°F) (domestic hot water). About one third of this low grade heat is available at higher temperatures 71°C (160°F) to 93°C (200°F) for space heating. The abrupt decline in available low grade heat with increasing supply temperature is due to the loss of the heat of condensation in the powerplant exhaust stream.

Ambient temperature has a small impact on the amount of available heat. Over the ambient temperature ranges studied, 2°C (35°F) to 43°C (110°F), there was less than a 10 percent change in the quantity of high grade heat available about the 21°C (70°F) reference point. The effect of ambient temperature on low grade heat is even smaller (about 1 to 2 percent) over the same temperature range.

2.2.4 Design Requirements for Heat Exchangers

Heat Exchanger design requirements were developed for the 40 KW powerplant at 35 and 40 percent electric generation efficiency and for the 26 MW powerplant for both Configuration 1 and Configuration 2. These design requirements are presented in Appendix A. These requirements in combination with the coolant properties determined in Task 3.3 provide design input for the heat exchanger test program definition.

2.3 Task 3.3 "Determination of Heat Transfer Properties of Fuel Cell Coolants"

The purpose of this task was the evaluation of the heat transfer related physical properties of two candidate fuel cell coolants.

2.3.1 Coolant Description

Documentation of these properties is required to support the design analysis of the related fuel cell system heat exchangers. The candidate coolants, (SF-97-50 and SF-1093-50), are both silicone oils which were selected for their high dielectric strength and relative inflammability at the expected fuel cell powerplant operating temperature range. High coolant dielectric strength is necessary since the present powerplant design philosophy results in the coolant being in direct electrical contact with the fuel cell stack; a low coolant dielectric strength could result in stack electrical leakage current which wastes power and compromises the stack life. Physical properties of these coolants are needed after exposure to powerplant operating conditions to support the design of the associated heat exchangers.

2.3.2 Test Approach

The fluid properties measured, along with the appropriate measurements method, are shown in Table II. The physical properties were evaluated for each of the two coolants in the as-received (new) condition and after subjecting them in the lab to typical powerplant environments of both long-term steady-state and start-stop operation.

Start-Stop Test

Samples of each silicone oil coolant were subjected to a series of simulated powerplant start-stop cycles. The samples were heated in a flask by an electrical immersion heater from room temperature to 191°C (375°F) where the heater was shut off and then the coolant was allowed to cool to room temperature. The upper limit on surface temperature of the immersion heater was controlled to a maximum of 315°C (600°F). This cycle was repeated 10 times on each 2000 cc coolant sample.

TABLE II

FLUID PROPERTY MEASUREMENT METHODS

Fluid Property	Measurement Method
Viscosity	Brookfield Viscometer Model RV
Density	Standard Lab Equipment
Specific Heat	Differential Scanning Calorimeter - DuPont 990 Thermal Analyzer
Thermal Conductivity	Wear Science Inc. Thermal Comparator
Volatility	Standard Laboratory Equipment
Flammability	Standard Laboratory Equipment
Flash Point	ASTM D92-52
Fire Point	ASTM D92-52
Auto Ignition	ASTM D2155-66
Dielectric Strength	Associated Research Model 4720-M7 Tester ASTM D877-49

2000-Hour Exposure Laboratory Test

A sample of each coolant type, SF-97-50 and SF-1093-50, was maintained at 191°C for 2000 hours in laboratory tests simulating powerplant operating conditions while being exposed to typical powerplant coolant loop type materials. The sample of SF-97-50 coolant was exposed only to a limited quantity of air representative of minor leakage into a sealed powerplant coolant system while the SF-1093-50 coolant sample was adequately exposed to air in accordance with the coolant manufacturers' recommendations to use this fluid in an open system.

Powerplant and Cell Stack Rig Coolant Samples

The physical properties of four samples of used coolants were measured to allow a comparison with the laboratory results; all coolants samples are SF-97-50. Three of the samples were removed from cell stack test stands and have exposure times of 1500, 3000 and 8000 hours. The remaining sample accumulated 461 hours while operating in an experimental fuel cell powerplant.

The sample descriptions are summarized in Table III and compared to the laboratory tests conducted under this contract. The physical properties of each coolant sample were evaluated after the completion of the individual test.

TABLE III

Coolant Sample Description Summary

Sample	Type	Source	Approx. Temp.	Start Stop Cycles	Hours
Start/Stop Test	SF-97-50	Lab Test	21 - 191°C (70 - 375°F)	10	—
	SF-1093-50	Lab Test	21 - 191°C (70 - 375°F)	10	—
Long Endurance Test	SF-97-50	Lab Test	191°C (375°F)	0	2000
	SF-1093-50	Lab Test	191°C (375°F)	0	2000
	SF-97-50	Cell Test Stand X-714	177°C (350°F)	*N/A	1500
	SF-97-50	Cell Test Stand X-707	177°C (350°F)	N/A	3000
	SF-97-50	Cell Test Stand X-708	177°C (350°F)	N/A	8000
	SF-97-50	Powerplant X-586-4	177°C (350°F)	21	461

*N/A - Not Available

Viscosity

An increase in coolant viscosity is considered to be an indication of fluid oxidation and is used as a measure of coolant degradation. The coolant manufacturer recommends coolant replacement when the viscosity exceeds twice the original value because coolant gelation is imminent. The initial viscosity values are shown in Figure 12. Viscosity is effectively the same for both fluids.

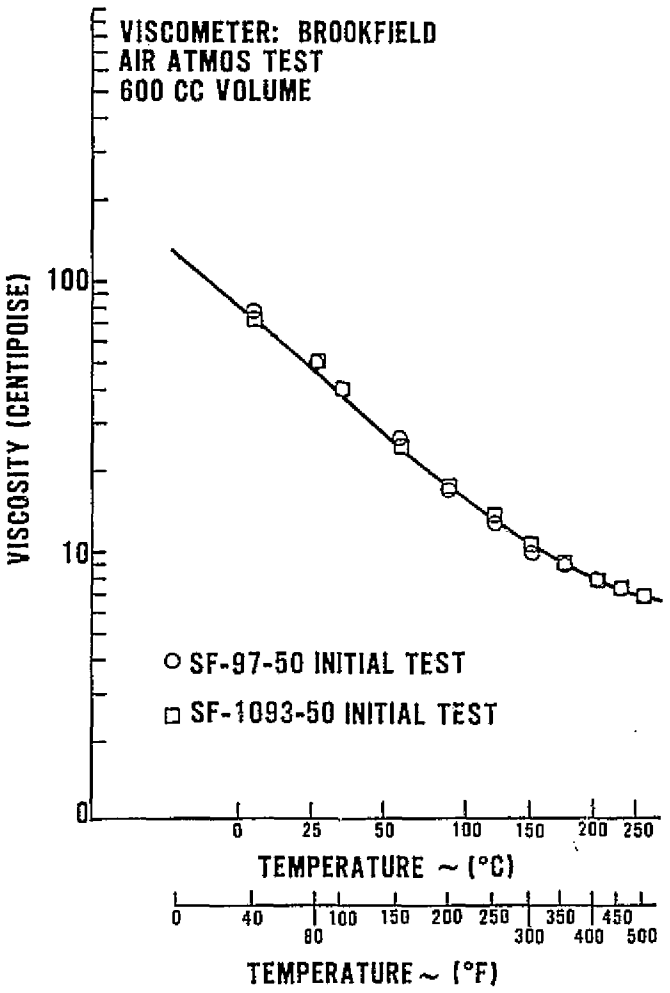

Figure 12 – Viscosity vs. Temperature, Initial Test

Post-test viscosity measurements for the start-stop samples are shown in Figure 13 and were found to be unchanged from the original values. An initially undetected difference in test technique resulted in exposing the SF-1093-50 sample to a high temperature for a longer period of time. However, the test result indicates this difference had insignificant impact.

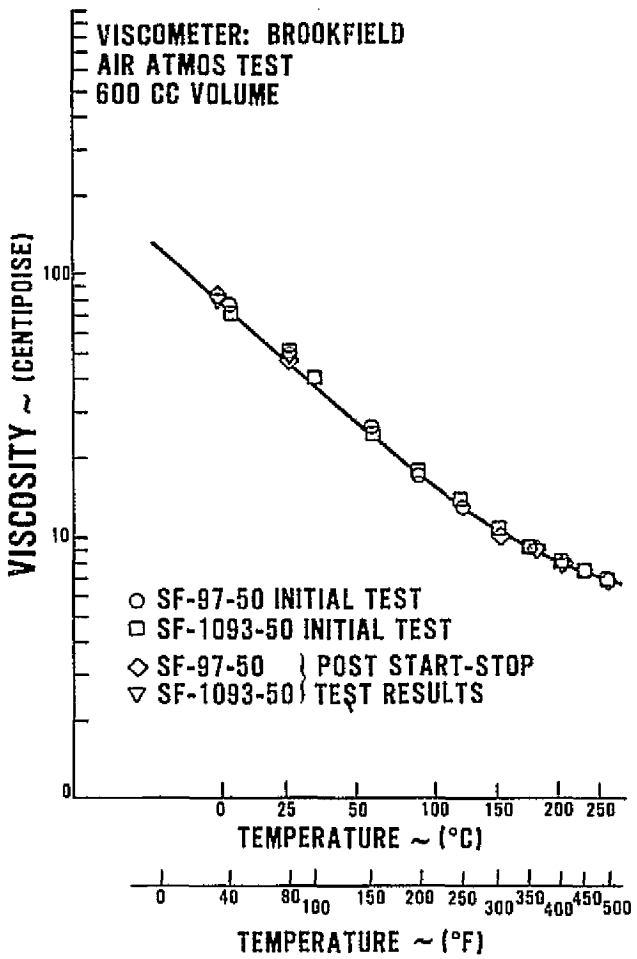

Figure 13 — Viscosity vs. Temperature, Post Start-Stop Tests

The viscosity increase of the SF-1093-50 2000-hour coolant sample was predictably small (Figure 14) since it contains an additional ingredient to retard oxidation which is the primary cause of the viscosity change. The viscosity increase of the 2000-hour SF-97-50 laboratory coolant sample was significant, and at room temperature conditions, approached doubling of the initial value (Figure 14). When viscosity doubles, coolant replacement is recommended by the manufacturer. The viscosity increase of SF-97-50 coolant with time is also apparent in the test results of the used coolant samples and the 8000-hour sample is nearing the recommended replacement level. Figure 15 shows that the used coolant viscosity increases with the operating time of the coolant sample. The more significant viscosity increase of the laboratory SF-97-50 coolant from the 2000-hour test compared to the used coolant samples is believed to be primarily due to the higher temperature at which the 2000-hour test was conducted (191 vs. 177°C; 375 vs. 350°F). Since the laboratory test conditions are more severe than the actual powerplant conditions, it appears that if 1 percent or more air by volume were present, SF-97-50 would require annual replacement in a site powerplant. As an alternative to annual replacement, manufacturing approaches and sealing could be developed to achieve an air-free environment for SF-97-50.

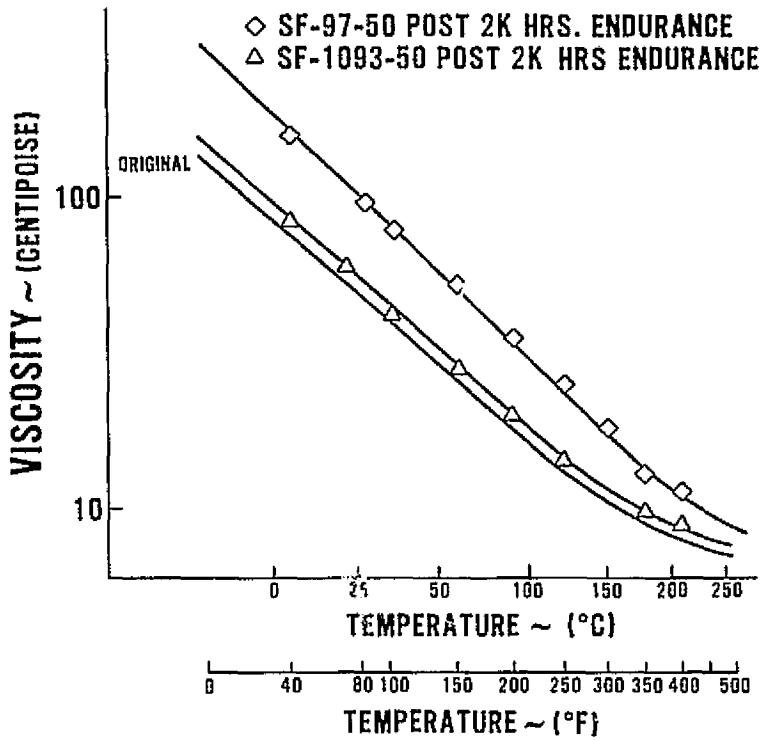

Figure 14 — Viscosity vs. Temperature After the 2000-hour Laboratory Test

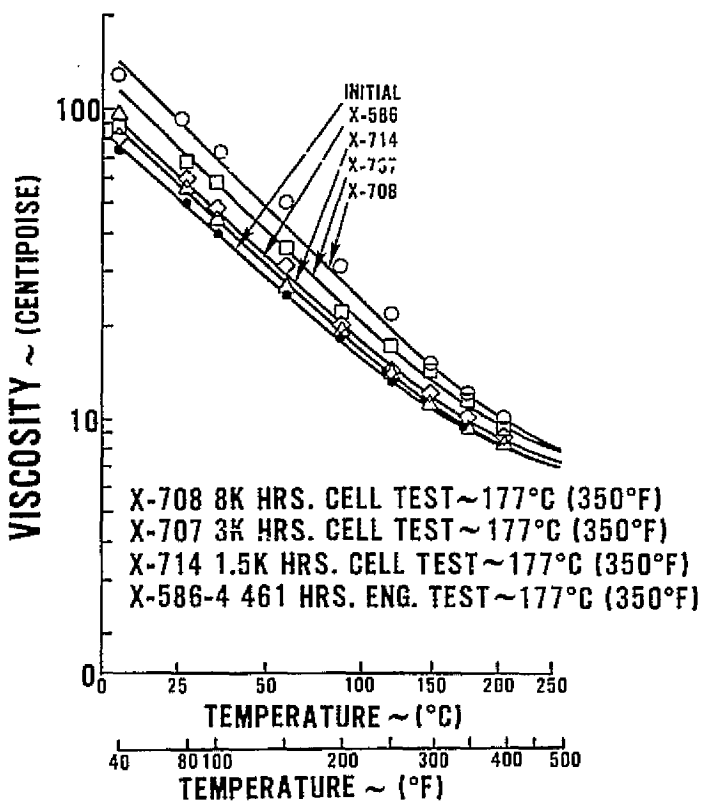

Figure 15 — Viscosity vs. Temperature SF-97-50, Rig Samples

Density

The initial coolant densities are equivalent as shown in Figure 16. No post test variation of density was detected after start-stop tests, 2000-hour endurance tests or after use in experimental rigs and powerplants as shown in Figures 17, 18, and 19.

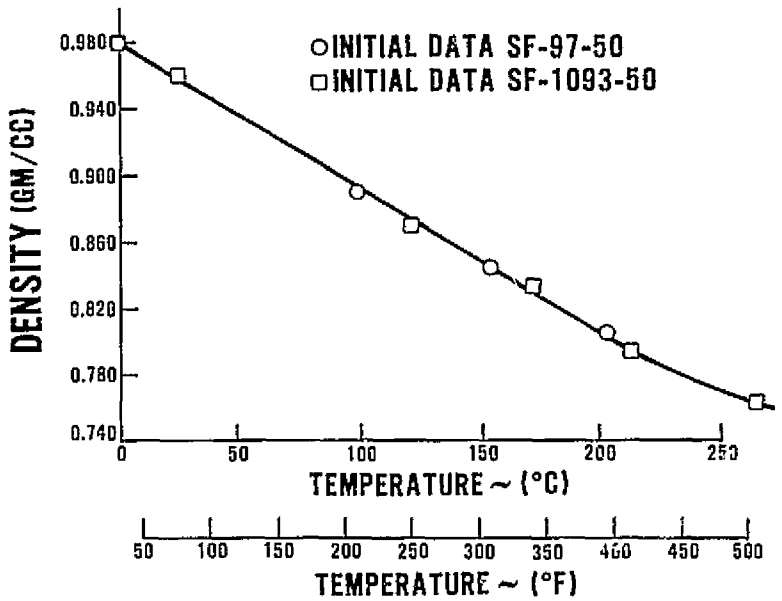

Figure 16 — Density vs. Temperature, Initial Data

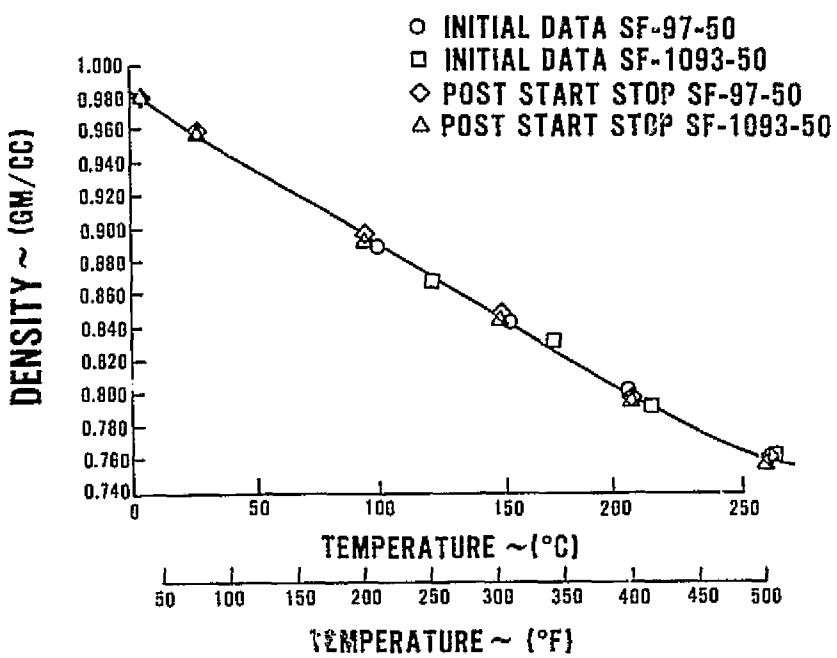

Figure 17 — Density vs. Temperature, Post Start-Stop Tests

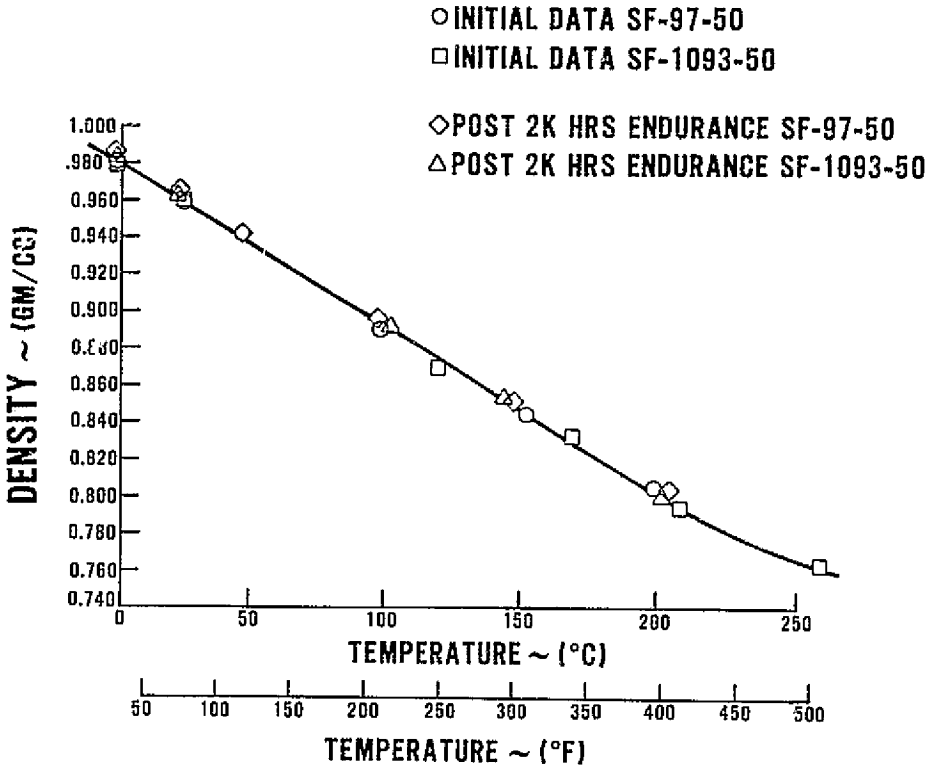

Figure 18 — Density vs. Temperature, After the 2000-hour Laboratory Test

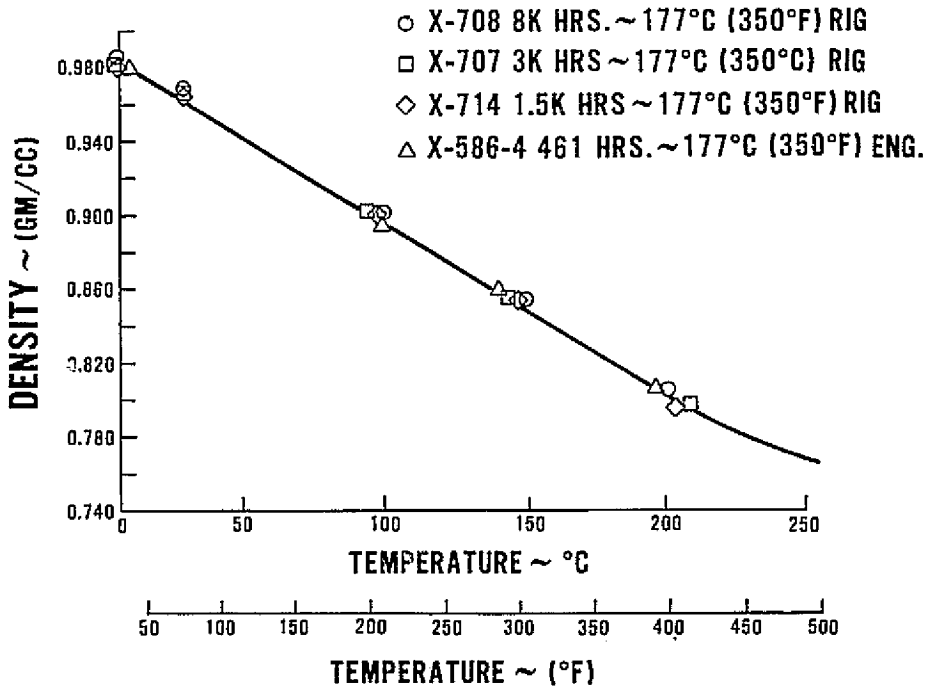

Figure 19 — Density vs. Temperature SF-97-50, Rig Samples

Specific Heat

A slight difference in the initial specific heat between the two coolants was detected at higher temperatures as shown by Figure 20. The post start-stop test results displayed in Figure 21 show a variation from the original values. However, the amount is considered insignificant (approximately 3 percent at powerplant operating temperature). The specific heat of all the rig coolant samples was found to decrease slightly at elevated temperatures. The amount of change appears to be somewhat time dependent as evidenced by the general trend of the used coolant samples toward lower values of specific heat with increased exposure time (Figure 22). The amount of specific heat change at elevated temperatures of the 2000-hour laboratory samples of SF-97-50 and SF-1093-50 was similar for both fluids but more significant than experienced with the used rig samples (Figure 23). The laboratory coolant samples were exposed to a uniformly higher temperature than that of the coolants operating in the cell test stand or in the fuel cell powerplant and this factor is believed to be primarily responsible for the variation in the test results between the two enduance situations.

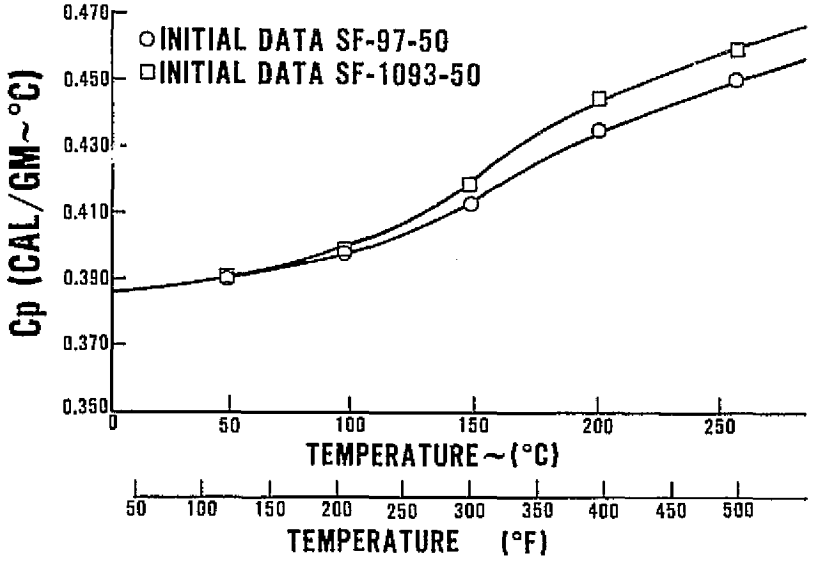

Figure 20 — Specific Heat vs. Temperature, Initial Data

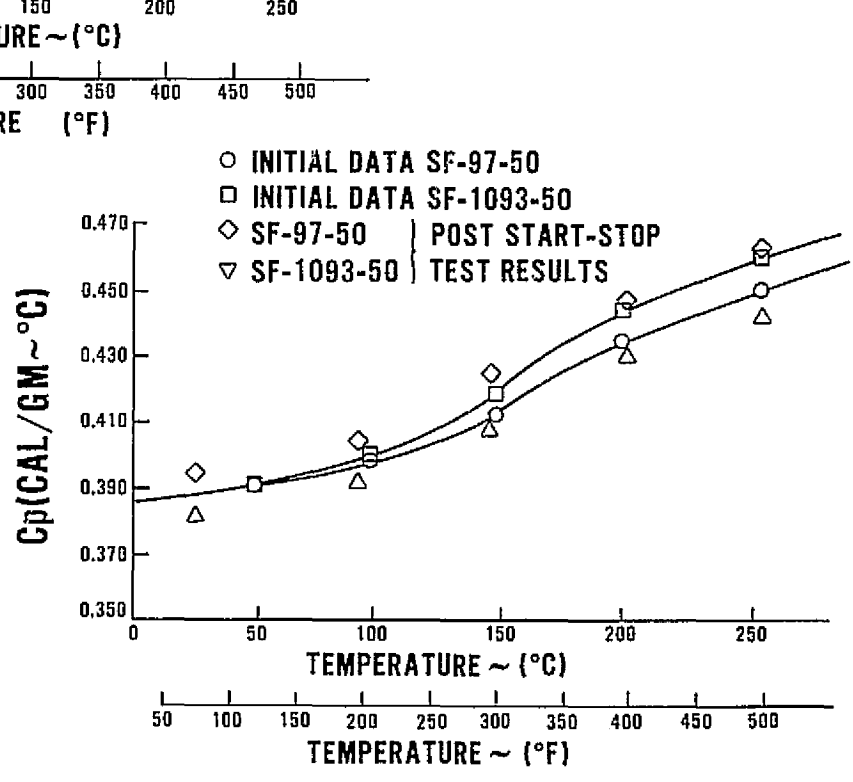

Figure 21 — Specific Heat vs. Temperature Post Start-Stop Tests

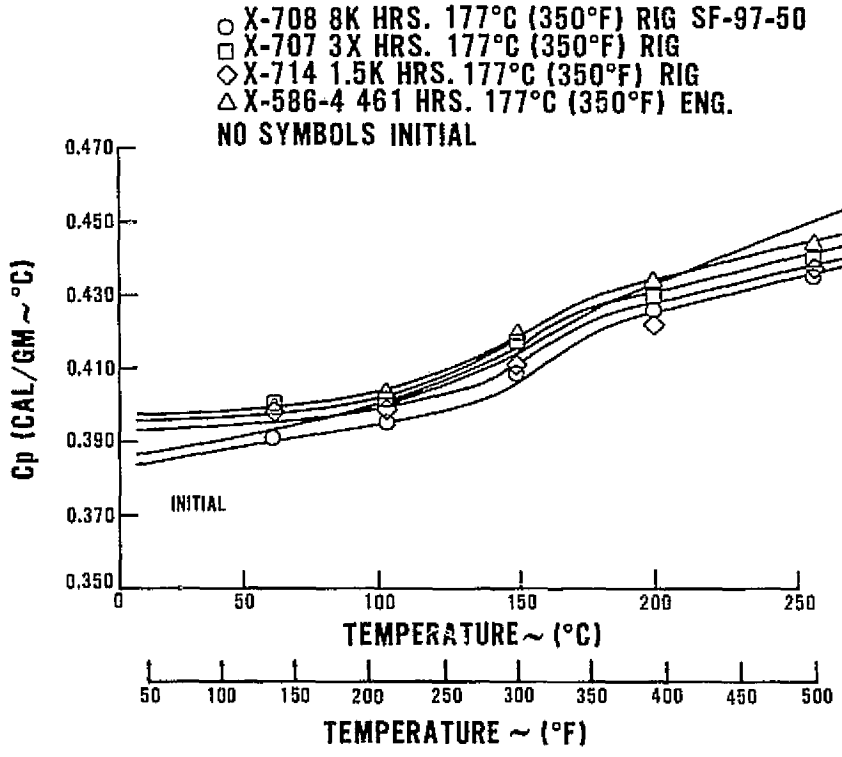

Figure 22 — Specific Heat vs. Temperature SF-97-50 Rig Samples

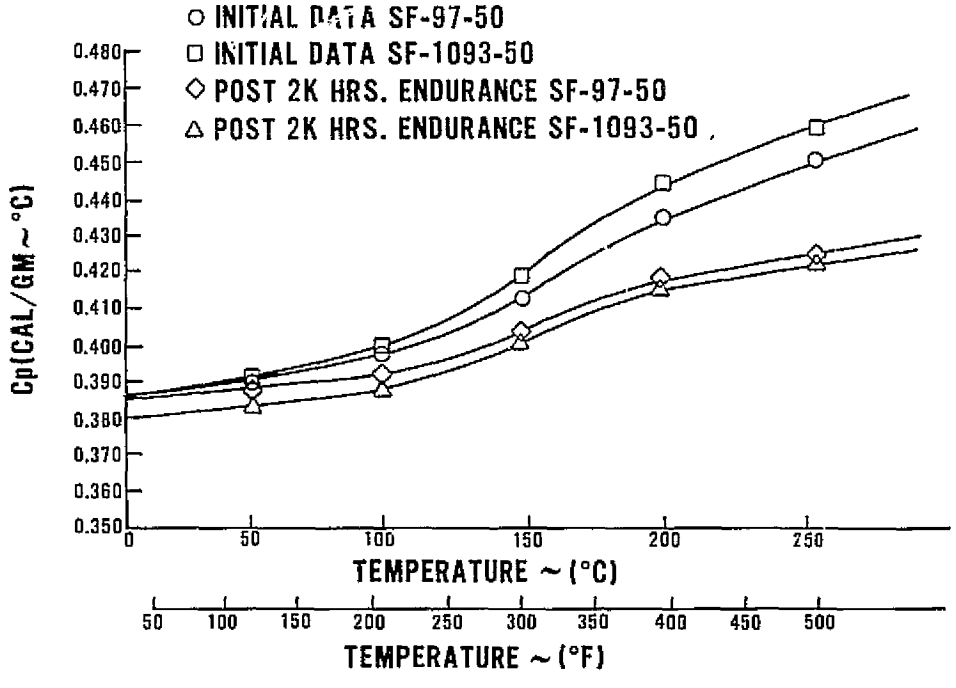

Figure 23 — Specific Heat vs. Temperature After the 2000-Hour Laboratory Test

Thermal Conductivity

The coolant thermal conductivity was evaluated by Wear Sciences Inc. The Wear Science test procedure and results are discussed in Appendix B.

The test results for SF-97-50 and SF-1093-50 coolants are shown in Figures 24 through 27. In general, the initial thermal conductivity of the coolants are similar in that they show the same thermal conductivity at room temperature. The initial conductivity increases with temperature up to a fluid temperature of 51.8 - 65.7°C (125 - 150°F) and then decreases with increasing fluid temperatures (Figure 24). The used powerplant and rig fluid samples indicated values of conductivity lower than the new fluids (Figure 25). This same trend appears for the lab 2000-hour endurance (Figure 26) and start/stop samples (Figure 27). Wear Sciences reported that a substantial amount of "dissolved" gas was present in the used SF-97-50 samples and that degassing prior to testing was required. The X-586 powerplant and X-707 rig samples of SF-97-50 actually showed increased values of thermal conductivity after de-gassing (Figures 28 and 29). However, these were still below the thermal conductivity of the new SF-97-50 sample.

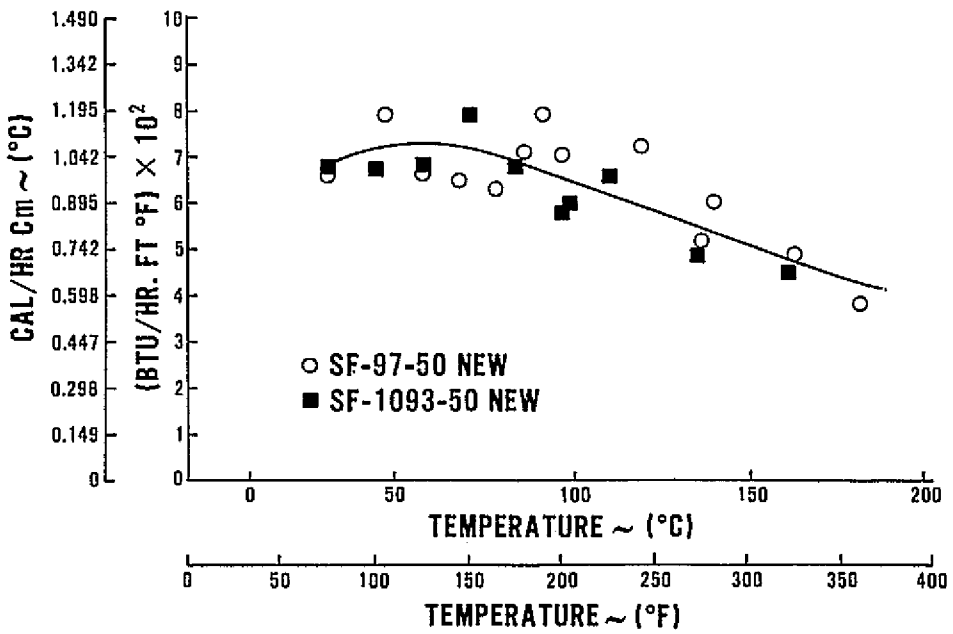

Figure 24 — Initial Thermal Conductivity vs. Temperature SF-97-50 and SF-1093-50

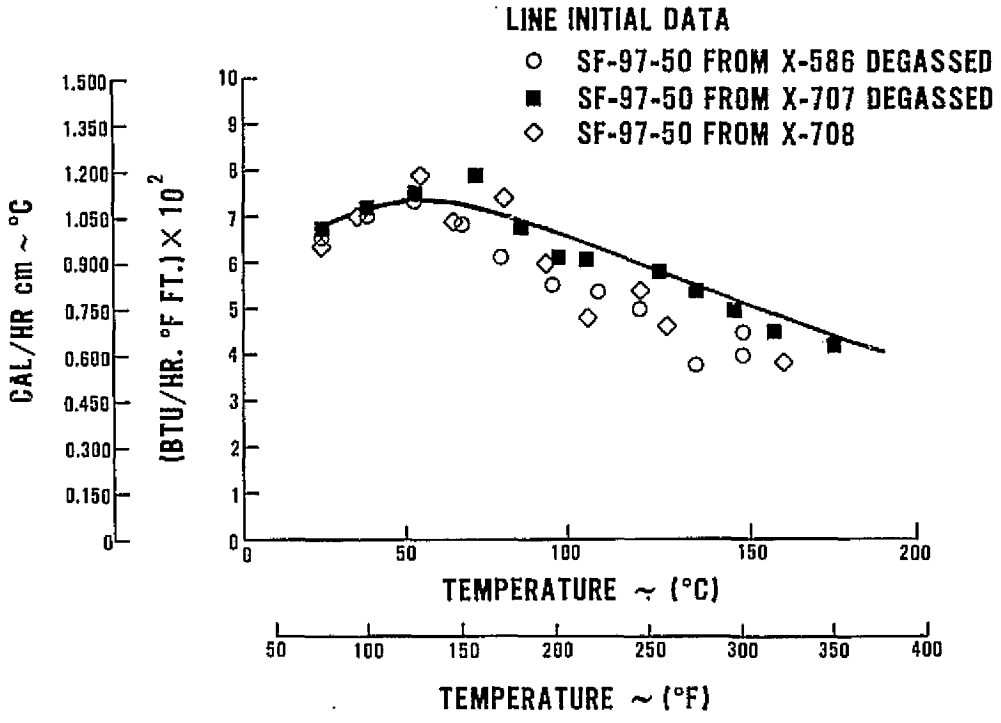

Figure 25 — Thermal Conductivity vs. Temperature SF-97-50, Rig Samples

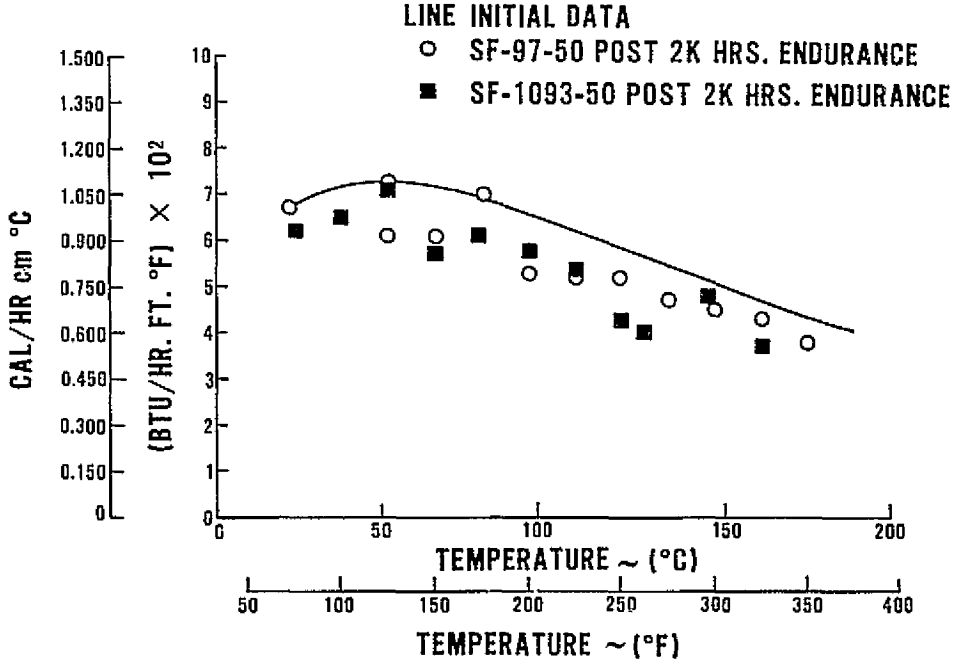

Figure 26 — Thermal Conductivity vs. Temperature After the 2000-hour Laboratory Test

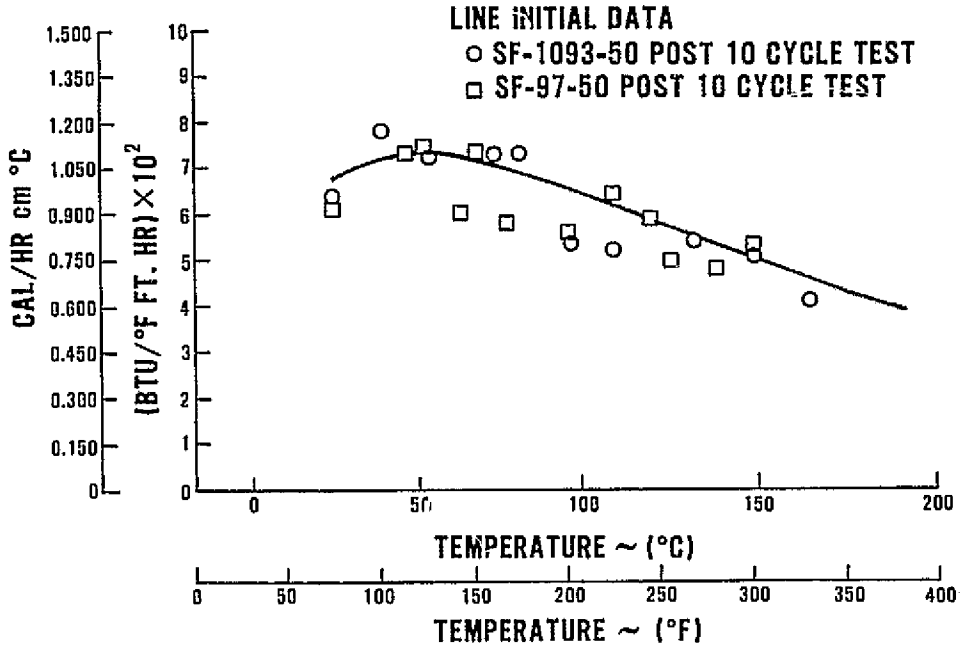

Figure 27 — Thermal Conducity vs. Temperature Post Start-Stop Tests

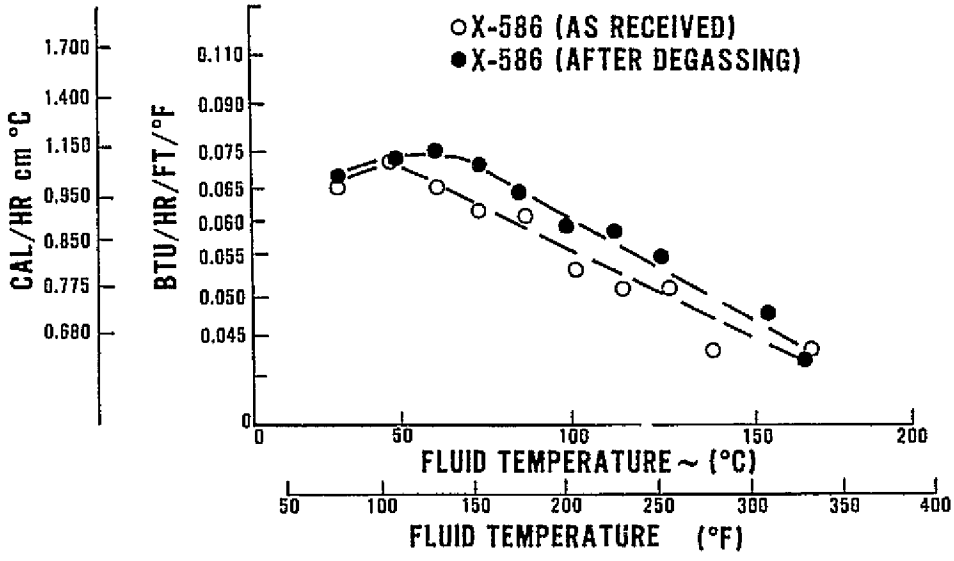

Figure 28 — Effect of Degassing on Measured Thermal Conductivity of SF-97-50, X-586

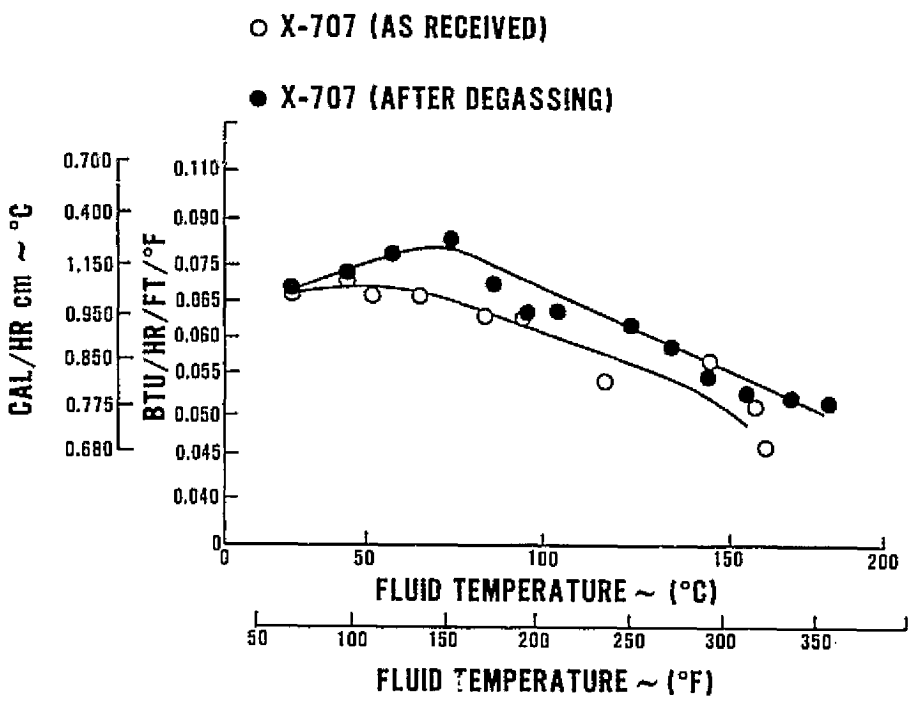

Figure 29 — Effect of Degassing on Measured Thermal Conductivity of SF-97-50, X-707

Volatility

The SF-97-50 coolant requires a sealed coolant system while the SF-1093-50 must have an open system, exposed to air, to function properly. To measure volatility, samples of each coolant are held at a constant temperature in an open container and the weight loss per unit time recorded as a function of exposed fluid surface. Figure 30 shows the results of the volatility test with new fluids. The coolant volatility was observed to decrease substantially after the start-stop testing as shown by Figure 31 (16-33 percent reduction at powerplant operating temperatures). The SF-97-50 laboratory 2000-hour sample was found to gel within 70 hours while being maintained at 260°C, thereby terminating the test since volatilization of the coolant effectively ceases after gelation. (See Figure 32). The SF-1093-50 laboratory sample also showed a decrease in volatility as shown in Figure 32. The used coolant samples experienced a drop in volatility below the original sample reference and the 8000-hour cell stack sample was observed to gel in less than 20 hours at 260°C. (See Figure 33.) These results indicate that the volatility of each coolant is low and that coolant loss should not present a problem at typical powerplant operating conditions.

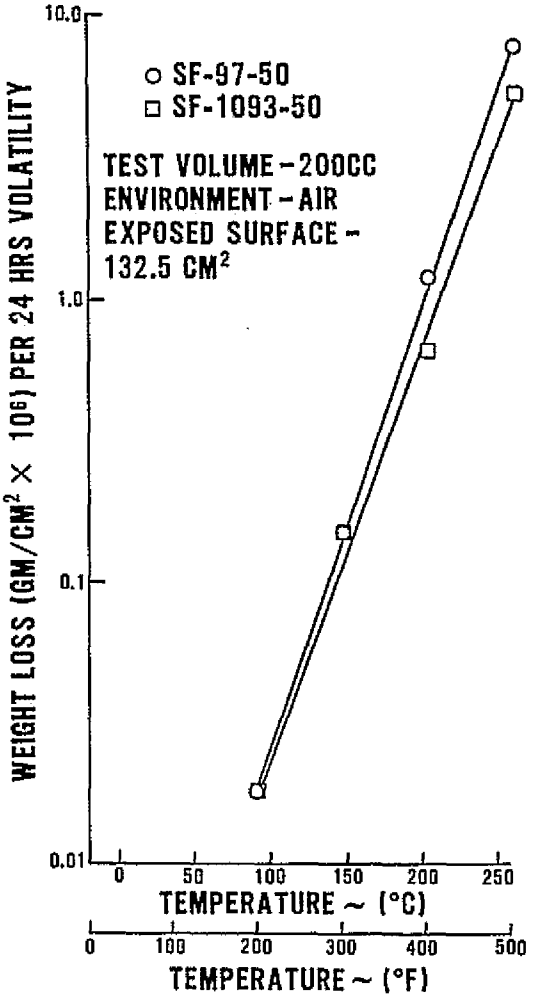

Figure 30 —

Volatility vs. Temperature, Initial Data

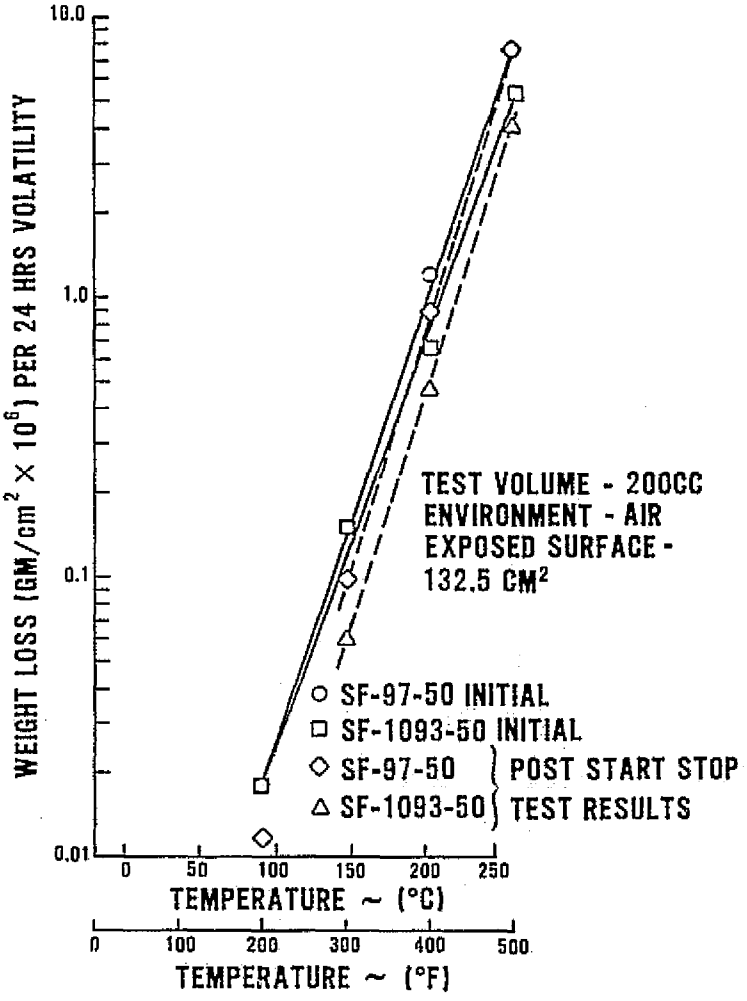

Figure 31 —

Volatility vs. Temperature, Post-Stop Tests

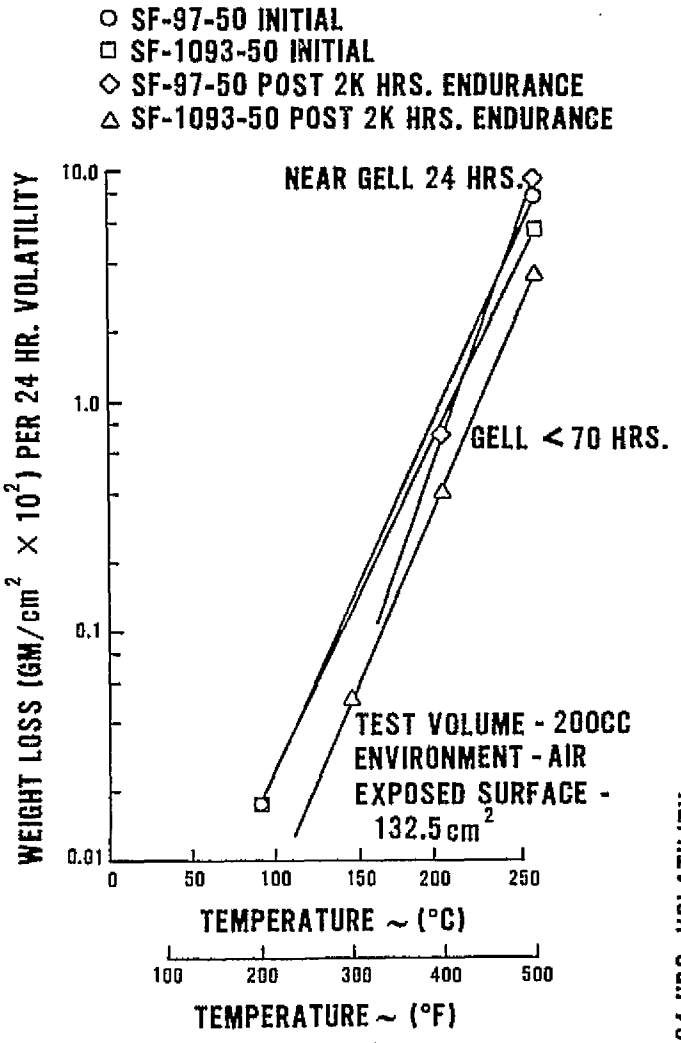

Figure 32 –

Volatility vs. Temperature After the 2000-hour Laboratory Test

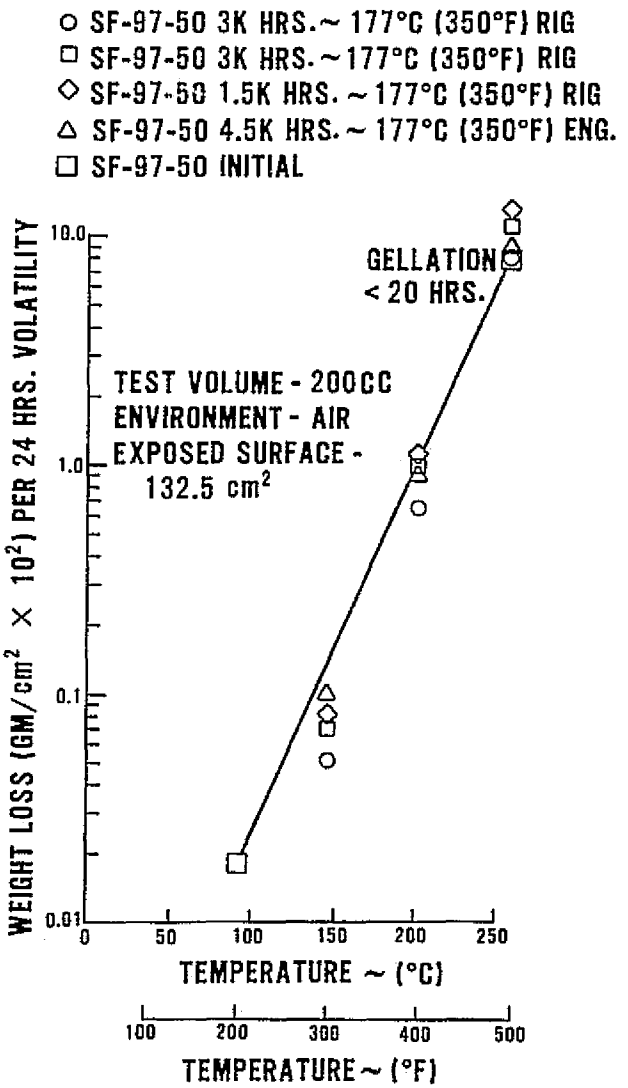

Figure 33 –

Voltatility vs. Temperature SF-97-50, Rig Samples

Flammability

Initial flammability limits are well above powerplant operating conditions. All coolant samples displayed some minor increase in flammability after exposure to powerplant operating conditions (Table IV). This is caused by a breakdown of the coolant polymer into a tetramers of higher flammability. However, the flammability of the mix is a function of the relative proportions of the two compounds and is not necessarily a function of operating time. Flammability limits are still well above powerplant conditions as shown in Table IV.

TABLE IV

FLAMMABILITY TEST RESULT SUMMARY

SF-1093-50	Flash Point	Fire Point	Autogenous Ignition
Original Sample	316°C (600°F)	343°C (650°F)	440°C (825°F)
Post 2000-Hour Sample	310°C (590°F)	336°C (635°F)	388°C (730°F)
Start-Stop Tests	288°C (550°F)	316°C (600°F)	413°C (775°F)
SF-97-50			
Original Sample	299°C (570°F)	343°C (650°F)	421°C (790°F)
Post 2000-Hour Sample	274°C (525°F)	330°C (625°F)	413°C (775°F)
Start-Stop Tests	274°C (525°F)	316°C (600°F)	371°C (700°F)
1500-Hour Stand Sample	302°C (575°F)	346°C (655°F)	390°C (735°F)
3000-Hour Stand Sample	288°C (550°F)	322°C (612°F)	334°C (635°F)
8000-Hour Stand Sample	291°C (555°F)	338°C (640°F)	365°C (690°F)
461-Hour Powerplant Sample	296°C (565°F)	323°C (615°F)	343°C (650°F)

Dielectric Breakdown

Table V shows that the initial dielectric strength of both coolants is acceptable. The dielectric strength of all coolants tested were found to be generally lower than the initial conditions. However, all are still satisfactory for use in fuel cell powerplants as illustrated in Table V.

Summary of Coolant Property Testing

The results of this testing indicates that both fluids are compatible with powerplant materials and operating temperatures. The differences between the two coolants' reaction with air requires different design considerations for powerplant plumbing. A key question to be resolved is whether it is more feasible to construct an air tight SF-97-50 system than a system in which adequate aeration of the SF-1093-50 coolant is possible. Further testing of each of the coolants under real powerplant conditions would be needed to resolve this issue.

TABLE V

DIELECTRIC BREAKDOWN TEST SUMMARY

Test Temperatures	Low 23.9°C (75°F)	Low 93°C (200°F)	Low 149°C (300°F)	Average 23.9°C (75°F)	Average 93°C (200°F)	Average 149°C (300°F)	High 23.9°C (75°F)	High 93°C (200°F)	High 149°C (300°F)
	Volts/MIL Kilovolt/meter x 10^{-6}								
SF-1093-50									
Original Sample	240 9.45	220 8.67	180 7.09	260 10.24	240 9.46	210 8.27	300 11.82	290 11.42	250 9.85
2000 Hour Lab Sample	200 7.88	–	–	240 9.46	–	–	280 11.42	–	–
SF-97-50									
Original Sample	250 9.85	210 8.27	160 6.30	280 11.03	240 9.46	180 7.09	350 13.79	290 11.42	210 8.27
2000 Hour Lab Sample	240 9.46	–	–	250 9.85	–	–	260 10.24	–	–
1500 Hour Stand Sample	230 9.06	–	240 9.46	250 9.85	–	260 10.24	290 11.24	–	280 11.03
3000 Hour Stand Sample	170 6.70	–	140 5.52	220 8.67	–	200 7.88	280 11.03	–	230 9.06
8000 Hour Stand Sample	190 7.49	–	250 9.85	220 8.67	–	250 9.85	260 10.24	–	250 9.85
461 - Hour Powerplant Sample	170 6.70	–	190 7.49	220 8.67	–	220 8.67	260 10.24	–	240 9.46

2.4 Task 3.4 "Experimental Program to Assess Heat Exchanger Core Characteristics"

Fuel cell powerplants present unique fouling conditions for the heat recovery heat exchangers. The component design requirements established in Task 3.2 were considered along with fluid properties determined in Task 3.3 and the heat exchanger background discussed in Section 4.4 to define an experimental program to establish basic heat exchanger data for designing heat exchangers for fuel cell powerplants with heat recovery. These data will be used to establish the impact of heat recovery on powerplant cost. The program encompasses four major tasks:

Task A – Materials Selection - The materials compatibility problems of heat exchangers interfacing with both fuel cell powerplant fluids and the water in the Integrated Utility System loop will be investigated and materials will be selected for use in this application. Initial materials selection will be made based upon known constraints. Follow-up testing of primary candidates will confirm these choices.

Task B – Definition of Fouling Considerations - The fouling characteristics experienced with fuel cell heat exchangers will be investigated and design factors and cleaning schedules to eliminate fouling effects on system performance will be established.

Task C – Definition of Required Integrated Utility System Water Loop Quality - The quality of water in the integrated utility system loop which is required to minimize corrosion and fouling on the system side of the heat exchangers will be identified.

Task D – Definition of Heat Exchanger Size and Cost Differential and Confirmation - Heat exchanger configurations will be selected for 40 KW and 26 MW fuel cell powerplants with heat recovery. The size of these heat exchangers will be defined and the cost differential between a fuel cell powerplant which rejects heat to air and a fuel cell powerplant which rejects heat to an integrated utility system loop will be determined. If heat exchanger core configurations different from those previously tested are selected, a short test will be conducted to confirm that the f and j factors and the fouling data are appropriate for the selected configurations.

The program, as defined, requires 18 months to complete: however, this depends upon several factors. For example, if core procurement and materials selection is accomplished in an on-going commercial program, a program as short as 12 months could result. Alternatively, if special cores or core materials are required, core porcurement could extend the program beyond 18 months. The individual program tasks are discussed in Figure 34.

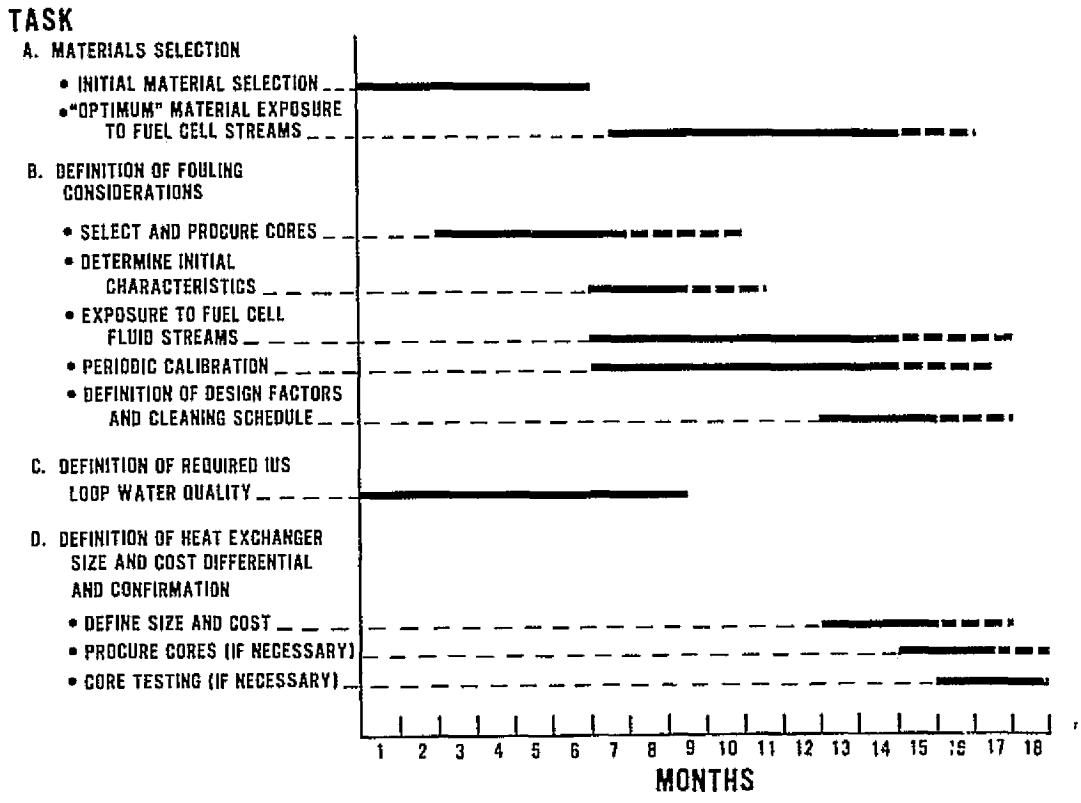

Figure 34 – Recommended Test Program

Task A – Materials Selection - The materials selected for fabrication of heat exchangers interfacing between the integrated utility system loops and fuel cell powerplant must be compatible with both the fuel cell fluids and the integrated utility system water coolant. The fuel cell thermal control heat exchanger materials are not a concern at this time since many materials compatible with the integrated utility system water loop are also compatible with silicone oil coolants. The heat exchangers which interface with the fuel cell exhaust gases do represent a potential material problem as discussed in Section 4.4. Samples of potential heat exchanger materials will be fabricated and placed within the fuel cell exhaust gas streams. The samples will be water cooled thereby exposing the material on both sides to the actual system fluids. Post-test examination of the samples will serve to identify materials for condenser fabrication. Consideration will be given to running dual sets of samples (one set on demineralized, deaerated water and the second set on available city water)in order to evaluate the effect of dissolved impurities.

Task B – Definition of Fouling Considerations - Several candidate vendor heat exchanger cores with representative geometry will be selected for testing based upon their availability. The cores being considered for potential integrated utility system use include the conventional round tube-type (possibly finned), the compact plate fin and the flattened finned tube. The cores will be purchased and experimental ducting added to allow accurate performance testing of the new, clean surfaces.

At the same time test rigs will be set up which expose the heat exchanger cores to three fuel cell exhaust streams (anode, cathode, and reformer). These rigs will utilize cell stacks from commercial programs to provide the proper exhaust conditions.

The initial characteristics of the test cores will be determined and then the cores will be exposed to the effluent gas streams of a fuel cell stack for an extended period of time with periodic performance calibrations to detect any loss of performance. The integrated utility system side of these cores will be deliberately cooled by clean air in order not to foul this surface. This technique will provide a more accurate evaluation of the fuel cell gas stream fouling tendencies. The cores will be functioning during this test and consequently should be experiencing realistic fouling environments on the fuel cell effluent side of the HEX.

Consideration will also be given to a parallel fouling test of cores exposed to the fuel cell coolant. However, this is not presently considered to be necessary. Fouling on the integrated utility system water side of the core may also be considered in this task if fouling characteristics for varying degrees of integrated utility system water purity are not available.

Interim and post-test calibrations of the cores will enable the detection of performance decay by a comparison with the initial data and these data will be analyzed to define design factors and cleaning schedules to accommodate fouling in fuel cell powerplant heat exchangers.

Task C – Definition of Required Integrated Utility System Water Loop Quality - Since water quality varies considerably with geography, it is uneconomic to design heat exchangers to accommodate the worst conditions which could be experienced in a mass produced powerplant for integrated utility system application. Accordingly, to define a practical level of

water quality for all integrated utility system applications, practical limitations of water treatment systems will be considered in conjunction with the results of the materials compatibility testing in Task A and the fouling characteristics for water (from the literature or Task B). The fuel cell powerplant heat exchangers will then be designed for this water quality and the necessary water treatment to achieve this quality will be installed at each site.

Task D — Definition of Heat Exchanger Size and Cost and Confirmation - The results of Tasks A, B, and C will be used together with data from commercial fuel cell programs to select the heat exchanger core configurations and sizes to meet the component design requirements established in Task 3.2 for 40 KW and 26 MW fuel cell powerplants with heat recovery (see Appendix B). The cost differential between an air cooled powerplant and a powerplant with heat recovery will be defined. If the selected core configurations are significantly different from those for which fouling data has been obtained, a short fouling test will be conducted to confirm the fouling data.

3.0 RECOMMENDATIONS

Further assessment of the use of fuel cell powerplants in integrated utility systems requires definition of the economic impact of heat recovery on capital cost and selection of the most economic heat recovery configuration. The following activities are recommended to make this assessment.

1. The heat exchanger experimental program defined in Task 3.4 should be implemented. Using data generated in the experimental effort, the capital cost impact of heat recovery should be evaluated for each heat recovery configuration.

2. The heat availability data generated in this contract, together with the data on the capital cost impact should be used as input to an analysis of total economics for fuel cell powerplants in typical integrated utility system installations. A computer program such as the Energy Systems Optimization Computer Program (ESOP) in use at NASA USPO could be used for this analysis.

3. The most attractive heat recovery configuration for fuel cell powerplants should be selected based on the results of the economic analysis carried out in recommendation 2.

In the effort described in this report, high grade heat was used to raise steam. Investigations of fouling characteristics under Task 3.4 shows that boiling concentrates dissolved solids and leads to fouling in steam generators. Avoiding the effects of fouling will require careful attention to water quality of the high grade heat recovery loop. It is recommended that the use of a pressurized water loop for heat recovery be considered in further studies to minimize fouling in the high grade heat recovery loop.

4.0 DISCUSSION

4.1 Introduction

The effort described in this report was performed under NASA Contract NAS9-14220 awarded by the Urban Systems Project Office at Johnson Space Center to the Pratt & Whitney Aircraft Division of United Aircraft. On January 1, 1975, the activities in this effort were transferred with other fuel cell activities to the Power Utility Division of United Aircraft. The effort took place during the period August 15, 1974 through February 15, 1975. In addition to the authors, W. Brunner, R. C. Nickols and E. K. Parenti of the Power Utility Division of United Aircraft contributed to this effort. Valuable technical assistance was provided by V. Shields and T. Redding of the NASA Urban Systems Project Office.

4.1.1 Brief Overview of Program

The study program approach is shown in Figure 35. Fuel cell powerplant designs being studied in commercial programs were examined using existing analytical techniques to define the availability of waste heat at rated power and at part load as a function of signficant parameters, such as powerplant rating and electric generation efficiency. The properties of dielectric fluids used for fuel cell coolants were defined experimentally and, together with system flow and pressure drop predictions, established the design requirements for heat recovery subsystem components. Heat exchanger design requirements and coolant properties were then examined to plan an experimental program for evaluating the characteristics of candidate heat exchangers for the heat recovery subsystem. The plan was based on the use of commercial program test stands and was designed to augment the present commercial effort.

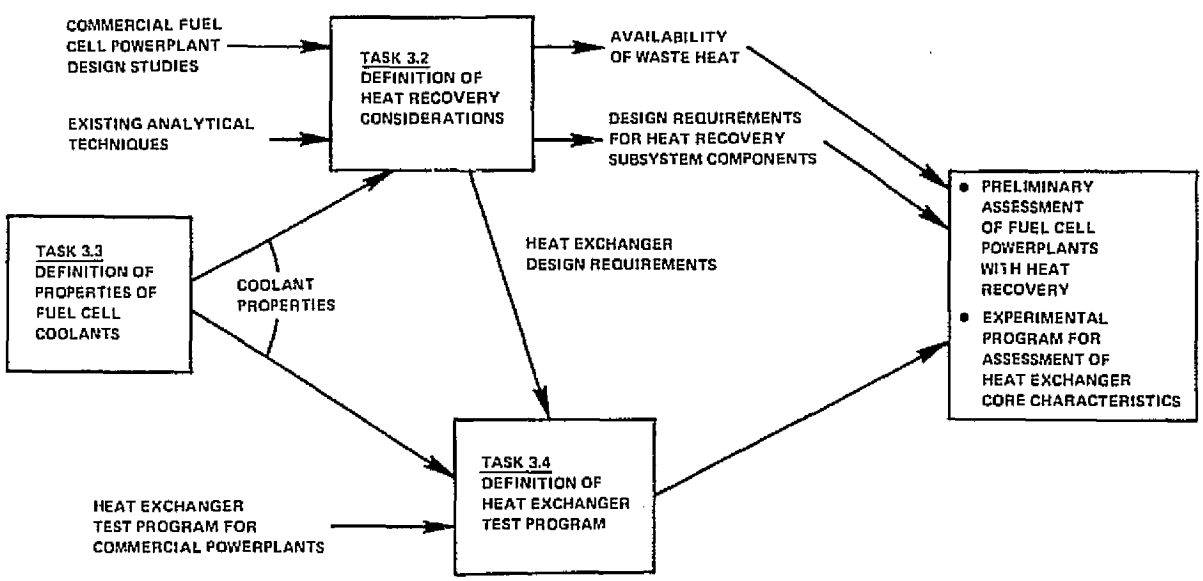

Figure 35 — Study Approach

The availability of waste heat and heat recovery subsystem design requirements provide a preliminary assessment of fuel cell powerplants with heat recovery. Implementation of the heat exchanger test program will provide data required to assess the capital cost impact of heat recovery. Discussion of the activity in each area follows.

4.2 Task 3.2, "Definition of Heat Recovery Considerations in Fuel Cell Powerplants"

4.2.1 Task Objectives

The object of this task is the definition of heat recovery considerations in fuel cell powerplants. Specific areas requiring study included:

- definition of a baseline powerplant
- definition of changes to powerplants to permit heat recovery
- definition of waste heat availability
- design requirements for heat recovery subsystem components

All thermodynamic analyses utilized in these studies were based on current analytical techniques developed for commercial fuel cell programs. Analyses include powerplant simulation techniques programmed for digital computers.

4.2.2 Characteristics of Baseline Fuel Cell Powerplants

The characteristics of a baseline fuel cell powerplant were defined to permit the evaluation of the impact of heat recovery. The baseline fuel cell powerplant was selected from designs which are presently under development in commercial fuel cell programs at Power Utility Division. Technology consistent with inital commercial powerplants was assumed.

The characteristics of two natural gas fueled powerplants are presented in this report. The first is the baseline powerplant of 40 KW rating which was used for the majority of the studies. The baseline 40 KW powerplant described here is being designed as one member of a family of fuel cell powerplants for on-site use. The overall thermodynamic characteristics of this powerplant are shown in Figure 36. The powerplant is designed for maximum overall efficiency at approximately half-rated power since this is a typical load point for on-site applications. Figure 36 indicates the 35 percent overall efficiency at 20 KW and shows the variation in overall efficiency from zero KW AC net to rated power, 40 KW AC net. Table VI below, summarizes the mechanical and electrical characteristics of the baseline 40 KW powerplant.

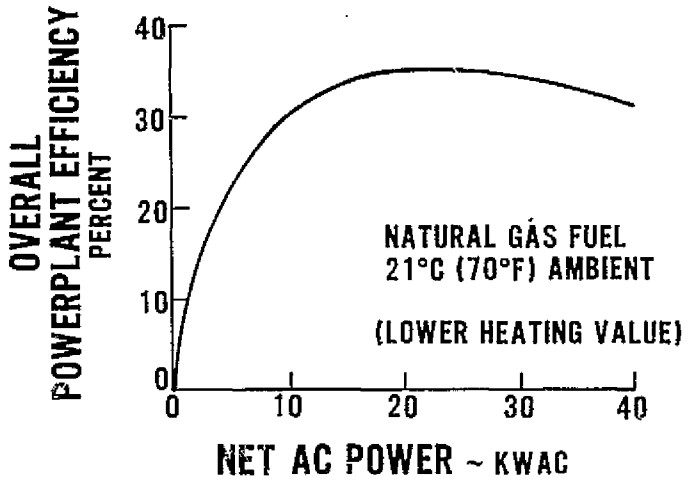

Figure 36 – 40 KW Baseline Powerplant Efficiency

TABLE VI

40 KW POWERPLANT CHARACTERISITCS

MECHANICAL

- Specific Weight: 55 kg/kw (120 lbs/kw)
- Envelope: 2.4 m x 1.2 m x 1.9 m (8 ft. x 4 ft. x 6 ft. 3 in.) high, about 5.67 m^3 (200 $ft.^3$) total volume
- Interfaces: Natural gas fuel line 19 kg/hr (42 lb/hr) natural gas maximum flow at start-up
  Water drain for excess condensed water

ELECTRICAL

- Power Form: 120/208 VAC, 4 wire, 3 phase, 60 Hz
- Steady State Rating (Maximum Continuous): 40 KW at .85 p.f.
- Overload Rating:
  - Motor Starting: (5 second rating): 56 KW at .7 p.f.
  - Fault Clearing: 300 amps
- Power Quality
  - Voltage Regulation: ±5 percent from zero net to full rated power
  - Frequency Regulation: ±.005 percent

A simplified fluid schematic of the baseline powerplant is shown in Figure 37. All major components of the baseline powerplant are shown in Figure 37 except for the inverter which converts the fuel cell DC output to 120/200 VAC. The only mechanical interfaces required are the natural gas fuel supply line and an excess water drain. The powerplant recovers sufficient process water by condensing water from fuel cell and burner exhaust streams. This eliminates the requirement for an external water supply. Final heat rejection is to air through two heat rejection components, the thermal control heat exchanger and the condenser. In this design, both units are air-cooled by a common cooling fan. The power section thermal control loop (right side of schematic) is a circulating oil loop which removes waste heat from the power section, provides heat to generate process steam for the reformer and then rejects any remaining heat to ambient in the thermal control heat exchanger. Control of the thermal loop in this design is maintained by bypass valves (not shown on schematic). One bypass controls the steam generation rate by shunting a portion of the coolant around the steam generator. The other bypass valve controls power section temperature by controlling coolant flow through or around the thermal control heat exchanger. There is no control required for the condenser; excess water recovered at temperatures below design is stored for use in very hot weather or discharged.

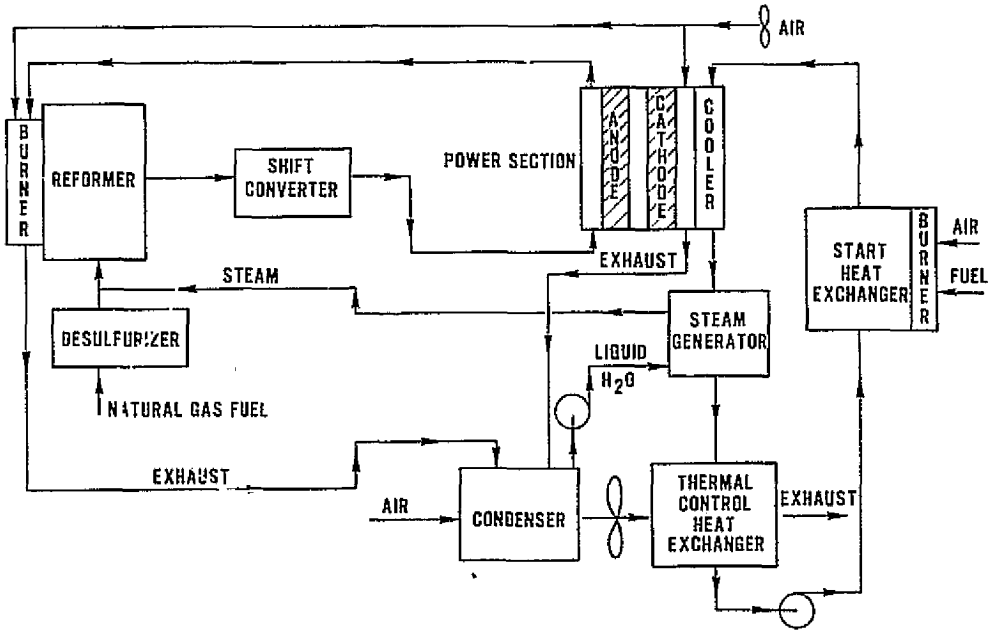

Figure 37 — 40 KW Baseline Powerplant Schematic

The second powerplant used in the study to define the effects of scale is a 26 MW design which is one of the configurations being considered for use in parallel with the network at electric utility sub-stations. The design uses a modular concept to minimize the number of

field connections; the modules would be factory assembled and tested and then truck transported to the installation site. Module size varies depending on the particular design. General mechanical and electrical characteristics of the 26 MW powerplant are indicated in Table VII:

TABLE VII

26 MW POWERPLANT CHARACTERISTICS

MECHANICAL

- Specific Weight: 37 kg/kw (80 lbs/kw)
- Envelopes: Overall 26 MW installation 54.3 m x 25.9 m x 5.5 m (178 ft x 85 ft x 18 ft)
- Interfaces: Natural gas fuel line 4926 kg/hr (10,850 lb/hr) maximum flow
  Water Drain for excess condensed water
  Module Interconnections

ELECTRICAL

- Power Form: 13,800 VAC, 3 phase, 3 wire, 60 Hz
- Steady State Rating (Maximum Continuous): 26 MW at unity p.f.
- Power Quality
  - Voltage: ±5 percent
  - Frequency: 60 Hz ±0.1

The power section thermal control loop of the 26 MW powerplant is essentially the same as that of the baseline 40 KW powerplant. The 26 MW unit uses separate air-cooled condensers to desuperheat and condese water from the powerplant exhaust streams. Figure 38 shows the trend of electric generation efficiency as a function of percent rated power for the 26 MW powerplant. Maximum efficiency occurs at approximately 50 percent of rated power.

4.2.3 Definition of Powerplant Changes Necessary for Heat Recovery

The recovery of available heat in this study is concerned with two categories defined by NASA as follows:

- High Grade Heat is required to produce 10.3×10^4 n/m^2 (15 psig) saturated steam with the condensate return temperature being 93°C (200°F.)

- Low Grade Heat is required to produce 71°C (160°F) hot water with the return temperature being 24°C (75°F.)

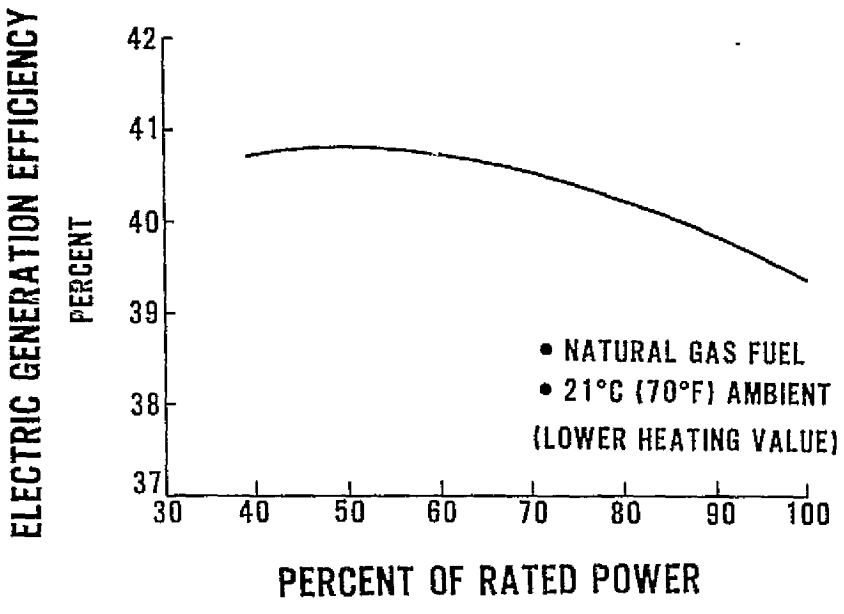

Figure 38 — 26 MW Powerplant Electric Generation Efficiency

As indicated in Figure 39, all waste heat in the present powerplant designs is rejected to cooling air streams. The final heat rejection components employed in the 40 KW baseline powerplant are the thermal control heat exchanger and the condenser. The thermal control heat exchanger is an oil to air heat exchanger which rejects waste heat from the power section coolant loop after the steam generator has extracted sufficient heat to produce steam for the reformer. All of the waste heat at the thermal control heat exchanger is available as high grade heat. The condenser rejects heat from the combined cathode exhaust and reformer burner exhaust streams by first desuperheating and then condensing water out of this mixed gas stream to provide sufficient water for the process steam generator. This air cooled heat exchanger can be replaced with either a single heat exchanger to produce 71°C (160°F) hot water or with two heat exchangers to supply both low grade and high grade heat.

Modifications to the baseline concept for heat recovery involve the substitution of heat exchangers and fluid streams which recover the waste heat in useable form. Three alternate heat recovery arrangements have been studied. Each arrangement assumes that all powerplant heat is rejected to the heat recovery loop at all times and that the integrated utility system can accept all excess heat. The first arrangement is shown in Figure 40A and indicates a 10.3×10^4 n/m^2 (15 psig) steam generator removing waste heat from the oil coolant loop and a water heat exchanger desuperheating and condensing the combined exhaust gas streams. This heat recovery arrangement is referred to as Configuration 1 throughout this report.

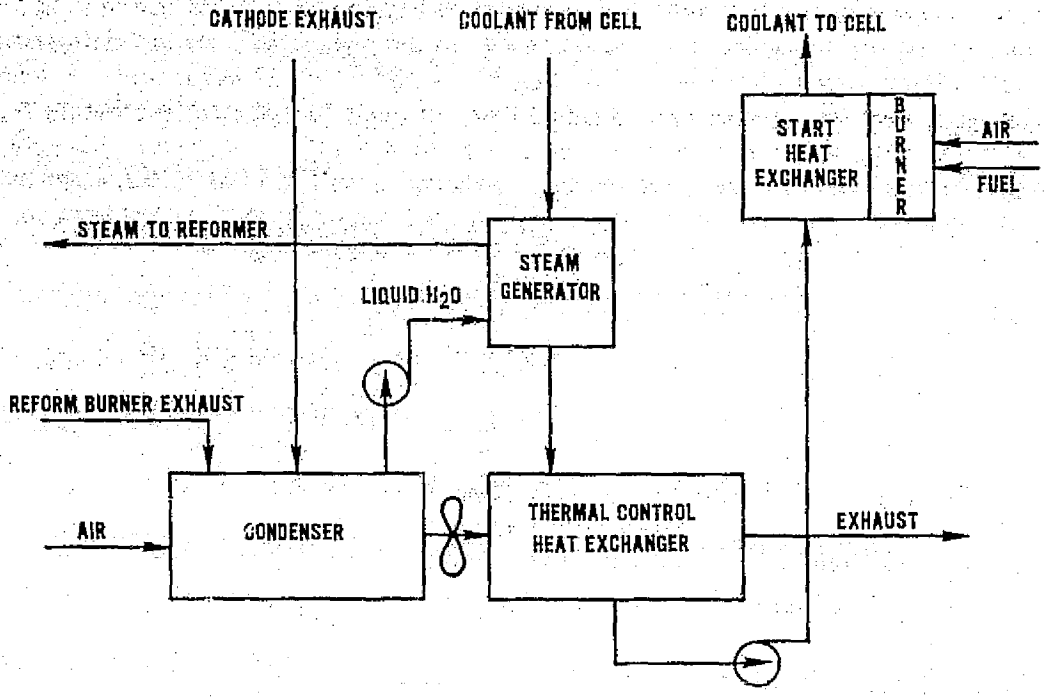

Figure 39 – 40 KW Baseline Thermal Management System Schematic

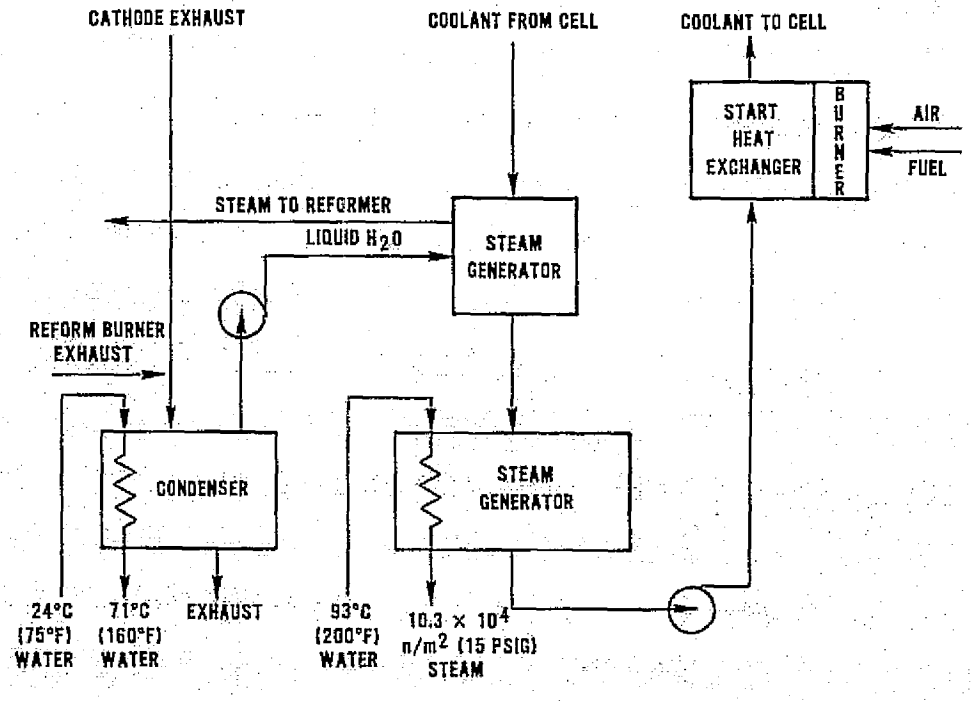

Figure 40A – Heat Recovery Subsystem – Configuration 1

A second arrangement, Configuration 2, is indicated in Figure 40B. In this configuration, the maximum amount of high grade heat is extracted from the powerplant. As in Configuration 1, all coolant loop waste heat is used to produce 10.3×10^4 n/m^2 (15 psig) steam. In addition, high grade heat from the combined exhaust stream waste heat is used to generate 10.3×10^4 n/m^2 (15 psig) steam and the remainder is used for the 71°C (160°F) water supply. A third arrangement is to remove all powerplant waste heat as 71°C (160°F) hot water as shown in Figure 40C. This arrangement, Configuration 3, results in the simplest system.

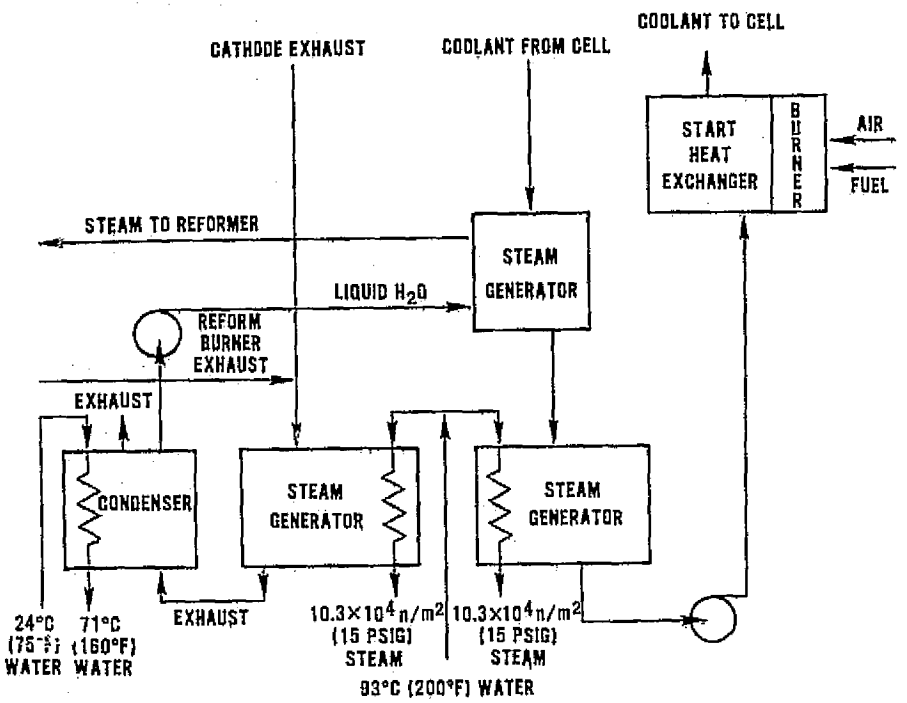

Figure 40B — Heat Recovery Subsystem — Configuration 2

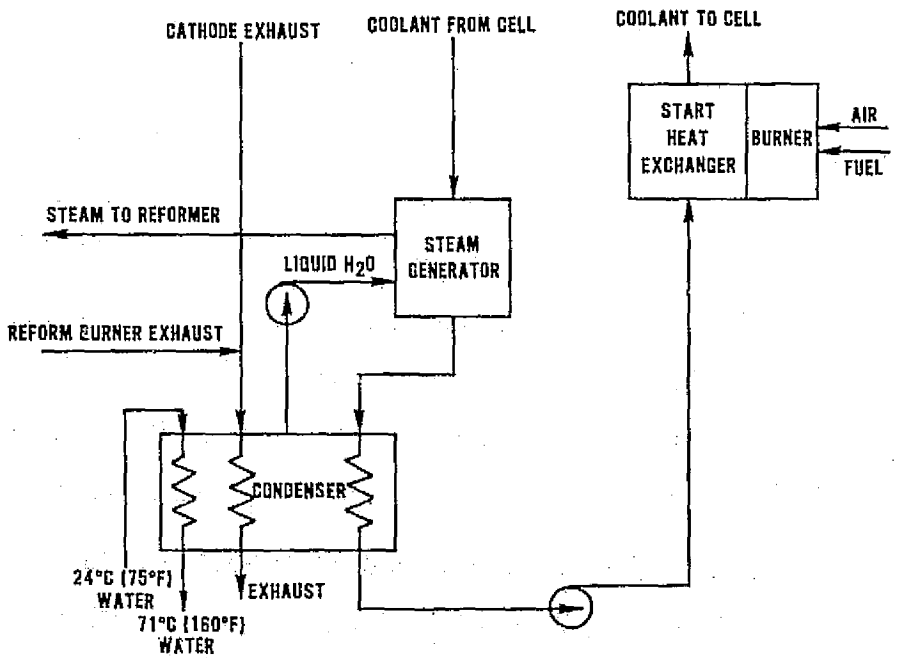

Figure 40C — Heat Recovery Subsystem — Configuration 3

The baseline power section heat removal method is a forced convection silicone oil loop. Alternate methods of heat removal from the power section were considered in this study. The prime alternate in present Power Utility designs is the use of two-phase water cooling directly in the power section. This concept is shown in Figure 41 with the necessary modifications for heat recovery. In this approach, water is circulated through the power section to remove waste heat. The resulting two-phase mixture flows to a steam separator which provides process steam to the reformer as required. All excess steam is diverted to a condenser which is used to generate 10.3×10^4 n/m^2 (15 psig) steam for heat recovery. The condenser is utilized as an interface between the powerplant and the heat recovery loop to avoid contamination of the powerplant loop by the building piping. The low grade heat recovery portion of the system is similar to the previously described systems. The use of heat pipes to remove waste heat from the power section would result in a similar final heat rejection concept. That is, heat from the heat pipes would be used to generate steam for process use and for excess heat remvoal via a condenser as in Figure 41. This approach has not been seriously considered to date because of relatively high cost estimates for heat pipes compared to other means of heat removal. Two factors which contribute to the high cost estimates are the large number of heat pipes required for intercell placement and the difficult stack environment.

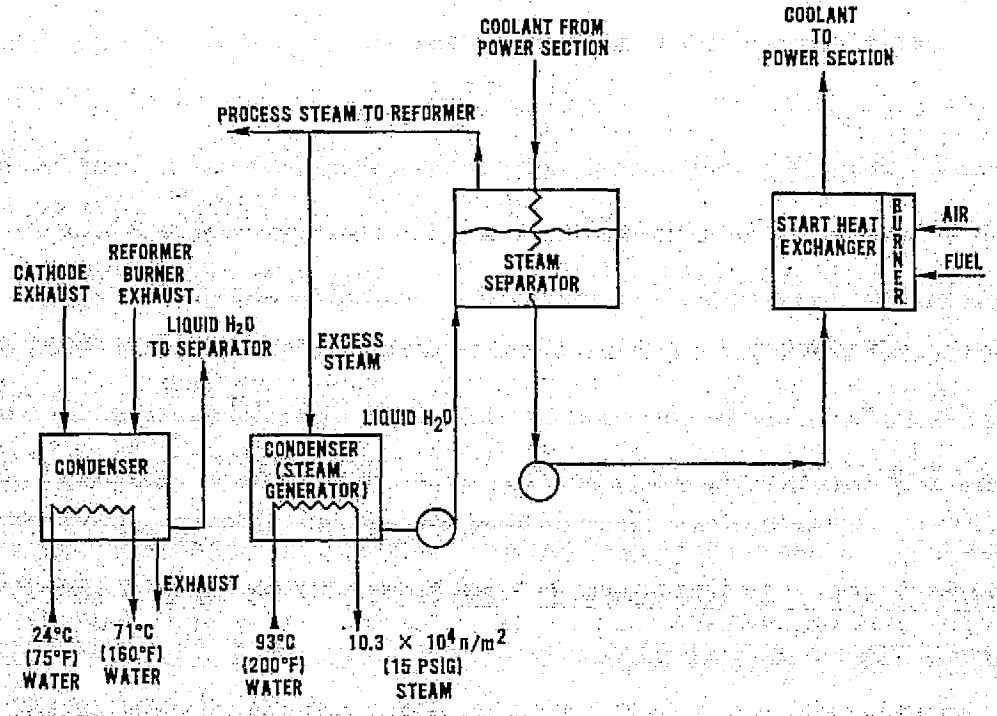

Figure 41 – Heat Recovery Subsystem for 2-Phase Water Cooled Power Section

Control of the baseline 40 KW powerplant in the heat recovery configuration does not require the addition of any controls. This applies to both the oil-cooled power section configuration and the two-phase water-cooled power section configuration described in the preceding paragraph. Normal control of the oil coolant loop is with a coolant bypass valve to control flow through the thermal control heat exchanger. This same bypass valve would be used to control oil flow through the steam generator in the heat recovery mode. Normal controls for the alternate two-phase water-cooled version include regulators to control steam flow to the process line and to the excess steam condenser. These controls are suitable for normal powerplant configuration or heat recovery configuration. These methods of control with the active control unit on the fuel cell side of the heat recovery loop will result in varying amounts of excess condensed water from the fuel cell powerplant. This water is available to the integrated utility system, if desired. Powerplant modifications to the 26 MW powerplant for heat recovery are similar to the 40 KW baseline powerplant.

4.2.4 Available Heat from 40 KW Powerplant

In defining available heat, the heat exchanger effectiveness must be considered.

From the effectiveness (ϵ) versus N.T.U. curves in the heat transfer literature and considerations of practical heat loss, axial conduction and maldistribution effects, the following conclusions can be made for small size heat exchangers:

- ϵ max. practical = 0.90 for counterflow
- ϵ max. practical = 0.80 for cross flow

For compact heat exchangers of the type being considered for fuel cell powerplants, header costs for counterflow units are substantially higher than for cross flow units resulting in higher overall heat exchanger costs. Economic considerations would dictate the use of the 0.80 effective cross flow unit except where special system thermodynamic requirements for higher effectiveness and higher cost existed. A heat exchanger effectiveness of 0.80 was selected as a practical design point for all heat exchangers involved in this study.

The quantities of available high grade and low grade heat for the baseline 40 KW powerplant in heat recovery Configuration 1 are indicated in Figure 42 as a function of net power level. In this configuration, the power section coolant loop is the sole source of high grade heat 10.3×10^4 n/m^2 (15 psig) steam. High grade heat drops from 19,400 KCAL/HR at 40 KW to zero at about 8 KW because the process steam requirements consume all available heat in the loop below this point. The low grade heat (71°C (160°F) hot water) decreases linearly from a maximum of 23200 KCAL/HR (92,000 Btu/hr) at 40 KW to 3020 KCAL/HR (12,000 Btu/hr) at zero net power. This heat recovery configuration (1) is the arrangement which causes a minimum of changes to the powerplant, yet produces reasonable quantities of both high and low grade heat.

Configuration 2 is somewhat more complex but maximizes the available quantity of high grade heat. This is, of course, at the expense of low grade heat since the total available heat remains constant. Figure 43 shows the available high and low grade heat for the 40 KW

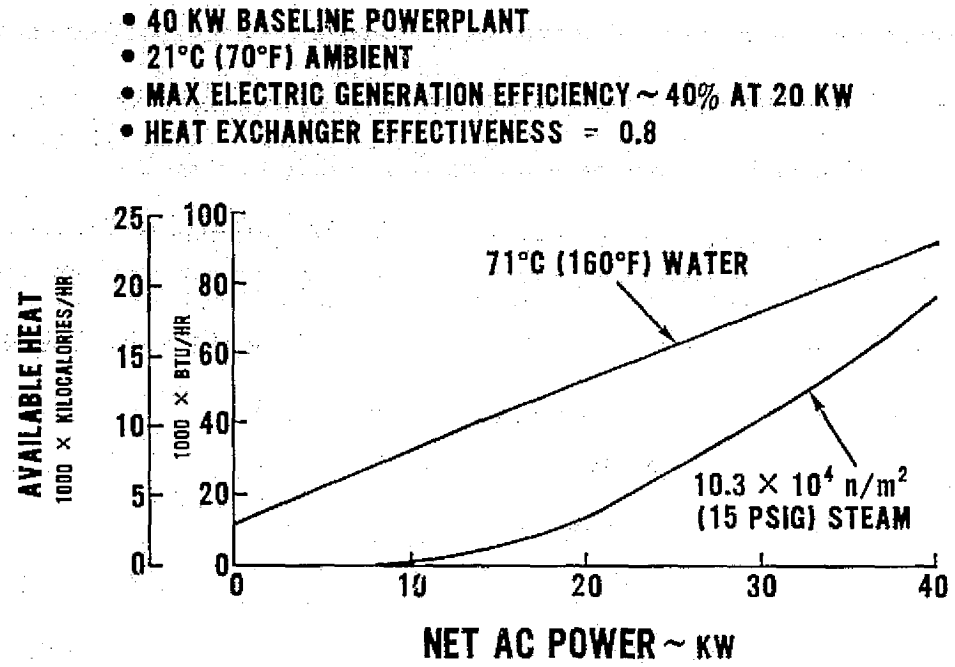

Figure 42 — Available Heat for the 40 Percent Efficient, 40 KW Powerplant — Configuration 1

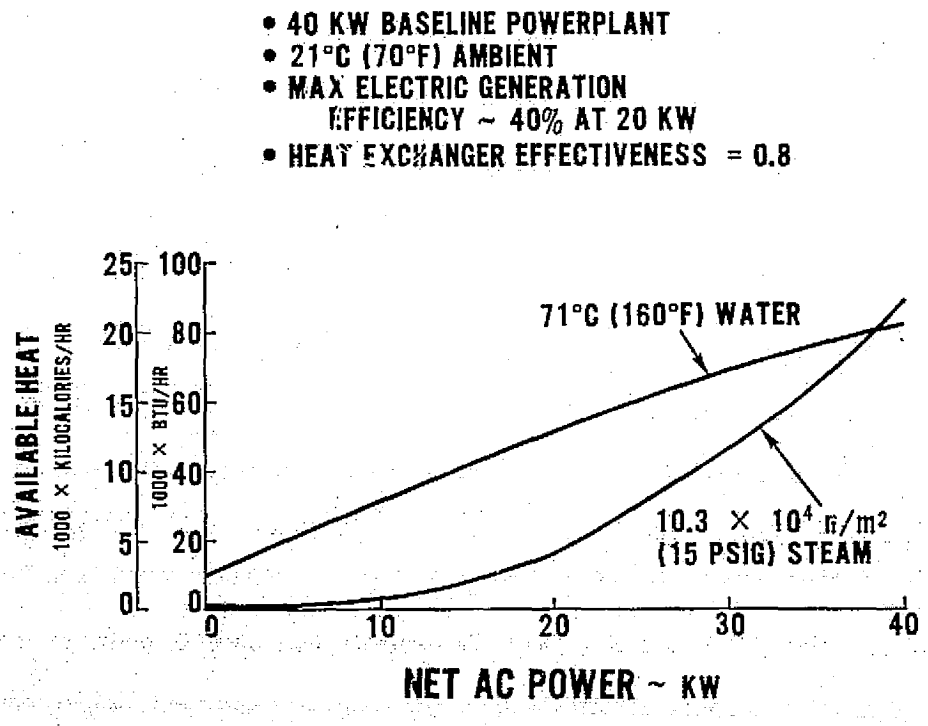

Figure 43 — Available Heat for the 40 Percent Efficient, 40 KW Powerplant — Configuration 2

powerplant in Configuration 2. In this configuration, some high grade heat remains available even at idle from the combined cathode/anode exhaust stream. The maximum quantity of 10.3×10^4 n/m^2 (15 psig) steam available at 40 KW has increased from 19300 KCAL/HR (76,500 Btu/hr) in Configuration 1 to 22000 KCAL/HR (87,300 Btu/hr) in Configuration 2. An equal amount of low grade heat has been sacrificed in all cases.

The available heat for the all low grade heat version, Configuration 3, is shown in Figure 44. Here all available heat from both the exhaust stream and from the power section coolant loop is used to generate 71°C (160°F) water. In this arrangement, the total available heat varies from 42300 KCAL/HR (168,000 Btu/hr) at 40 KW to 3020 KCAL/HR (12,000 Btu/hr) at 0 KW.

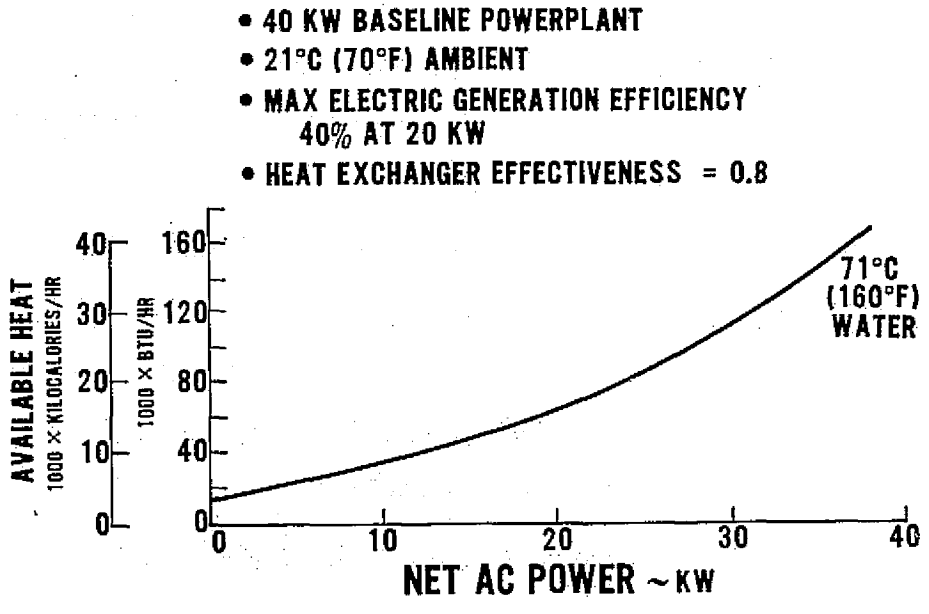

Figure 44 — Available Heat for the 40 Percent Efficient, 40 KW Powerplant — Configuration 3

4.2.5 The Impact of Independent Variables on Available Heat

Electric Generation Efficiency

The impact of electric generation efficiency on available high grade heat is shown in Figure 45. Efficiency levels of 30 percent, 35 percent, and 40 percent were investigated. The quantity of high grade heat increases rapidly with decreasing electric generation efficiency since the level of waste heat from the power section is increasing. The largest increase in high grade heat occurs between 40 percent and 35 percent efficiency. A smaller increase occurs as efficiency is further lowered to 30 percent. This is due to design restrictions imposed by power section operating restraints. Similar curves are presented in Figure 46 to illustrate that the impact of efficiency on available low grade heat. Again, the quantity of available heat is increasing rapidly between 40 percent and 30 percent electric generation efficiency. The largest change occurs between 35 percent and 30 percent where the decreasing efficiency of the fuel conditioner contributes more strongly to available low grade heat.

- 40 KW BASELINE POWERPLANT
- HEAT RECOVERY CONFIGURATION 1
- 21°C (70°F) AMBIENT
- HEAT EXCHANGER EFFECTIVENESS = 0.8

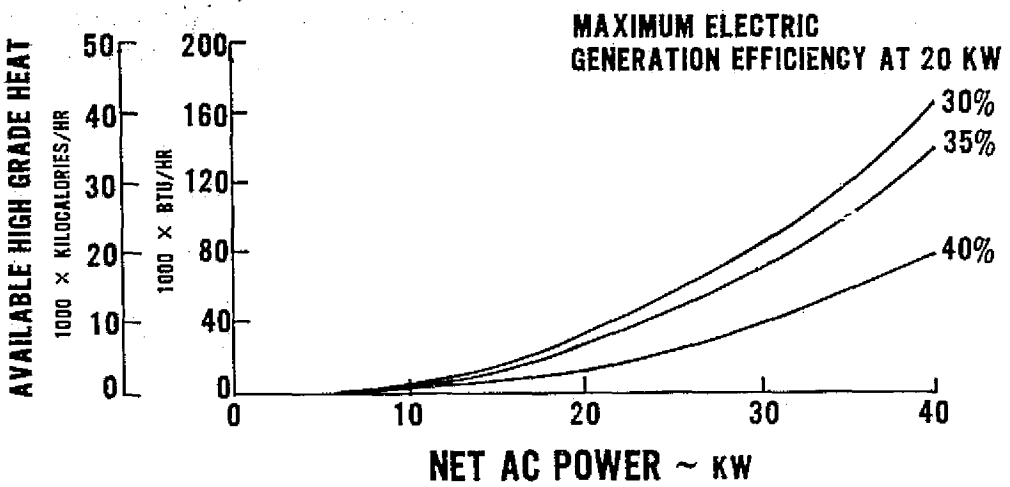

Figure 45 — The Impact of Electric Generation Efficiency on High Grade Heat

- 40 KW BASELINE POWERPLANT
- HEAT RECOVERY CONFIGURATION 1
- 21°C (70°F) AMBIENT
- HEAT EXCHANGER EFFECTIVENESS = 0.8

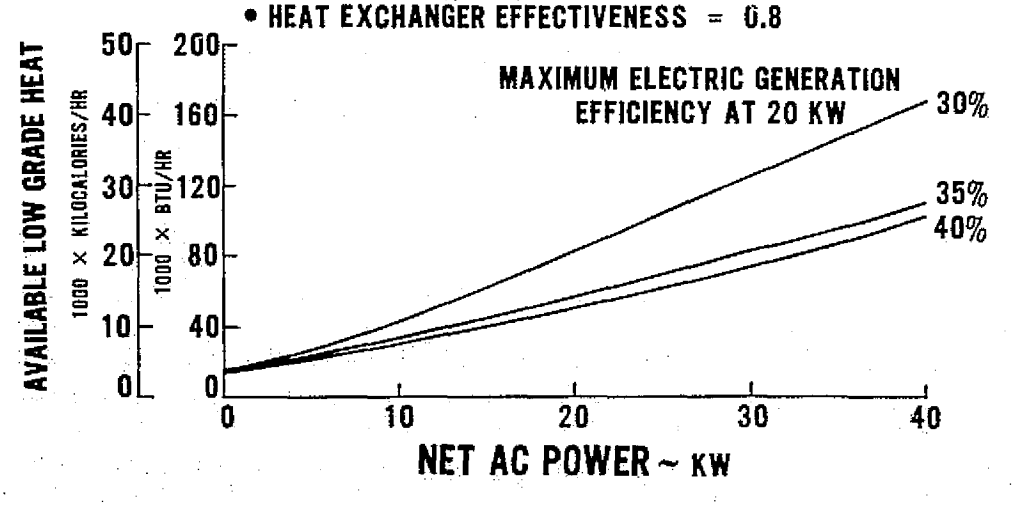

Figure 46 — The Impact of Electric Generation Efficiency on Low Grade Heat

Figure 47 is shown to illustrate the impact of electric generation efficiency on total useable energy. This curve is expressed as percent of fuel lower heating value and shows the trend at full power (40 KW) and half-power (20 KW). In general the change in useable energy from 40 percent to 35 percent are relatively small both at full and half-power. A more significant change is shown between the 35 percent and 30 percent powerplant designs. The primary factor causing the sharp decline in useable energy at 30 percent is the electric generation efficiency at full power which drops off much faster between half-power and full power for the low efficiency powerplant. This is due to design restrictions on the powerplant subsystems.

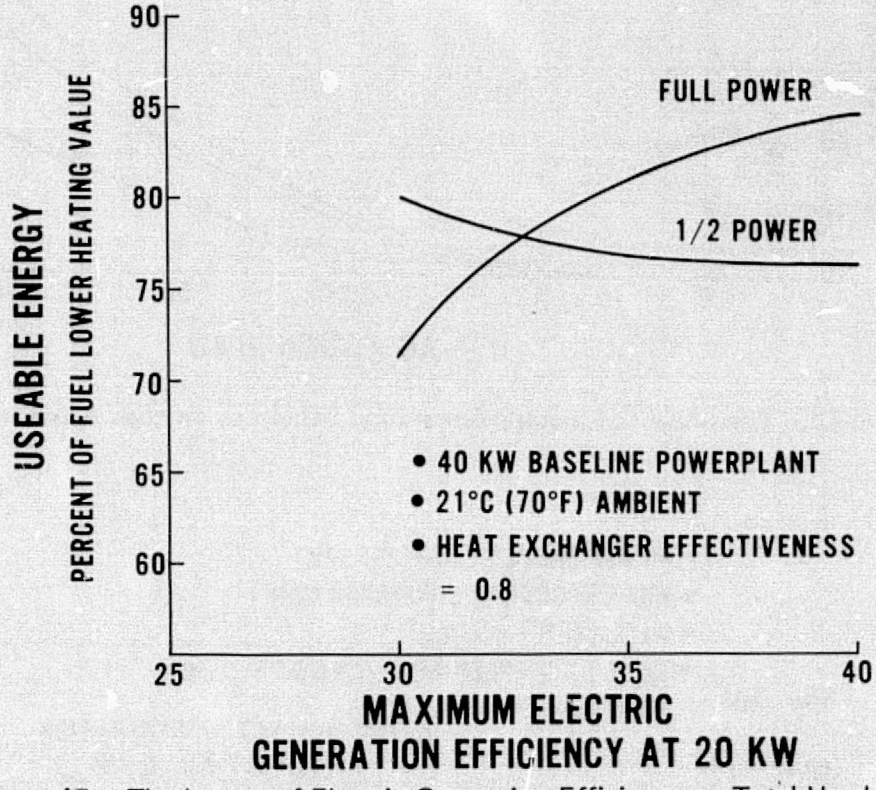

Figure 47 — The Impact of Electric Generation Efficiency on Total Useable Energy

Ambient Temperature

The effect of ambient temperature on available high grade and low grade heat was studied. A temperature range of 2°C (35°F) to 43°C (110°F) was investigated and the impact was found to be small. Figure 48 shows less than a 10 percent change in available high grade heat from 21°C (70°F) to 43°C (110°F) or 21°C (70°F) to 2°C (35°F) at any power level. The effect of ambient temperature on low grade heat is even smaller (about 1 to 2 percent maximum) as temperature is increased or decreased about the 21°C (70°F) reference point. The larger impact of ambient temperature on high grade heat as compared to low grade can be attributed to the difference in the amount of power section waste heat removed by the process air stream. This stream enters the power section at ambient temperature and always exists at average cell temperature. Heat removed from the power section to heat incoming air in this manner is heat that is unavailable to the power section coolant loop.

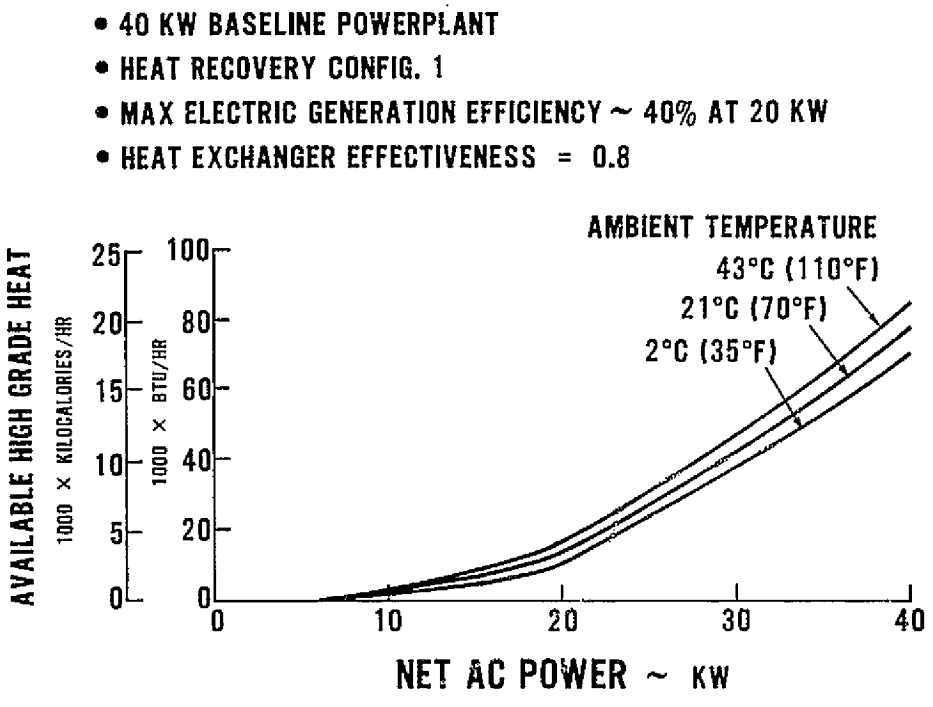

Figure 48 — The Effect of Ambient Temperature on Available High Grade Heat

Varying Recovery Loop Steam Pressures

Figure 49 shows the results of studies to determine the impact of varying recovery loop steam pressures on available high grade heat. A range of 10.3×10^4 n/m^2 to 62.1×10^4 n/m^2 (15 to 90 psig) was selected as compatible with the possible range of coolant temperatures. The study was conducted using Configuration 2 for maximum effect. The maximum steam pressure available is limited by the coolant exit temperature from the power section. Limits are indicated over the range of interest 149 to 177°C (300 to 350°F). These results are shown in Figure 49 at the 40 KW net AC power level only. They indicate only a minor effect of recovery loop pressure on high grade waste heat availability. This effect is associated with maintaining an effectiveness of 0.8 for the exhaust gas heat exchanger.

Low Grade Heat Recovery Loop Temperature

A study of the effect of varying temperatures in the low grade heat recovery loop was conducted for the 40 KW baseline powerplant. Specific cases studied were: 24°C (75°F) return temperature with 71°C (160°F) supply (the baseline case - low grade heat used for domestic hot water), 60°C (140°F) return with 93°C (200°F) supply (low grade heat used for space heating), and a two-stage recovery arrangement with 24°C (75°F) return, 71°C (160°F) supply and 71°C (160°F) return with 93°C (200°F) supply. The quantities of low grade heat available at 40 KW, (21°C (70°F) ambient, 40 percent electric generation efficiency at 20 KW) are shown in Table VIII.

The sharp decline in available heat between 24°C (75°F) and 60°C (140°F) water return temperatures is due to the loss of the heat of condensation in the powerplant exhaust stream. The combined exhaust stream dewpoint for this configuration is approximately 66°C (150°F).

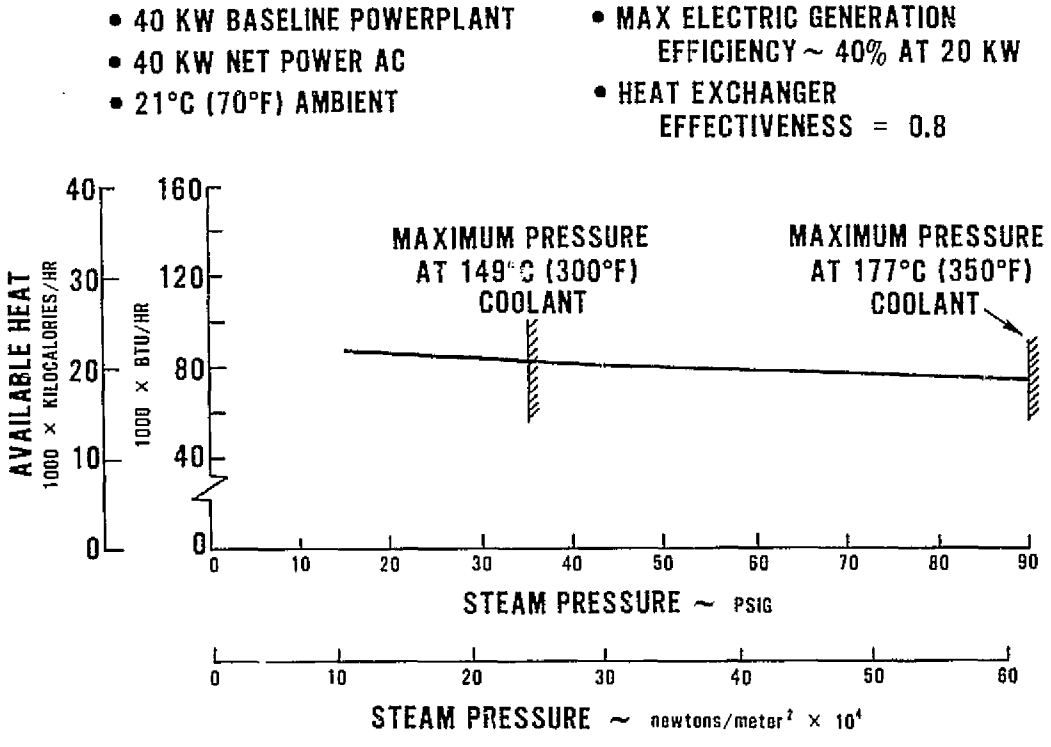

Figure 49—The Effect of Steam Pressure on Available High Grade Heat for the 40 Percent Efficient, 40 KW Powerplant—Configuration 2

TABLE VIII

LOW GRADE HEAT AVAILABLE AT 40 KW

40 PERCENT EFFICIENCY AT 20 KW

	Water Return Temperature °C	(°F)	Water Supply Temperature °C	(°F)	Available Low Grade Heat KCAL/HR	(Btu/hr)
Baseline	24	(75)	71	(160)	23,000	(91,900)
Case 1	60	(140)	93	(200)	7,600	(30,000)
Case 2	24	(75)	71	(160)	16,300	(64,600)
	71	(160)	93	(200)	6,880	(27,300)

Powerplant Rating

The effect of scale (powerplant rating) was studied by evaluating the quantities of available high grade and low grade heat for the 26 MW powerplant; these quantities are indicated in Figure 50 over the range of half-power to full power. Heat recovery Configurations 1 and 2 are both shown in this figure. The overall impact of scale is obtained by comparing the total useable energy for the 40 KW baseline and the 26 MW powerplants. The total useable energy at rated power for the 26 MW powerplant is 96 percent of the fuel lower heating value compared to 84 percent for the 40 KW powerplant. Since the 26 MW powerplant is a modular powerplant, it is obvious that this same 96 percent holds true at the module rating (typically 4 MW). Estmates have indicated that the useable energy remains nearly constant down to about the 500 KW level and then decreases slowly to the 84 percent value for the 40 KW baseline powerplant. The primary factors producing this trend toward slightly lower useable energy at lower power levels are inverter performance, component parasite power and thermal losses. All items show strong scale effects between 40 and several hundred KW to produce this trend in total useable energy.

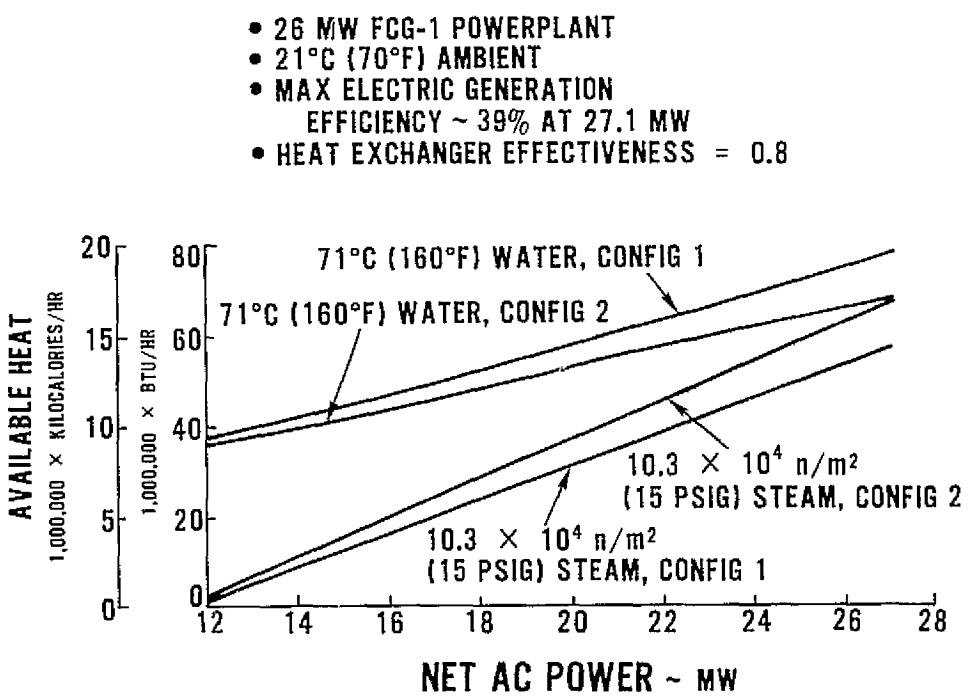

Figure 50 – Available Heat for the 26 MW Powerplant – Configurations 1 and 2

4.2.6 Component Design Requirements for Heat Recovery

Component design requirements were developed for the 40 KW powerplant at 35 and 40 percent electrical generation efficiency and for the 26 MW powerplant. Requirements were analyzed for heat recovery Configurations 1 and 2 for both powerplants. These design re-

quirements are provided in Appendix A. Items included in the design requirements are function, heat transfer requirements and a complete description of both cold side and hot side streams. The latter includes mass flow rates, inlet and exit temperatures, and detailed stream compositions. Pressure drop allocations are also indicated wherever they are considered critical. The 26 MW powerplant design requirements are written in terms of 4 MW independent modules.

These design requirements plus the coolant properties determined in Task 3.3 provide complete component design requirements for the definition of a heat exchanger test program to assess the basic characteristics of candidate heat exchanger cores.

4.3 Task 3.3, "Determination of Heat Transfer Properties of Fuel Cell Coolants"

4.3.1 Method and Equipment for Measuring Each Fluid Property

Initial fluid property data for the two candidate silicone oil coolants, SF-97-50 and SF-1093-50, were limited at fuel cell powerplant operating conditions and no data was available on changes to the coolant properties after exposure to powerplant operation. Since definition of the impact of heat recovery on fuel cell powerplant size and cost requires coolant property data, important properties were measured as part of this contract effort. The properties which were evaluated included:

- Viscosity
- Density
- Specific Heat
- Thermal Conductivity
- Volatility
- Flammability
- Dielectric Strength

The test method for each measurement is discussed below.

Viscosity

Viscosity measurements were performed by using a Brookfield Viscometer; the device functions by detecting the effort required to rotate a test "wheel" in the fluid sample while the fluid is maintained at specific temperatures. The test unit is shown in Figure 51.

Density

Originally, density measurements were planned to be made with Hydrometers. However, an alternate approach was selected which is considered to be more accurate. A 250 Ml narrow-neck glass vessel was carefully weighed empty and after being filled with the test coolant. The density was calculated from the weight-volume relationship. This was repeated at elevated temperatures with the excess fluid volume (due to thermal expansion) being removed as required.

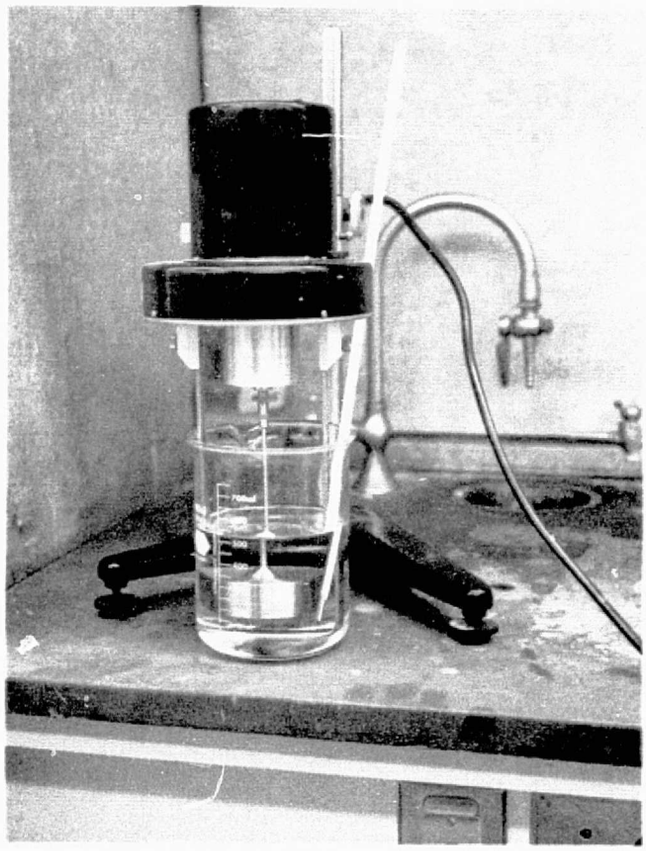

Figure 51 – Brookfield Viscometer

Specific Heat

Specific heat measurements were performed using a Dupont Differential Scanning Calorimeter. A sample of coolant is placed within the calorimeter and is automatically heated in a manner to change its temperature at constant rate. The calorimeter readout is proportional to the heating energy required and is a measure of the coolant specific heat. The test instrument is shown in Figure 52.

Thermal Conductivity

Coolant Thermal Conductivity

The thermal conductivity of the test coolant samples was evaluated by Wear Sciences, Inc. The test instrument employed by Wear Sciences is a Thermal Comparator utilizing a specially constructed test probe from Technometrics, Inc. The equipment is illustrated in Figure 53.

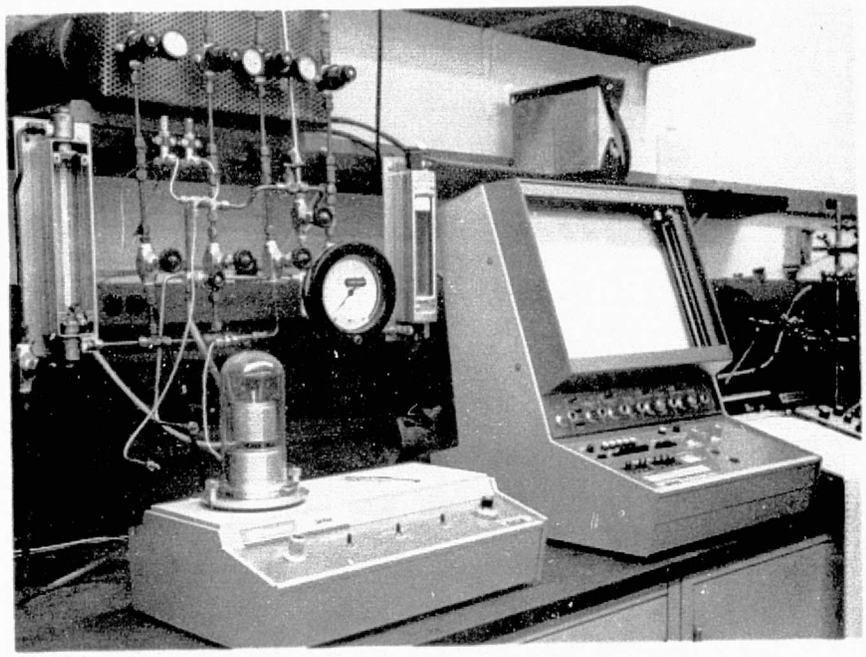

Figure 52 – Dupont Differential Scanning Calorimeter

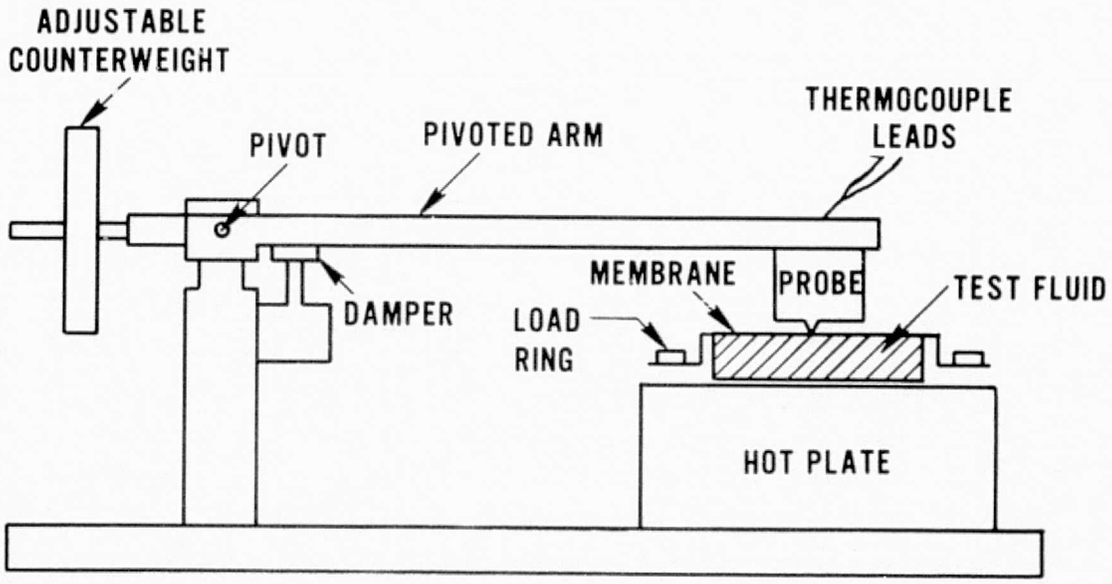

Figure 53 – Thermal Comparator

The probe consists of an electrically heated metal block which is maintained at a specific temperature and an unheated, "pointed" end containing a thermocouple temperature read-out. The probe is mounted on a balance arm similar to that used for a record turntable stylus. The test fluid is placed in a shallow heated dish and maintained at a temperature approximately 21.2°C (70°F) lower than the probe. A thin membrane is placed over the fluid to minimize secondary effects such as evaporation or variations in fluid surface tension. The test method is to allow the thermocouple end of the probe to gently contact the fluid surface (i.e., membrane) which allows heat conduction from the probe into the fluid. The "tip" of the probe in contact with the fluid will reach a lower temperature than the metal block depending upon the relative conductivities of the probe material and the test fluid. Since the highest temperature is at the top of the test sample, convection currents are minimized and the temperature differential between the metal block and the test sample is proportional to the thermal conductivity of the coolant sample. The thermal conductivity is determined by comparing the temperature differential of the sample to the temperature differential observed with a liquid of known conductivity. This instrument and the test method are described further in Appendix B.

Volatility

The volatility of the coolants was evaluated by monitoring the rate of weight loss from coolant samples while maintaining the fluid at specific temperature levels in open containers. The test arrangement is shown in Figure 54.

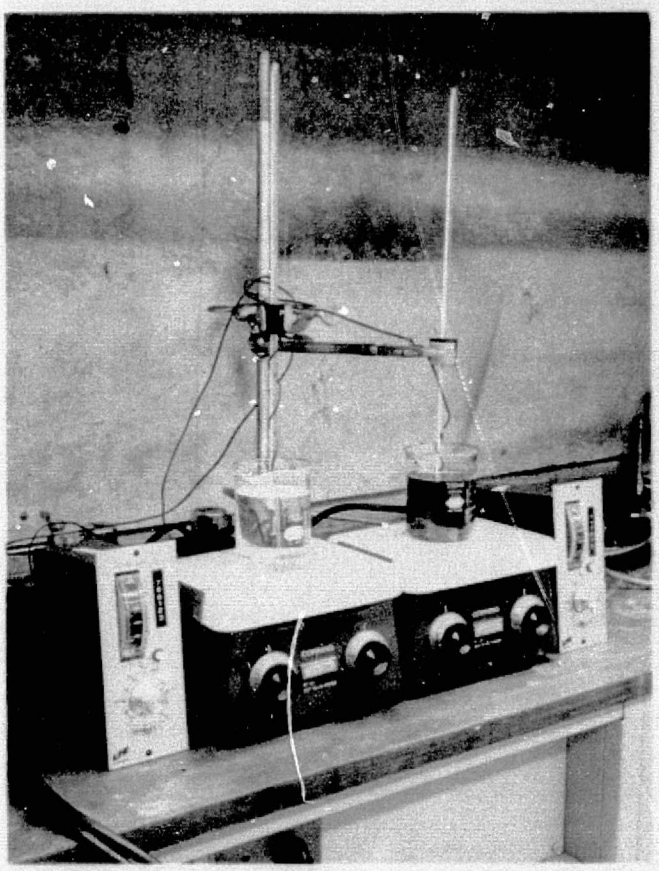

Figure 54—Test Arrangement for Volatility

Flammability

The flammability tests were performed according to standard ASTM procedures D92-52 and D2155-66. In these procedures, samples of each coolant were heated in an open container while a flame is passed back and forth across the top of the container as the temperature rises. The temperature at which the vapor initially ignites was recorded as the "flash point". When the flame ignites and burns for a minimum of 5 seconds the temperature is recorded as the "fire point". Continued heating of the coolant without using an open flame eventually resulted in the fluid self igniting; this is referred to as the "autogeneous ignition temperature". Figure 55 shows the test in process.

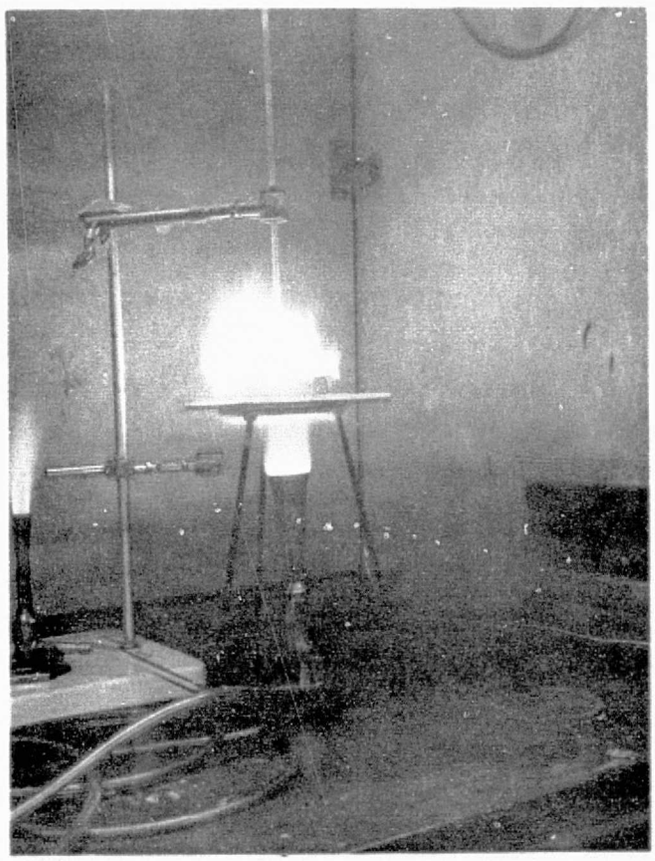

Figure 55 – Flammability Test in Process

Dielectric Strength

This test was performed using an Associated Research inc. test machine model 4720-M7 and ASTM procedure D877-49. The dielectric strength test was performed by placing the electrodes of the tester in a coolant sample. The voltage between the plates was increased until arcing occurred which indicates coolant dielectric breakdown. This test was repeated with a fresh coolant sample six times at each temperature. The test equipment is shown in Figure 56.

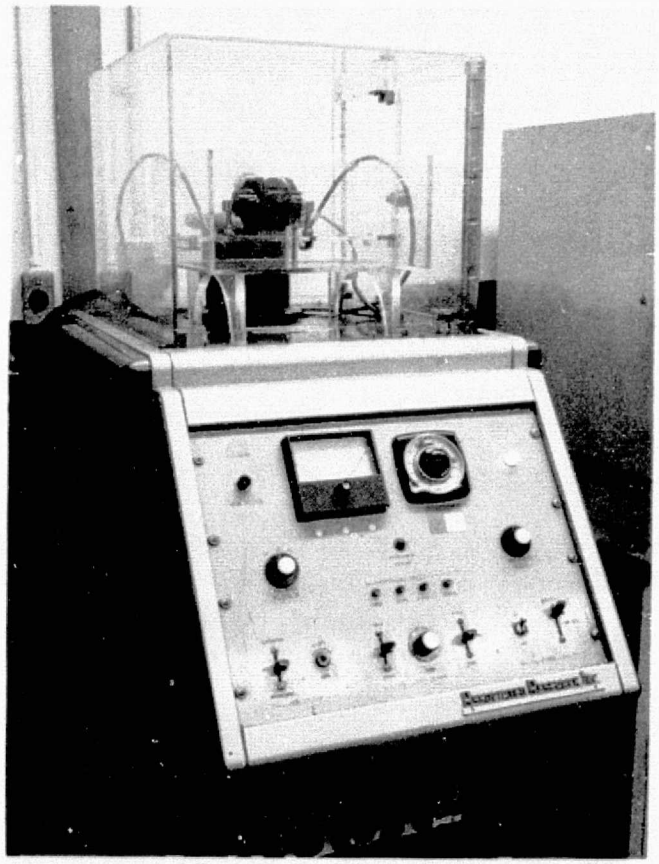

Figure 56 – Dielectric Strength Test Equipment

4.3.2 Description of Test Program

The test program is shown in out-line form in Figure 57 and described below. The results of the test program are presented in Section 2.3.

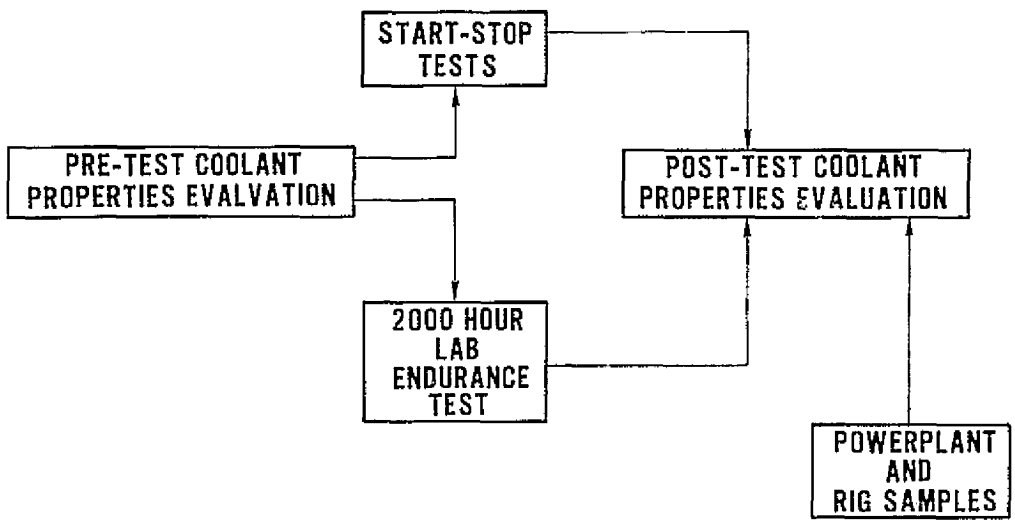

Figure 57 — Outline of Test Program

Pre-Test Coolant Properties Evaluation

Sufficient quantities of both the SF-97-50 and the SF-1093-50 were obtained from the manufacturer to support all testing required of the task. Samples of each coolant were tested to establish the initial values of coolant physical properties.

The 2000-Hour Exposure to Powerplant Conditions

The long-term steady-state test consisted of exposing approximately 1 liter of each coolant to selected powerplant materials while maintaining the fluid at 190.5°C (375°F) for a period of 2000 hours. The specific test conditions for each coolant were tailored to conform closely to the coolant manufacturers recommendations while also considering realistic powerplant limitations. The manufacturer recommends minimizing the amount of air which comes in contact with the SF-97-50 coolant to prevent oxidation of the fluid. Filling a powerplant cooling loop usually results in the inclusion of a small quantity of air and, as a result, approximately 1 percent air by volume was sealed into the SF-97-50 container at the start of the long-term exposure test. The SF-1093-50 coolant is manufactured with an additive to prevent oxidation and actually requires being exposed to air to prevent degradation of the fluid.

A powerplant system using this coolant would be designed with a membraneless accumulator to encourage air exposure to the coolant. Therefore, the long term sample of SF-1093-50 was placed in an open container such that the ratio of coolant surface area in air contact to the total coolant volume approximated that expected in a typical powerplant; 2.5×10^{-3} cm^2/cm^3. The test arrangement for the SF-97-50 samples is shown in Figure 58. The arrangement for the SF-1093-50 was similar.

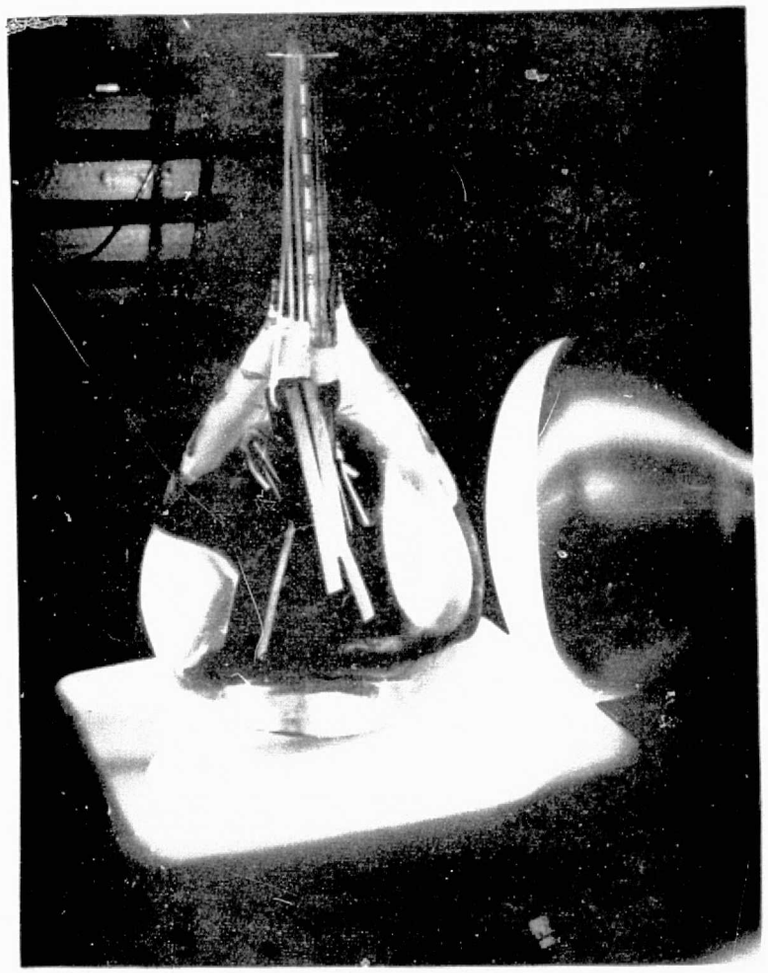

Figure 58 – 2000-Hour Laboratory Test Arrangement

The Start-Stop Exposure to Powerplant Conditions

The start-stop test cycle performed on samples of each coolant consisted of heating the fluid with an electrical immersion heater from room temperature to the powerplant operating temperature of 190.5°C (375°F) and then allowing the fluid to air cool to room temperature. The surface temperature of the heater was monitored to assure it did not exceed a maximum temperature of 315°C (600°F) during the heat-up cycle. According to the coolant manufacture, temperatures in excess of 315°C could cause fluid degradation; each coolant sample adequately abosrbed the heat energy so that the bulk remained well below the 315°C limit. Ten thermal cycles were accumulated on each of the coolants.

Several samples of SF-97-50 with varying exposure times (1500, 3000 and 8000 hours) were obtained from fuel cell stack test stands, and one (461 hours) SF-97-50 sample was obtained from an experimental powerplant for evaluation along with the lab samples. These fluid samples provided a cross check against the lab results.

4.4 Task 3.4 — "Definition of an Experimental Program to Assess Heat Exchanger Core Characteristics"

4.4.1 Introduction to Heat Exchanger Design for Fuel Cells in Integrated Utility System

Heat exchanger design requirements are established by the power system thermodynamic and system analysis. These requirements include fluid flows, temperatures and pressure drops. The requirements for fuel cell powerplants in integrated utility system were established in Task 3.2 (see Sections 2.2, 4.2, and Appendix A). Fluid properties are also required; these properties were defined for the silicone oils used as fuel cell coolants in Task 3.3 (see Sections 2.3 and 4.3). The heat exchanger design process involves selecting the heat exchanger configuration and dimensions which deliver the required performance at minimum cost.

The techniques used to evaluate the system performance level of a given heat exchanger configuration require the use of mathematical models and experimentally determined characteristics for the specific geometry considered. The experimentally determined characteristics for heat transfer is the "j" factor (Coburn Factor); it is expressed as follows:

$$j = \frac{h}{GC_p}\left(\frac{C_p \mu}{k}\right)^{2/3}$$

where:

h	= Unit Thermal Conductance	$\frac{\text{Calories}}{\text{HR cm}^2\,^\circ\text{C}}$	$\frac{\text{Btu}}{\text{HR Ft}^2\,^\circ\text{F}}$
G	= Mass Velocity	$\frac{\text{gm}}{\text{cm}^2\text{ - sec}}$	$\frac{\text{lb m}}{\text{FT}^2\text{-HR}}$
Cp	= Specific Heat	$\frac{\text{Calories}}{\text{gm }^\circ\text{C}}$	$\frac{\text{Btu}}{\text{lb m }^\circ\text{F}}$
μ	= Viscosity	$\frac{\text{gm}}{\text{cm - sec}}$	$\frac{\text{lb m}}{\text{FT - HR}}$
k	= Thermal Conductivity	$\frac{\text{Calories}}{\text{HR cm }^\circ\text{C}}$	$\frac{\text{Btu}}{\text{HR - FT - }^\circ\text{F}}$

The experimentally determined characteristic for pressure drop is the "f" factor (friction factor). It is expressed as follows:

$$f = \Delta P \left(\frac{D_H/^2 \, gp}{LG^2} \right)$$

where:

ΔP	= Pressure Drop	$\frac{dyne}{cm^2}$	, $\frac{lb\ f}{Ft^2}$
L	= Flow Length	cm	, Ft
D_H	= Hydraulic Diameter	cm	, Ft
g	= Gravity Constant	$\frac{cm}{Hr^2}$	, $\frac{Ft}{Hr^2}$
ρ	= Density	$\frac{gm}{cm^3}$	, $\frac{lb\ m}{Ft^3}$

The Coburn and friction factors are defined for a large number of core configurations as a function of Reynolds number in the literature. However, the choice of silicone oil as a candidate fuel cell coolant requires the use of heat exchangers with generous heat transfer characteristics. Heat exchangers for use with silicone oil also require a generous cross sectional area to minimize pressure drop since the fluids are relatively viscous. Studies to date indicate that compact surface-type heat exchangers offer potential system cost savings compared to more conventional round tube-type designs when considered for mass-produced fuel cell systems using silicone oil. The potential economic advantage of compact surface type heat exchangers over more conventional round tube-type designs is somewhat diminished when an alternate coolant, such as water, is considered in place of an oil. The characteristics of many of the compact cores which are suitable for use with silicone oils are not available in the literature. Therefore, it is often necessary when performing the selection of a heat exchanger for a specific fuel cell system application to also perform the basic testing of candidate heat transfer surfaces to determine the f and j factors. This testing has been conducted in the on going commercial fuel cell programs at United Aircraft.

Once the basic core configuration is established, heat exchanger materials must be selected to minimize corrosion in use. This presents no difficulty on the heat exchanger surfaces used with silicone oil because the oils are relatively inert and non-corrosive. However, the hot fuel cell exhaust streams which are fed to the various condensers in the 40 KW and 26 MW powerplants contain water vapor and in some cases, carbon dioxide. As a result, there is formation of a mild carbonic acid in fuel cell condensers which requires choosing corrosion resistant materials for the hot side of the condenser. The cold side of the condenser presents no difficulty in present fuel cell designs because air is used to cool the powerplant. However,

in integrated utility systm applications, condenser heat will be used to heat domestic hot water and impurities normally found in city water could introduce additional corrosion problems which must be considered in selecting heat exchanger core materials. This problem may also require treatment of the city water before it is used in the fuel cell powerplants.

Another factor to be considered in designing heat exchangers is the tendency of heat exchangers to foul in use. Fouling is the total of all surface heat transfer rate reductions caused by contamination carried by the fluids or by reactions between the fluids and the heat exchanger materials. As a result of fouling, the heat exchanger loses capacity during operation. Fouling in general can be minimized through proper selection of materials (to reduce fouling caused by corrosion), through proper selection of fluid velocities (to reduce accumulation of deposits) and through additions of filters or treatment systems to minimize deposits or change the fluid chemistry. Even with these steps, however, some fouling will take place. The impact of the remaining fouling on system performance must be eliminated through periodic cleaning of the heat exchanger and by proper sizing of the heat exchanger to allow for fouling. As in the case of materials selection, the fuel cell exhaust streams present unique fouling conditions and the fouling characteristics must be determined experimentally. In addition, specification of heat exchangers which discharge heat to the integrated utility system water or steam loops requires definition of design water quality levels and associated fouling characteristics for these streams.

4.4.2 Heat Exchanger Calibration Test Stands

The starting point for a heat exchanger, steam generator, or condenser design requires the accurate definition of the heat transfer coefficients and pressure drop characteristics of the selected core configuration.

The method used to obtain the required data is to test a small elemental heat exchanger core which is very carefully instrumented to obtain accurate data. The core is tested with steam as one fluid and air as the second fluid. The abundant heat available from condensing steam enables an isothermal temperature distribution to be obtained on one side of the core and confines any thermal resistance to the air side thereby allowing performance evaluation of the core geometry on that side. The test is repeated after reversing the fluid sides. A comparison of the heat lost by one fluid to the heat gained by the second fluid serves as a cross-check and adds confidence to the data. The test data is used to calculate the j (Coburn) factor and the f (friction) factor which can then be used to predict the performance of this core geometry on other fluids and other conditions of temperature and pressure.

A test stand at Power Utility used to obtain this type of data is shown in Figure 59. These stands have been utilized to develop the analytical procedures used in the present fuel cell programs and will be utilized for any future integrated utility system effort. This data obtained from tests on this stand yields an overall heat balance within 7 percent indicating that the instrumentation is sufficiently accurate for obtaining heat exchanger data. To further validate this stand, Coburn factor and friction factor were determined for a simple

bare round tube core presently described in the literature. The Coburn factor established in these tests is within 4 percent of that reported in the literature and the friction factor is within 20 percent of that reported in the literature. Data obtained using this stand have been used successfully to predict the performance of fuel cell powerplant steam generators, condensers and single-phase heat exchangers.

4.4.3 Experimental Program

An experimental program to define heat exchanger characteristics unique to fuel cells has been defined. The program assumes the use of the stand described above. A description of the experimental program is presented in Section 2.4.

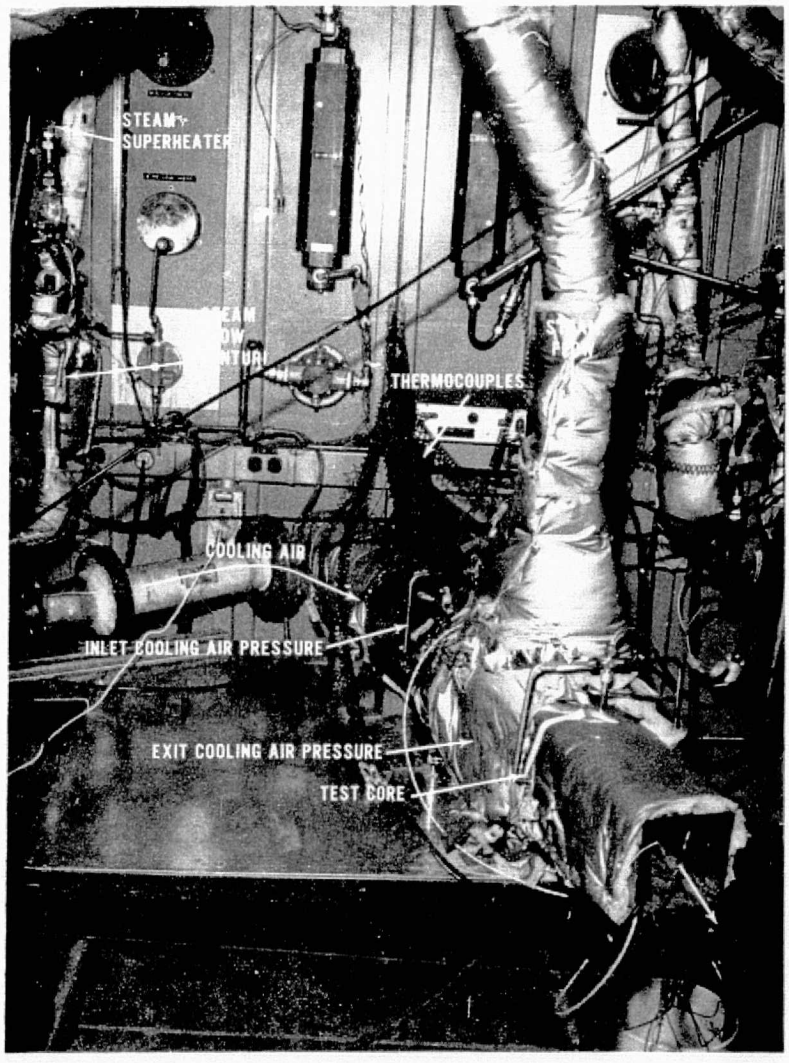

Figure 59 – Heat Exchanger Test Stand

APPENDIX A

COMPONENT DESIGN REQUIREMENTS

APPENDIX (CDR'S)

Component design requirements contained in this appendix are for the 40 KW powerplant at 35 and 40 percent electric generation efficiency and for the 26 MW powerplant. Figures CDR-1 through CDR-4 describe the 40 KW, 35 percent efficient powerplant. Figures CDR-5 through CDR-8 are the requirements for the 40 KW, 40 percent efficient powerplant. The remaining Figures, CDR-9 through CDR-18 describe the heat exchanger requirements for the 26 MW powerplant in heat recovery configurations 1 and 2.

Design Requirement

Component: Steam Generator
(Heat Recovery Configuration #1 and #2)

Powerplant: 40 KW Baseline
(35% Electric Generation Efficiency)

Function

Generate 10.3×10^4 n/m^2 (15 PSIG) steam from heat supplied by powersection coolant

Heat Transferred

28,425.6 $\frac{\text{Kilocalories}}{\text{HR}}$ (112,800 Btu/hr)

Flow Conditions

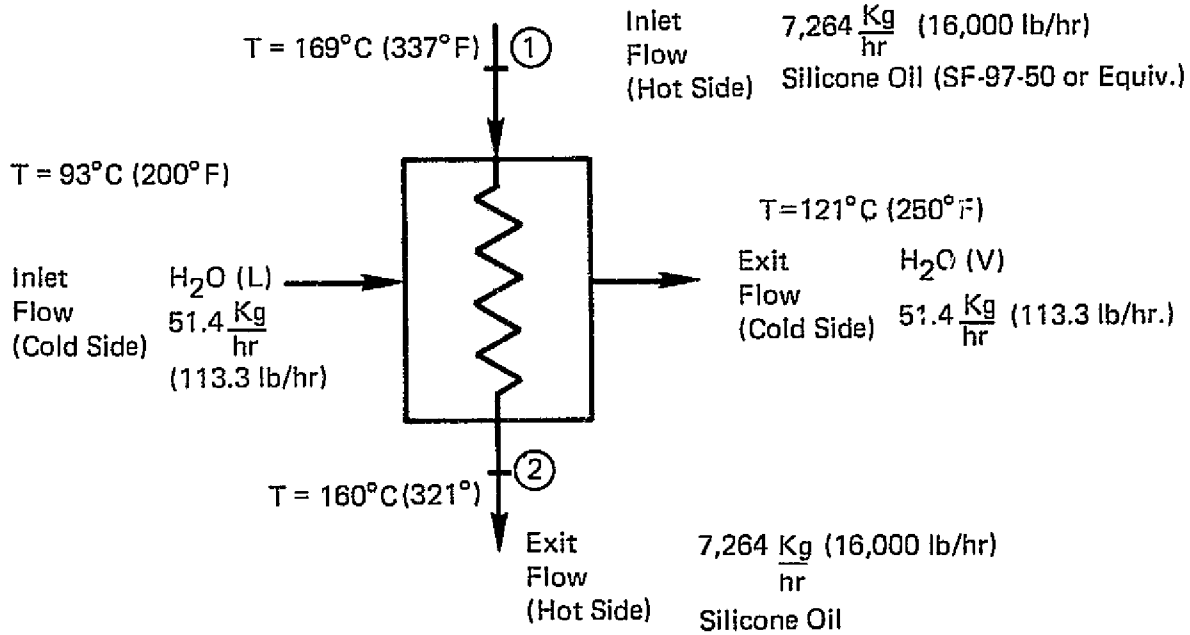

Pressure Drop

$\Delta P(1)-(2) = 6.895 \times 10^3$ n/m^2 (1psi)

Figure CDR-1 — Design Requirement 40 KW Baseline Steam Generator (Configuration 1 and 2)

Design Requirement

Component: Condenser
(Heat Recovery Configuration #1)

Powerplant: 40 KW Baseline
(35% Electric Generation Efficiency)

Function

Generate 71°C (160°F) Hot water (24°C (75°F) return temp.)

Desuperheat and condense H_2O from powerplant exhaust stream to 52°C (126°F) dewpoint

Provide for separation of condensed H_2O from the hot side exit stream

Heat Transfer

25,704 $\frac{\text{Kilocalories}}{\text{HR}}$ (102,000 Btu/hr)

Flow Conditions

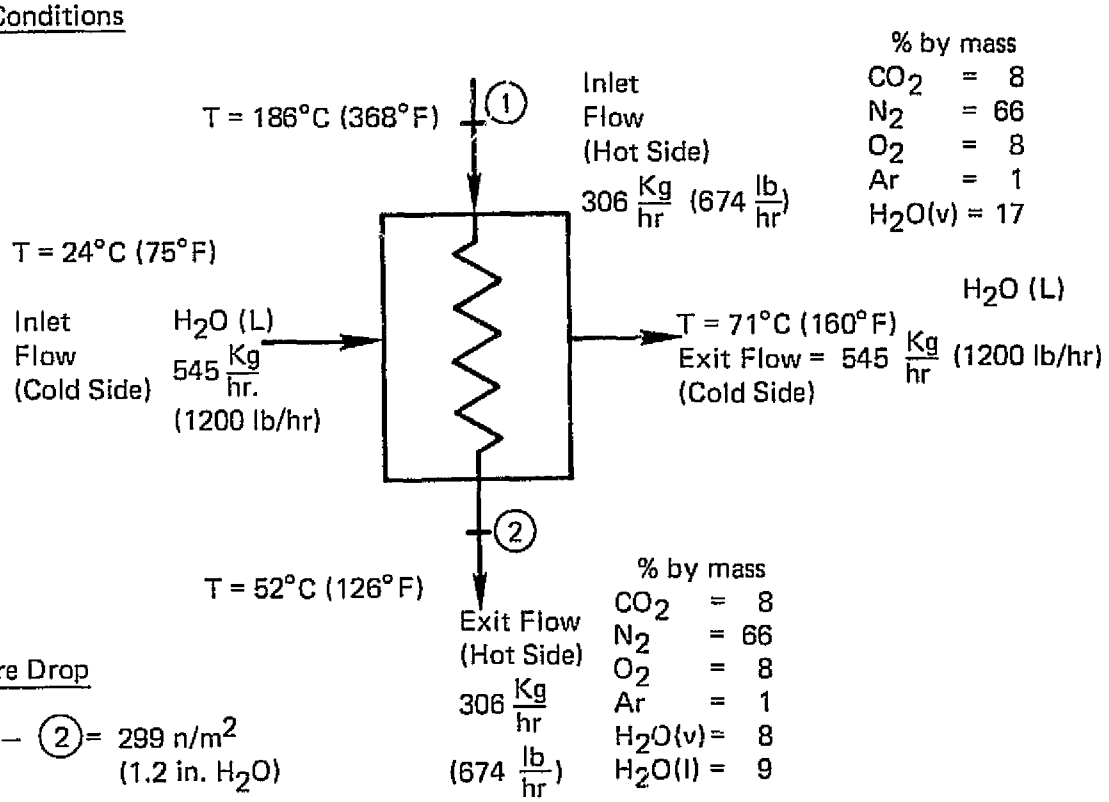

Pressure Drop

ΔP (1) – (2) = 299 n/m^2
(1.2 in. H_2O)

CDR-2 — Design Requirement 40 KW Baseline
Condenser (Configuration 1)

Design Requirement

Component: Exhaust Steam Generator
(Heat Recovery Configuration #2)

Powerplant: 40 KW Baseline
(35% Electric Generation Efficiency)

Function

Generate 10.3×10^4 n/m^2 (15 PSIG) steam from heat supplied by powerplant exhaust stream

Heat Transfer

4,334 $\frac{\text{Kilocalories}}{\text{HR}}$ (17,200 Btu/hr)

Flow Conditions

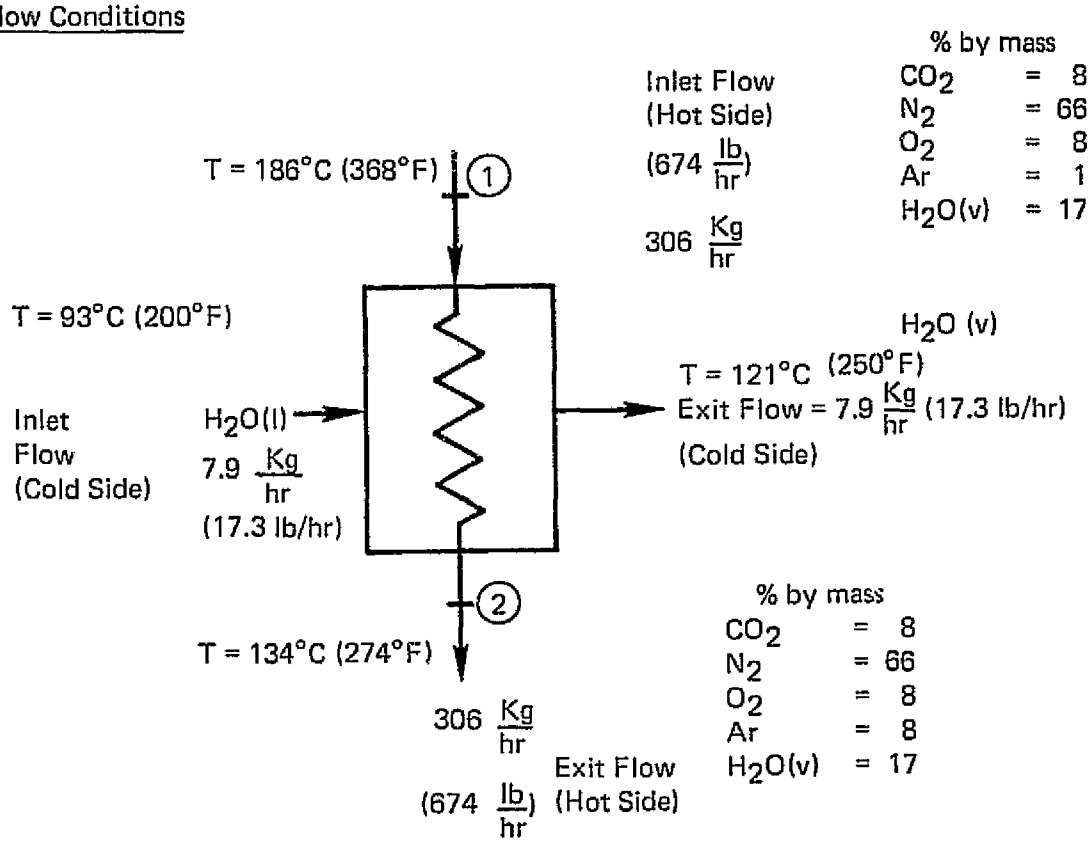

Pressure Drop

ΔP (1) – (2) = 149 $\frac{n}{m2}$ (0.6 in H_2O)

CDR-3 – Design Requirement 40 KW Baseline Exhaust Steam Generator (Configuration 2)

Design Requirement

Component: Condenser
(Heat Recovery Configuration #2)

Powerplant: 40 KW Baseline
(35% Electric Generation Efficiency)

Function

Generate 71°C (160°F) hot water (24°C (75°F) return temp.)

Desuperheat and condense H_2O from powerplant exhaust stream to 52°C (126°F) dew point

Provide for separation of condensed H_2O from hot side exit stream

Heat Transfer

21,370 $\frac{\text{Kilocalories}}{\text{HR}}$ (84,800 Btu/hr)

Flow Conditions

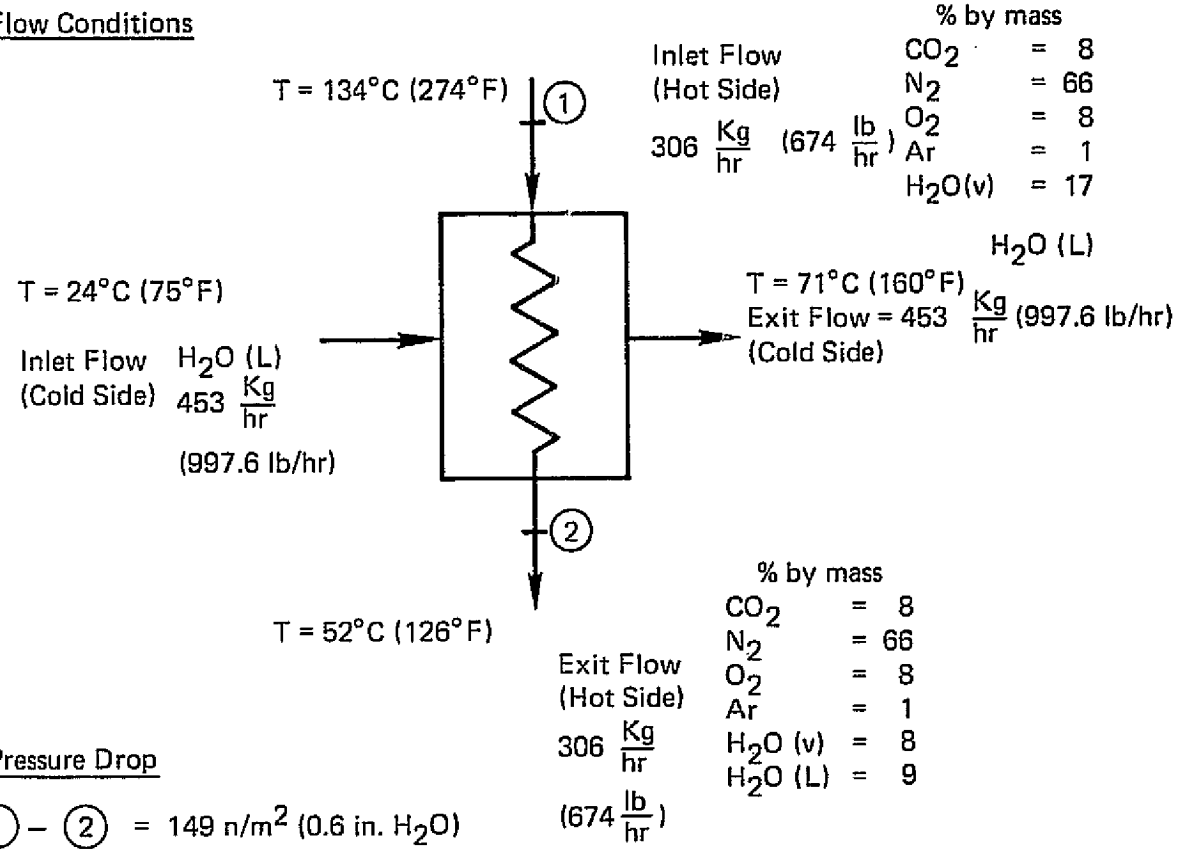

Pressure Drop

① – ② = 149 n/m^2 (0.6 in. H_2O)

CDR-4 – Design Requirement 40 KW Baseline Condenser (Configuration 2)

Design Requirement

Component: Steam Generator
(Heat Recovery Configuration #1 and #2)

Powerplant: 40 KW Baseline
(40% Electric Generation Efficiency)

Function

Generate 10.3×10^4 n/m^2 (15 PSIG) steam from heat supplied by power section coolant

Heat Transfer

19,399 $\frac{\text{Kilocalories}}{\text{HR}}$ (76,980 Btu/hr)

Flow Conditions

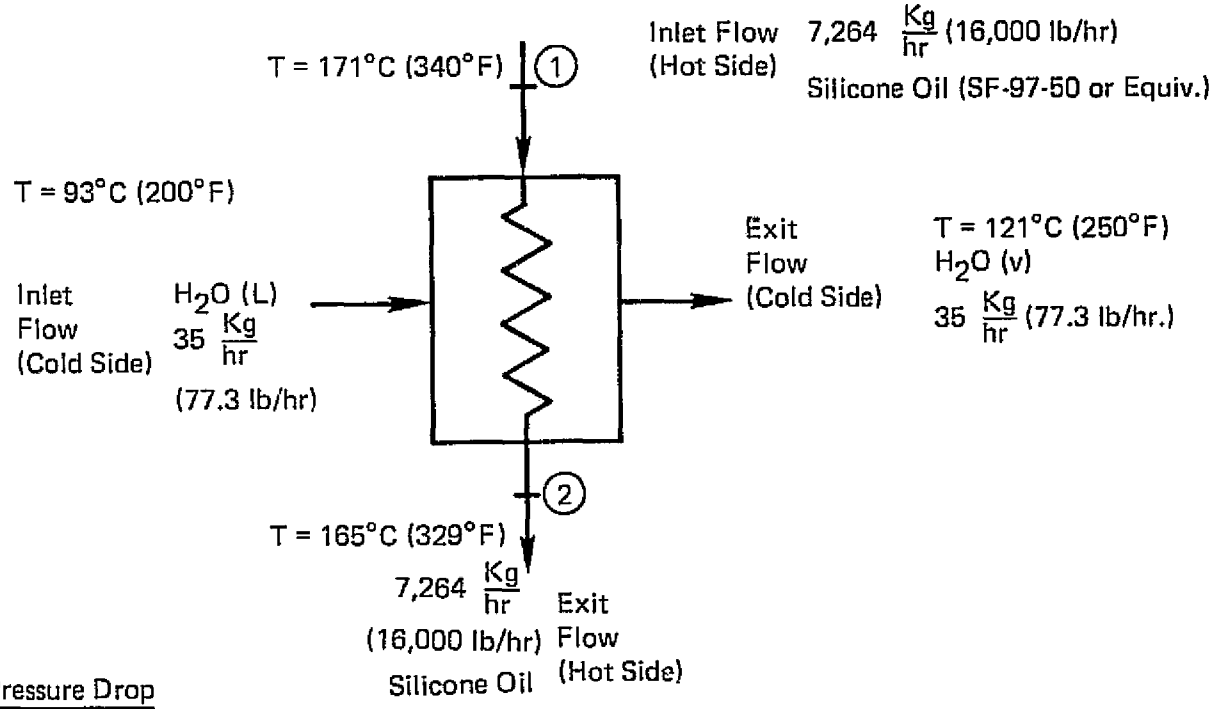

Pressure Drop

ΔP (1) – (2) = 6.895×10^3 n/m^2 (1 psi)

CDR-5 – Design Requirement 40 KW Baseline Steam Generator (Configuration 1 and 2)

Design Requirement

Component: Condenser
(Heat Recovery Configuration #1)

Powerplant: 40 KW Baseline
(40% Electric Generation Efficiency)

Function

Generate 71°C (160°F) hot water (24°C (75°F) return temp.)

Desuperheat and condense H_2O from powerplant exhaust stream to 47°C (117°F) dewpoint

Provide for separation of condensed H_2O from the hot side exit stream

Heat Transfer

23,151 $\frac{\text{Kilocalories}}{\text{Hr}}$ (91,870 Btu/hr)

Flow Conditions

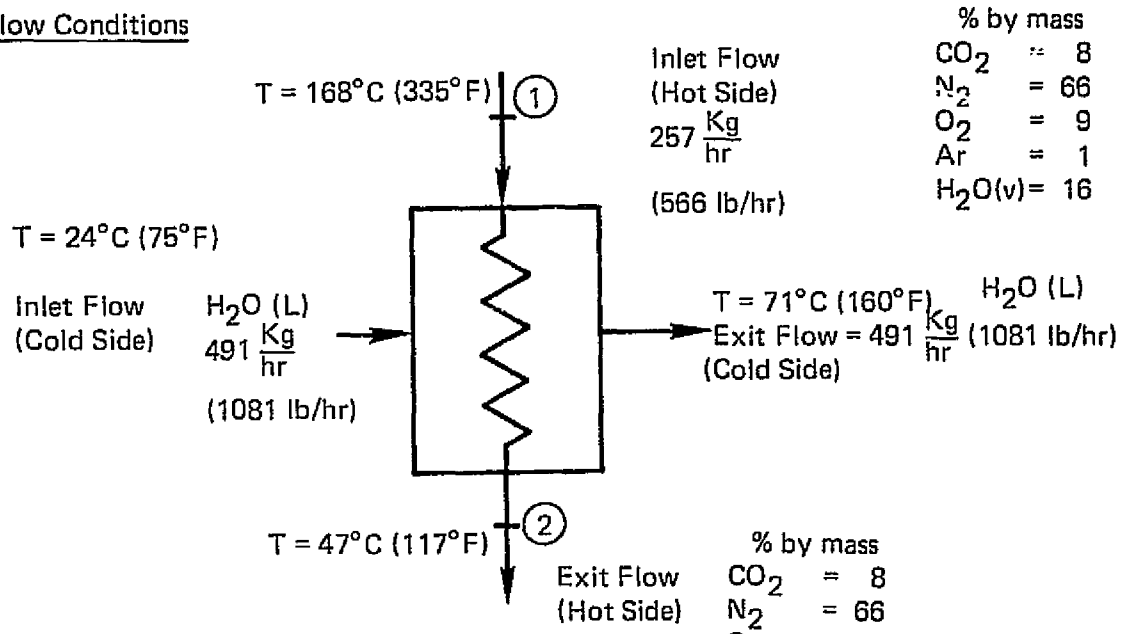

Pressure Drop

ΔP (1) – (2) = 299 n/m^2
(1.2 in. H_2O)

CDR-6 — Design Requirement 40 KW Baseline Condenser (Configuration 1)

Design Requirement

Component: Exhaust Steam Generator
(Heat Recovery Configuration #2)

Powerplant: 40 KW Baseline
(40% Electric Generation Efficiency)

Function

Generate 10.3×10^4 n/m^2 (15 PSIG) steam from heat supplied by powerplant exhaust stream

Heat Transfer

2,621 $\frac{\text{Kilocalories}}{\text{HR}}$ (10,400 Btu/hr)

Flow Conditions

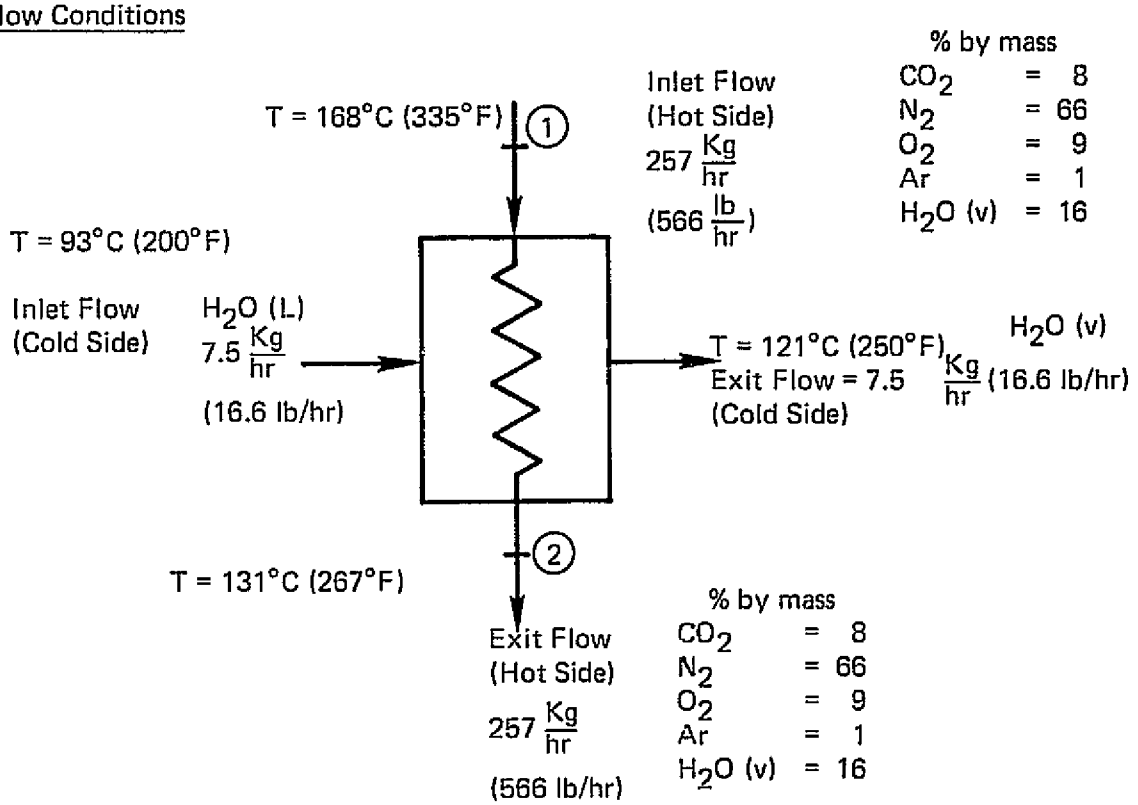

Pressure Drop

ΔP (1) – (2) = 149 n/m^2 (0.6 in H_2O)

CDR-7 – Design Requirement 40 KW Baseline Exhaust Steam Generator (Configuration 2)

Design Requirement

Component: Condenser
(Heat Recovery Configuration #2)

Powerplant: 40 KW Baseline
(40% Electric Generation Efficiency)

Function

Generate 71°C (160°F) hot water (24°C (75°F) return temp.)

Desuperheat and condense H_2O from powerplant exhaust stream to 47°C (117°F) dewpoint

Provide for separation of condensed H_2O from hot side exit stream

Heat Transfer

20,529 $\frac{\text{Kilocalories}}{\text{HR}}$ (81,465 BTU/HR)

Flow Conditions

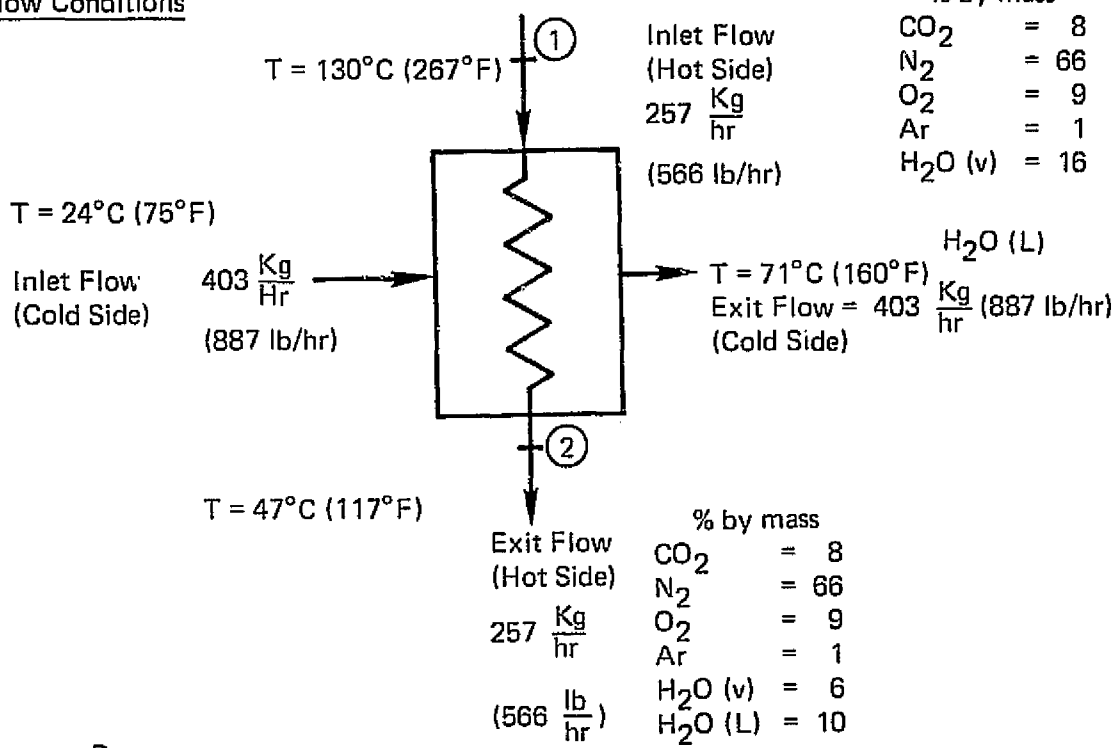

Pressure Drop

(1) – (2) = 149 n/m^2 (0.6 in. H_2O)

CDR-8 – Design Requirement 40 KW Baseline Condenser (Configuration 2)

Design Requirement

Component: Steam Generator
(Heat recovery configuration #1 and #2)

Powerplant: 4.33 MW module for 26 MW powerplant
(39% Electric Generation Efficiency)

Function

Generate 10.3×10^4 n/m^2 (15 PSIG) steam flow from heat supplied by power section coolant

Heat Transfer

$2.4 \times 10^6 \frac{\text{Kilocalories}}{\text{HR}}$ (9.53×10^6 Btu/hr)

Flow Conditions

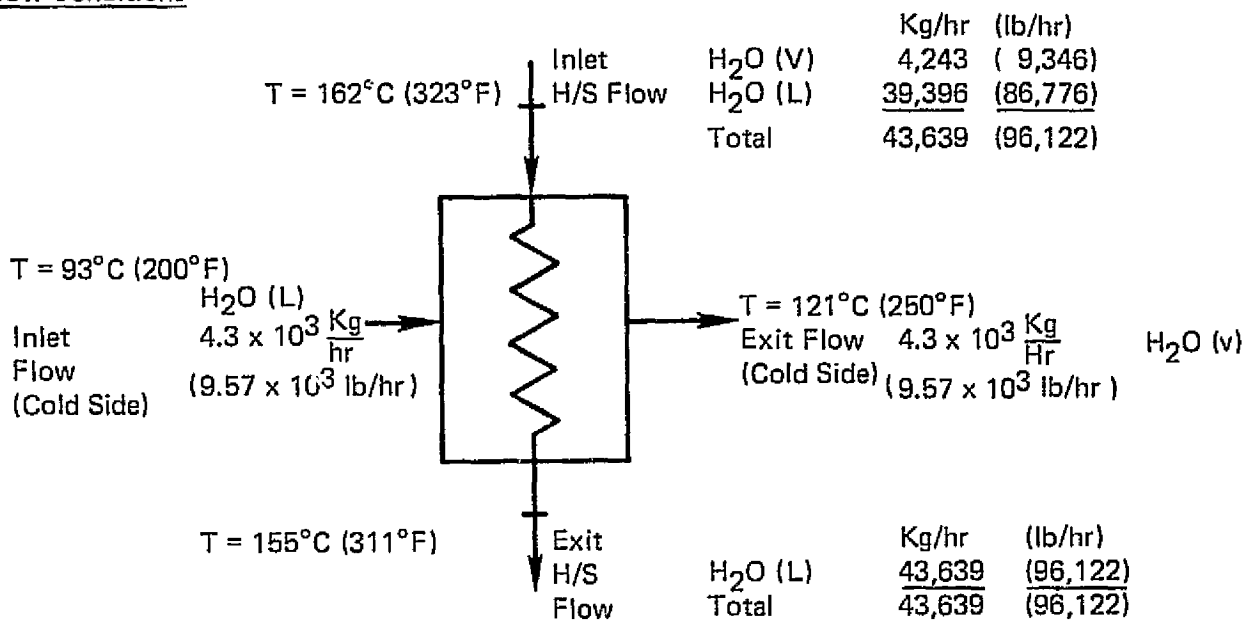

		Kg/hr	(lb/hr)
Inlet H/S Flow	H_2O (V)	4,243	(9,346)
	H_2O (L)	39,396	(86,776)
	Total	43,639	(96,122)

		Kg/hr	(lb/hr)
Exit H/S Flow	H_2O (L)	43,639	(96,122)
	Total	43,639	(96,122)

CDR-9 — Design Requirement 26 MW Steam Generator (Configuration 1 and 2)

Design Requirement

Component: Cathode Condenser
(Heat recovery configuration #1)

Powerplant: 4.33 MW module for 26 MW powerplant
(39% Electric Generation Efficiency)

Function

Generate 71°C (160°F) hot water

Desuperheat and condense H_2O from cathode exhaust to 58°C (137°F) dewpoint

Provide for separation of condensed water

Heat Transfer

$1.88 \times 10^6 \frac{\text{Kilocalories}}{\text{HR}}$ (7.47×10^6 Btu/hr)

Flow Conditions

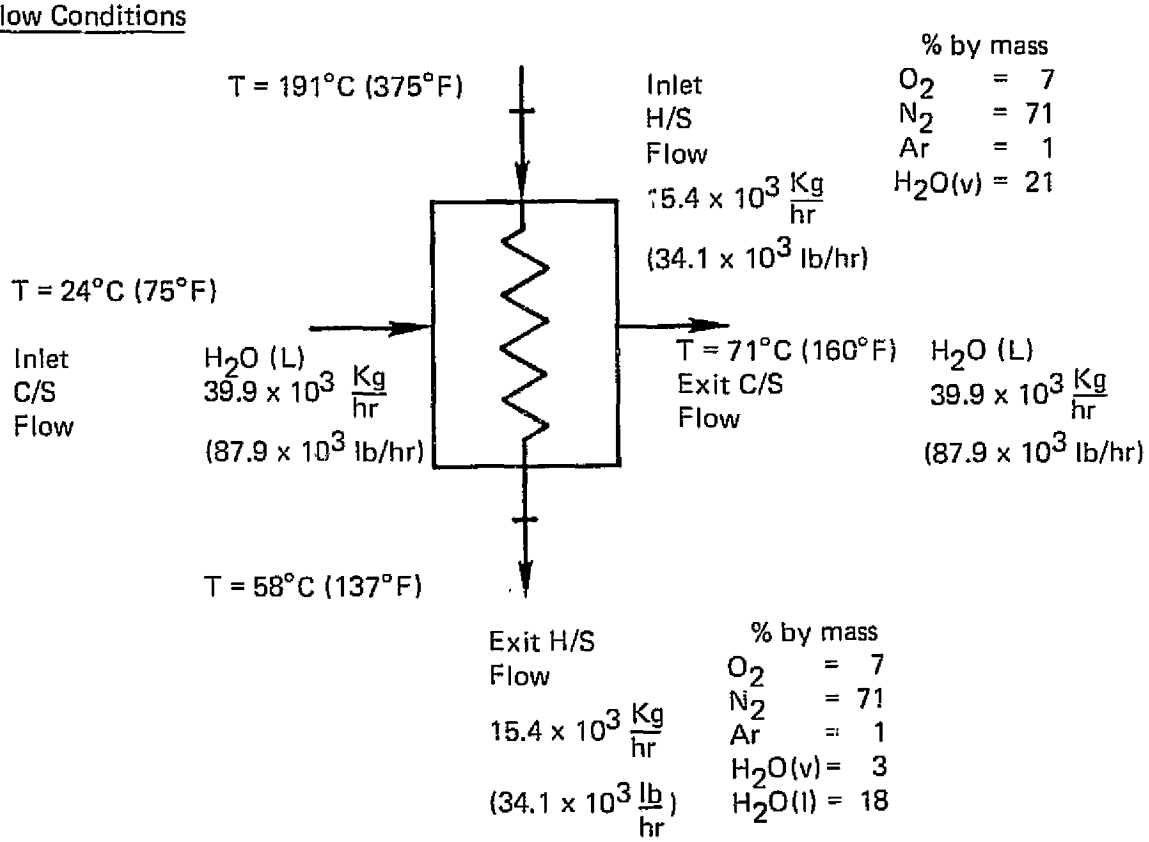

CDR-10 — Design Requirement 26 MW Cathode Condenser (Configuration 1)

Design Requirement

Component: Anode Condenser
(Heat recovery configuration #1)

Powerplant: 4.33 MW module for 26 MW powerplant
(39% Electric Generation Efficiency)

Function

Generate 71°C (160°F) hot water

Desuperheat and condense H_2O from anode exhaust to 58°C (137°F) dewpoint

Provide for separation of condensed water

Heat Transfer

$0.43 \times 10^6 \frac{\text{Kilocalories}}{\text{HR}}$ $(1.74 \times 10^6$ Btu/hr)

Flow Conditions

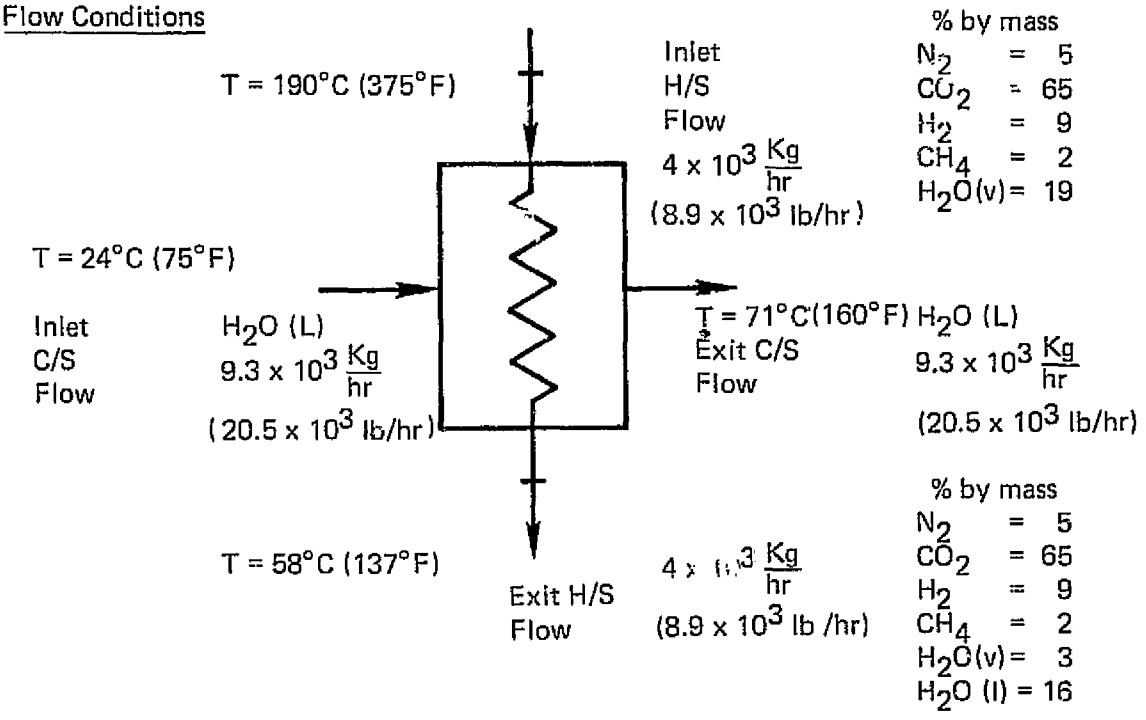

CDR-11 -- Design Requirement 26 MW Anode Condenser (Configuration 1)

Design Requirement

Component: Exhaust Condenser
(Heat recovery configuration #1)

Powerplant: 4.33 MW module for 26 MW powerplant
(39% Electric Generation Efficiency)

Function

Generate 71°C (160°F) hot water

Desuperheat and condense H_2O from exhaust to 52°C (126°F) dewpoint

Provide for separation of condensed water

Heat Transfer

$0.97 \times 10^6 \frac{\text{Kilocalories}}{\text{HR}}$ (3.85×10^6 Btu/hr)

Flow Conditions

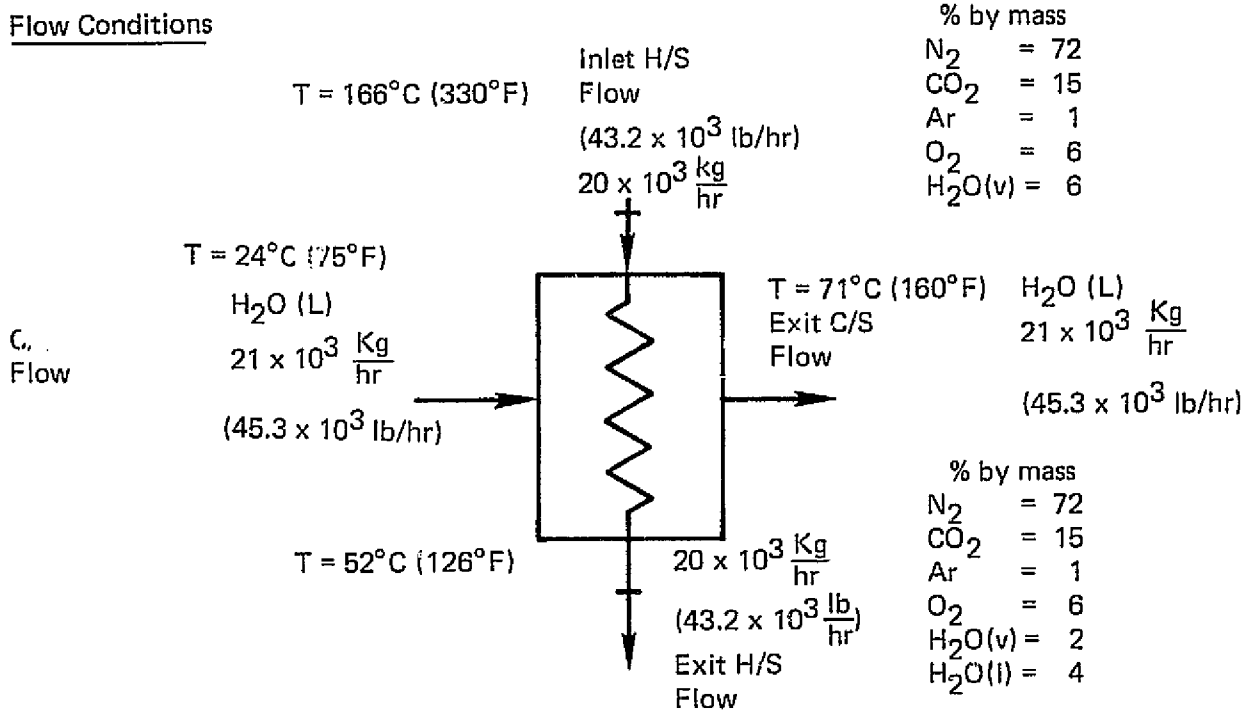

CDR-12 — Design Requirement 26 MW Exhaust Condenser (Configuration 1)

Design Requirement

Component: Cathode Steam Generator
(Heat recovery configuration #2)

Powerplant: 4.33 MW module for 26 MW powerplant
(39% Electric Generation Efficiency)

Function

Generate 10.3×10^4 n/m^2 (15 PSIG) steam flow

Heat Transfer

$0.2468 \times 10^6 \frac{\text{Kilocalories}}{\text{Hr}}$ (0.9797×10^6 Btu/hr)

Flow Conditions

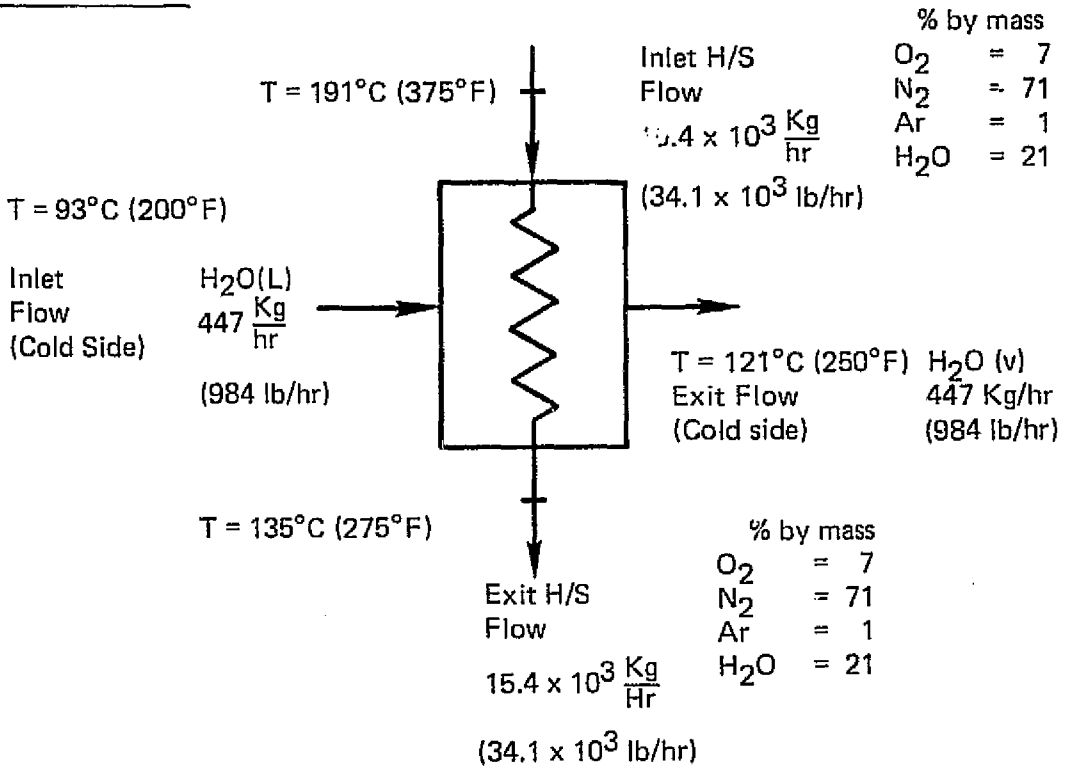

CDR-13 — Design Requirement 26 MW Cathode Steam Generator (Configuration 2)

Design Requirement

Component: Cathode Condenser
(Heat recovery configuration #2)

Powerplant: 4.33 MW module for 26 MW powerplant
(39% Electric Generation Efficiency)

Function

Generate 71°C (160°F) hot water

Desuperheat and condense H_2O from cathode exhaust to 58°C (137°F) dewpoint

Provide for separation of condensed water

Heat Transfer

$1.635 \times 10^6 \frac{\text{Kilocalories}}{\text{HR}}$ (6.491×10^6 Btu/hr)

Flow Conditions

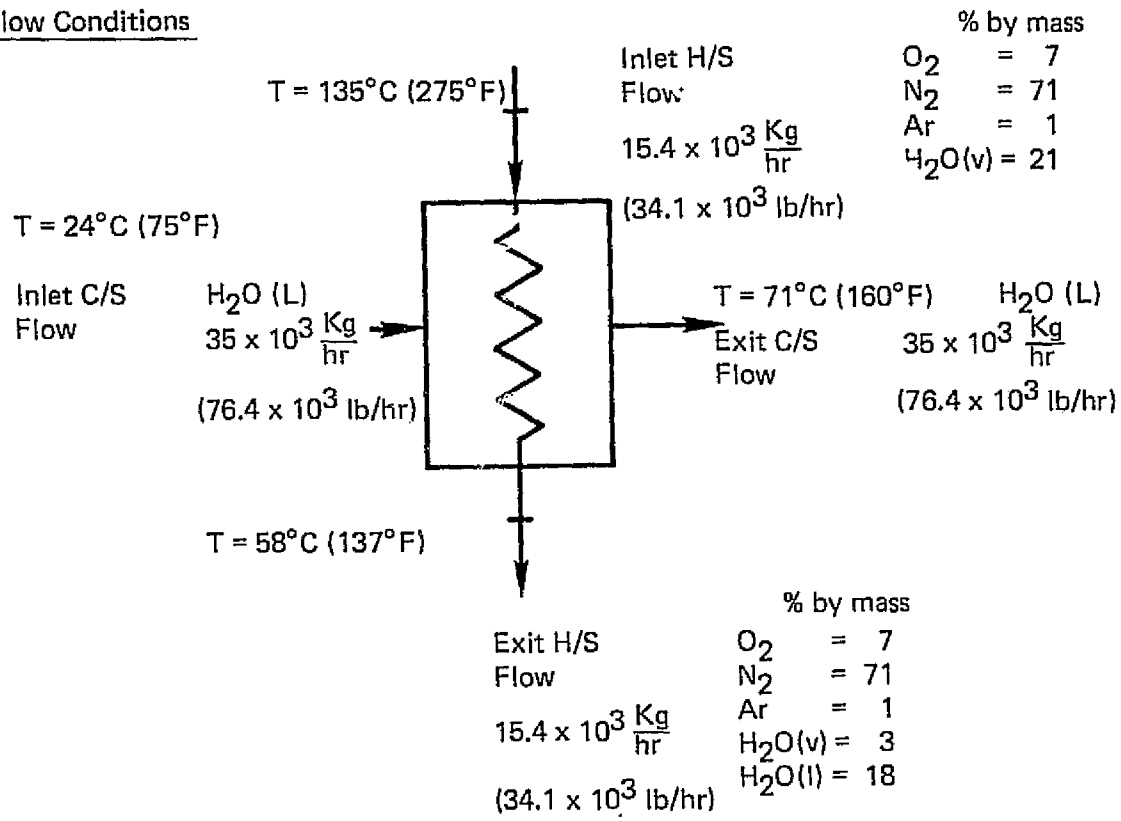

CDR-14 — Design Requirement 26 MW Cathode Condenser (Configuration 2)

Design Requirement

Component: Anode Steam Generator
(Heat recovery configuration #2)

Powerplant: 4.33 MW module for 26 MW powerplant
(39% Electric Generation Efficiency)

Function

Generate 10.3×10^4 n/m^2 (15 PSIG) steam flow

Heat Transfer

$0.121 \times 10^6 \frac{\text{Kilocalories}}{\text{HR}}$ (0.481×10^6 Btu/hr)

Flow Conditions

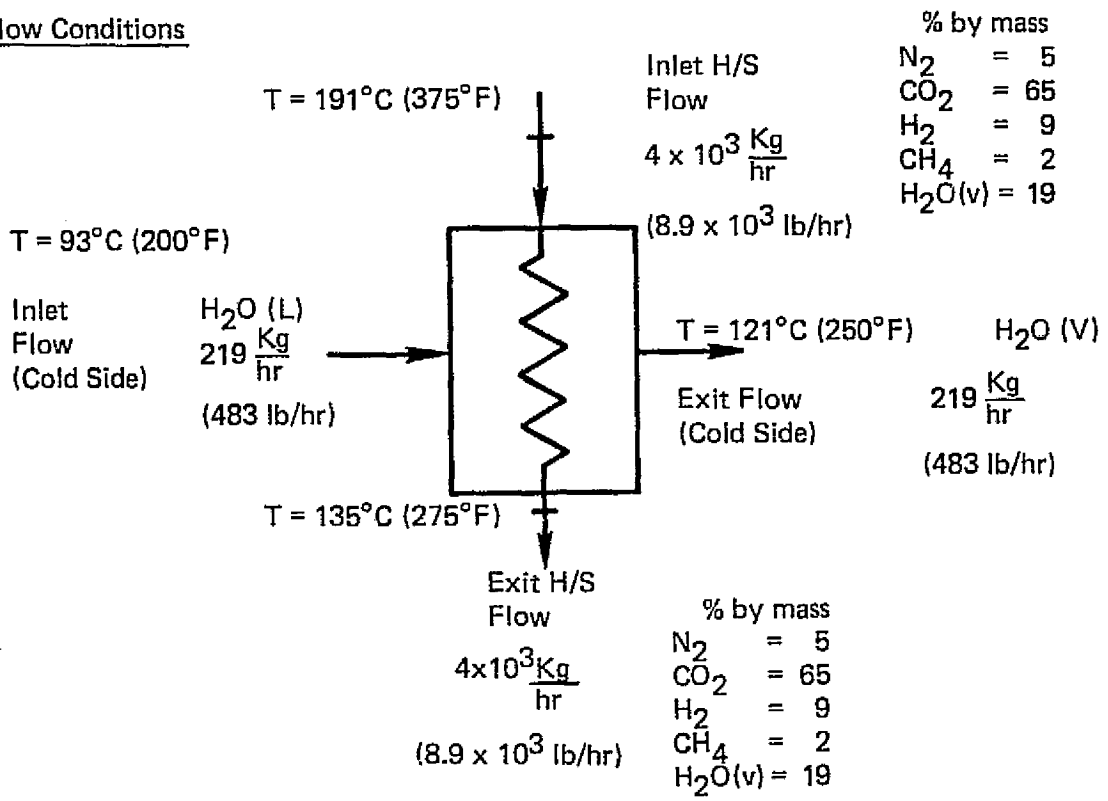

CDR-15 — Design Requirement 26 MW Anode Steam Generator (Configuration 2)

Design Requirement

Component: Anode Condenser
(Heat recovery configuration #2)

Powerplant: 4.33 MW module for 26 MW powerplant
(39% Electric Generation Efficiency)

Function

Generate 71°C (160°F) hot water

Desuperheat and condense H_2O from anode exhaust to 58°C (137°F) dewpoint

Provide for separation of condensed water

Heat Transfer

$0.303 \times 10^6 \frac{\text{Kilocalories}}{\text{HR}}$ (1.202×10^6 Btu/hr)

Flow Conditions

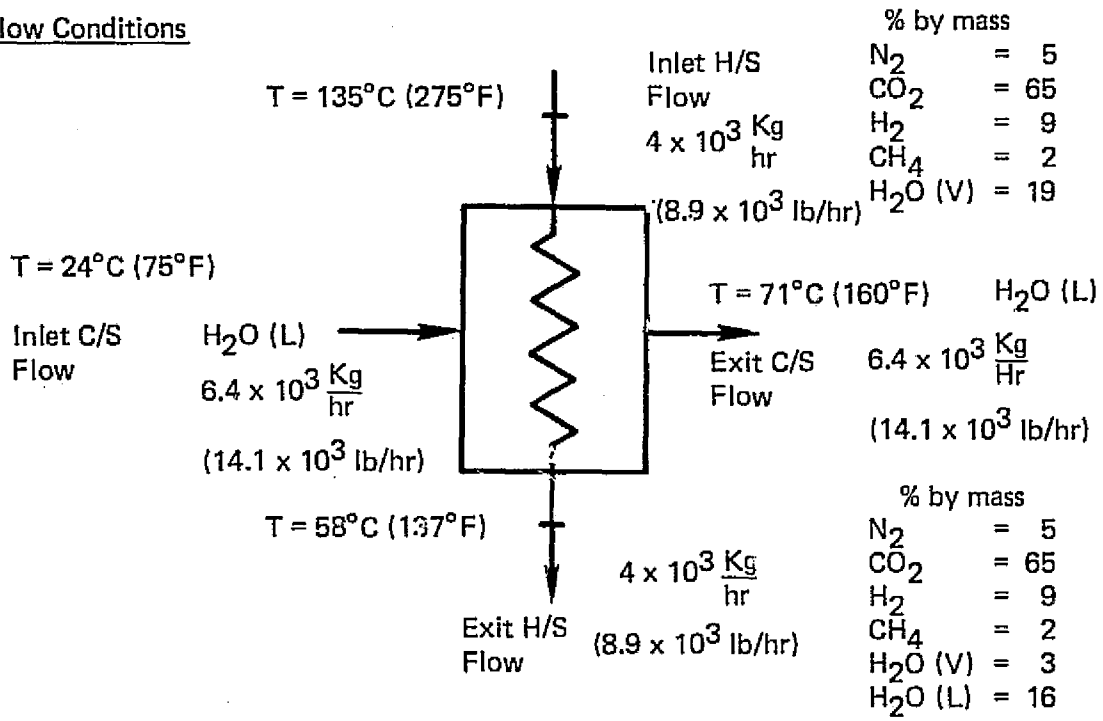

CDR-16 — Design Requirement 26 MW Anode Condenser (Configuration 2)

Design Requirement

Component: Exhaust Steam Generator
(Heat Recovery Configuration #2)

Powerplant: 4.33 MW module for 26 MW powerplant
(39% Electric Generation Efficiency)

Function

Generate 10.3×10^4 n/m^2 (15 PSIG) steam flow

Heat Transfer

$0.017 \times 10^6 \frac{\text{Kilocalories}}{\text{HR}}$ (0.069×10^6 Btu/hr)

Flow Conditions

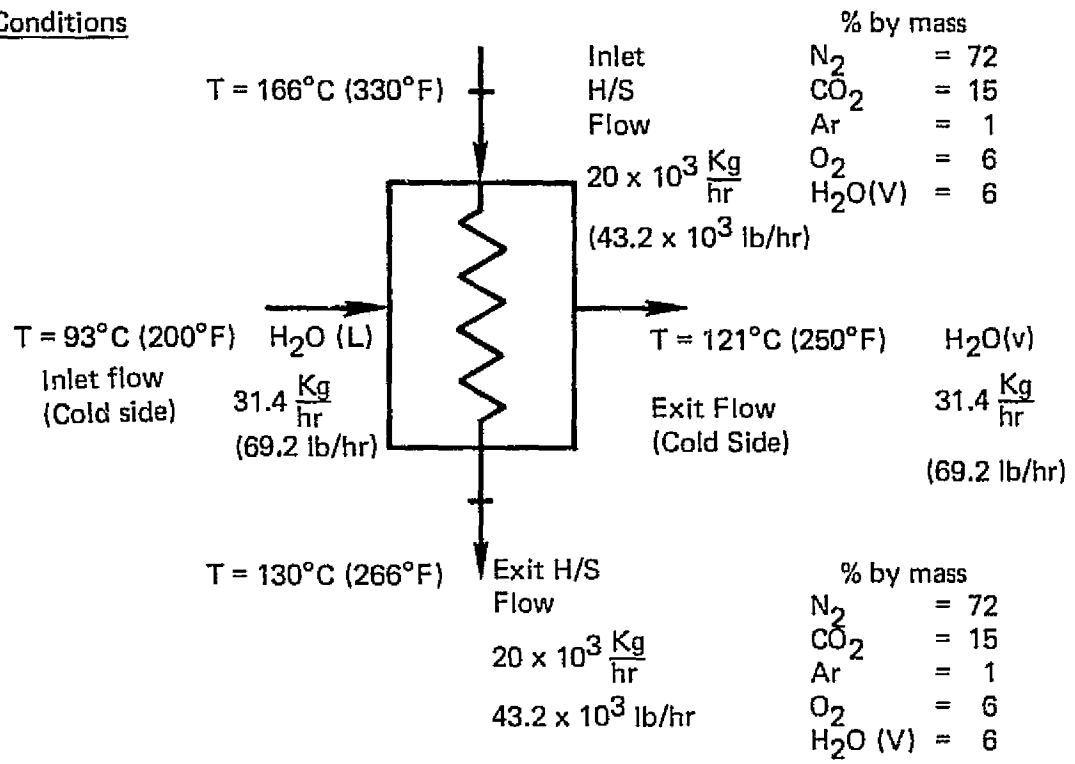

CDR-17 — Design Requirement 26 MW Exhaust Steam Generator (Configuration 2)

Design Requirement

Component: Exhaust Condenser
(Heat recovery configuration #2)

Powerplant: 4.33 MW module for 26 MW powerplant
(39% Electric Generation Efficiency)

Function

Generate 71°C (160°F) hot water

Desuperheat and condense H_2O from exhaust to 52°C (126°F) dewpoint

Provide for separation of condensed water

Heat Transfer

0.95×10^6 Kilocalories/Hr (3.78×10^6 Btu/hr)

Flow Conditions

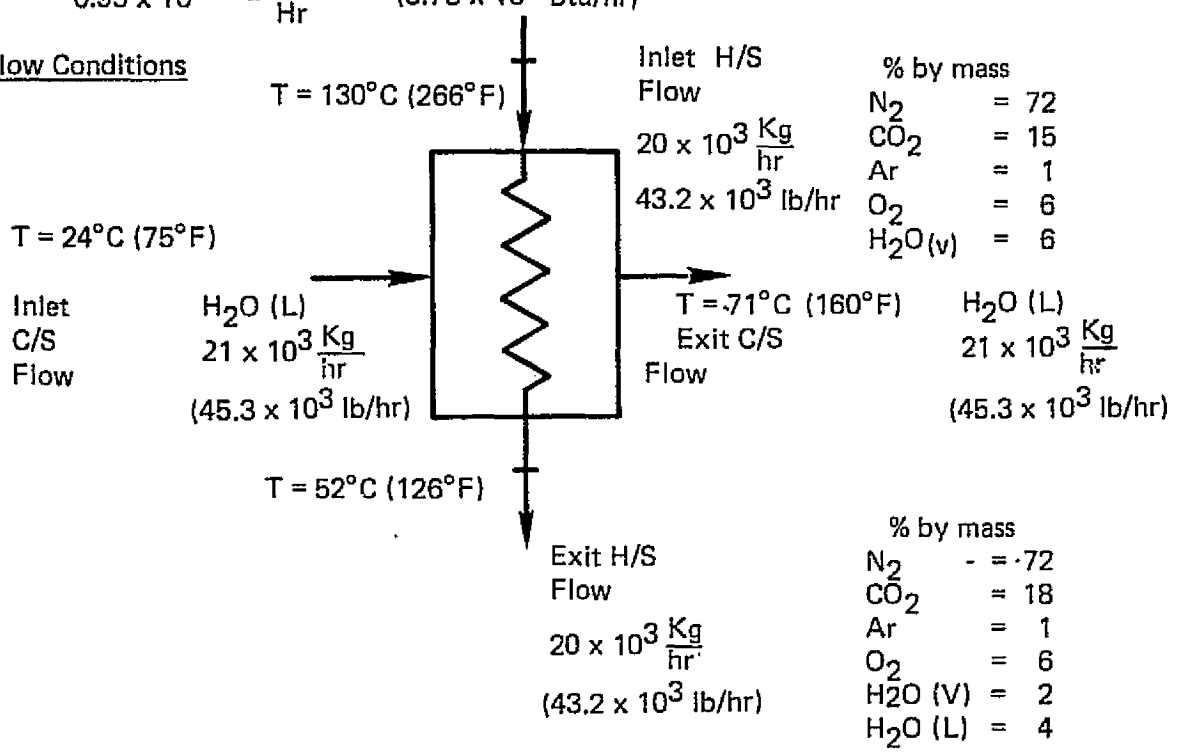

CDR-18 — Design Requirement 26 MW Exhaust Condenser (Configuration 2)

APPENDIX B

THERMAL CONDUCTIVITY MEASUREMENTS OF SILICONE FLUIDS WITH A THERMAL COMPARATOR

M. B. Murray
Wear Sciences, Inc.

THERMAL CONDUCTIVITY MEASUREMENTS OF SILICONE FLUIDS WITH A THERMAL COMPARATOR

M.B. Murray
Wear Sciences, Inc.

Prepared for: Pratt and Whitney Aircraft
SWES Engineering
South Windsor, Connecticut 06074

Summary

Thermal conductivity measurements have been made, as a function of temperature, on nine new and used silicone fluid samples. These measurements were made by the thermal comparator method and cover the temperature range from 70 to 350F.

The following fluids were evaluated:

1. SF-97 (50) New
2. SF-97 (50) After ten cycle test
3. SF-97 (50) 2000 hour endurance
4. SF-1093-50 New
5. SF-1093 After ten cycle test
6. SF-1093 2000 hour endurance
7. X-708(38655) 8000 hour test
8. X-707(38596) 3000 hour test
9. X-586

Test Equipment

The thermal comparator method used in this work was developed by Powell (Ref.1). This method is based on the fact that when two materials of different thermal conductivities, such as aluminum and plastic, are touched, the material with the higher thermal conductivity (in this case, the aluminum) will feel colder to the touch. This is simply because the aluminum conducts heat away at a faster rate. The thermal comparator is a means of quantitatively measuring this effect. This technique has three major advantages over other means of measuring thermal conductivity. First, it is simple to use and does not require an elaborate setup. Secondly, the method is rapid and a num-

---

Ref.1. Thermal Conductivity. Edited by R.P. Tye, Academic Press, New York 1969. Ch. 6: Thermal Conductivity Determinations by Thermal Comparator Methods, By R.W. Powell

ber of points can be measured in a short period of time. Finally, since it is a relative measurement, there is much less risk that an error in procedure or measurement will negate the value of the results.

A specially constructed Thermal Comparator probe was purchased from Technometrics, Inc. for this work. Figure 1 shows a schematic of the construction of this probe. A thermocouple, mounted within 0.001" of the sensing tip of the probe, is differentially connected to a copper thermal reservoir which is held at temperature T_o by means of a Nichrome wire heater mounted in the copper block. Upon contact of the probe tip, of thermal conductivity K_1 with the surface of a test material having a thermal conductivity K_2, the tip of the probe quickly drops to an intermediate temperature T, resulting in a temperature differential signal given by the expression $(T_o-T)=T_o\left[K_2/(K_1+K_2)\right]$. In the tests conducted by Wear Sciences this temperature differential signal was recorded on a Leeds and Northrup Speedomax XL recorder which was set up to measure signals in the microvolt range.

A photograph of the test setup is shown in Figure 2. Figure 3 is a schematic of the test equipment.

In this test the Thermal Comparator probe was mounted on one end of an aluminum arm which was held in a ball bearing mount so that the arm was free to pivot in the vertical plane. An adjustable counterweight, mounted on the other end of the aluminum arm beyond the fulcrum point, was used to counterbalance the weight of the probe. This counterbalance feature was necessary since experience has shown that the load of the probe tip against the specimen must be small and consistent to obtain reproducible data. A uniform probe loading of 5 grams was used throughout these tests.

In order to measure the thermal conductivity of a fluid with this equipment, it has been found that a thin membrane cover must be used so that the probe will not be in direct contact with the fluid. Otherwise, the area of contact between the probe tip and the fluid would be too large, and would vary with the surface tension of the fluid. Evaporative cooling effects from an open fluid surface would also be an unknown factor that would influence the results. Powell showed that

a thin film of plastic, stretched tautly over the fluid, would be an effective barrier as long as the plastic film was inert to the fluid. He used a proprietary material, Melinex, 0.00025" thick and found that this thin film had little effect on the readings obtained with both solid and liquid samples. In the Wear Sciences tests, a polyimide film, Kapton, was used because this plastic could withstand much higher temperatures. The Kapton film was 0.0005" thick.

The Kapton film was mounted in an embroidery hoop, and then stretched to form a smooth surface. The fluid sample was placed in a shallow evaporating dish about 0.5" deep x 5" in diameter. Powell found this size dish to be the optimum for achieving uniform heating and for minimizing the effects of thermal convective currents. The dish was filled to the brim so that the meniscus of the fluid was raised above the level of the top of the dish. Then the plastic film, stretched tautly over the embroidery hoop, was placed over the fluid surface, being careful to be sure that no air bubbles were trapped under the film. Finally, a concentric steel ring was placed on the edge of the embroidery hoop to weigh this assembly down. In this way, the plastic film would remain tightly stretched over the surface, even when the fluid was heated. Since this technique requires that the probe tip be hotter than the fluid surface, a temperature differential of about 70F between the probe and the fluid was maintained throughout these tests. The temperature of the probe was controlled with a variable power supply. The dish containing the test fluid was heated on a stepless control hot plate. The temperature of the test fluid was measured with a bare chromel-constatan thermocouple which penetrated through the side of the glass evaporating dish and extended into the center of the dish, just below the point where the probe came into contact with the plastic film. This thermocouple was sealed into the dish to prevent fluid leakage.

Test Procedure

Instead of trying to maintain the temperature differential between the probe and the fluid at exactly 70F, the actual temperatures of the probe and the fluid were measured with a thermocouple potentiometer just before each test. The microvolt readings, measured with the Leeds and Northrup recorder,

were divided by the actual temperature differential to convert these readings to microvolts /°F and then the readings were corrected to a 70°F temperature differential. Actually, small errors in the temperature measurements would have very little effect on the final results.

Each test was run using the following procedure:

1. The probe and the test fluid were heated slowly to the desired temperature levels and temperature differential.

2. Just before each test, the actual probe and fluid temperatures were measured and recorded. The recorder chart was started and the zero was set.

3. The probe arm was released and allowed to drop down in contact with the plastic film which covered the fluid surface. (A dashpot controlled the drop rate and contact between the probe and the film so as to prevent sudden impact and bounce).

4. As soon as the probe contacted the plastic film, a peak emf signal was recorded. This signal decayed rapidly until a plateau was reached which represented a near-steady-state temperature level. It was this level that constituted the reading related to thermal conductivity.

To convert these emf readings to thermal conductivity values, a calibration curve must also be prepared, using standard fluids of known thermal conductivity. A series of tests were made with the Thermal Comparator probe on the following standard fluids:

Water	Toluene
Glycerol	Nujol (medicinal paraffinic mineral oil)
Methyl alcohol	Carbon Tetrachloride

A calibration curve was then prepared by plotting the thermal conductivity values (from the literature) versus the Thermal Comparator emf readings for each of these fluids. This graph is shown as Figure 4. Using this curve, the emf readings for

any sample fluid can then be converted into thermal conductivity values by determining the intercept coordinates on the calibration curve.

It should be noted that a limiting reading for the comparator was determined by setting up a test with the Kapton film covering an empty evaporating dish. The comparator reading was then essentially the thermal conductivity of the Kapton plus some contribution from the air in the dish. For a temperature differential of 70F between the probe and the film, the emf reading was 15 micro-volts. Since the thermal conductivity of the Kapton film is approximately 5-6 x 10^{-4} milliwatts/cm^{o}C, this lends justification to the extrapolated shape of the calibration curve shown in Figure 4.

Test Results

The graphs of Thermal Comparator microvolt readings versus fluid temperature are shown in Figures 5 to 11. A second scale is included on these graphs to show the approximate corresponding conductivity values for some of these microvolt readings.

It was not possible to obtain data on any of these fluids at temperatures above 350 to 400F. The emf traces became very erratic and low readings were obtained. It is believed that volatile constituents in the fluid could be forming a vapor barrier under the plastic film which can act as a partially insulating layer.

Figure 5 shows the results obtained with the SF 97(50) and, for comparison, the data which had previously been obtained with SF 96(100). The SF 97(50) gave more scattered values, which may have been due to the lower viscosity of this oil. It also showed a sharper decrease in conductivity at temperatures above 275F. These low values at high temperature could be the result of vapor being trapped under the plastic film.

Figure 6 shows the results obtained with SF 97(50) after the ten cycle run and the 2000 hour endurance test. There is a trend toward lower conductivity with running time. There is also a shift in the curve for the fluid which was run for 2000 hours. At temperatures up to 175F, the conductivity of this sample was approximately the same as it was for the oil

C. 2

that had been run for ten cycles. Above this temperature, the conductivity dropped and then followed a new curve. Normally, this would be considered as experimental error, but similar results were also obtained with other fluids; for example, the SF 1093 after 10 cycles - Fig. 7, the X-586 - Fig. 9, the X-707 - Fig. 10 and the X-708 - Fig. 11. The reason for this behavior is not known.

Figures 7 and 8 show the curves obtained with the three samples of the SF 1093 fluid. The curve for the original oil, and the oil which had been run for ten cycles, is essentially the same (as shown in Fig. 7), although there is a drop in conductivity for the ten cycle test oil above 175F, and then a recovery at a lower level of conductivity. The SF 1093 fluid which was run for 2000 hours (Fig. 8) gave lower conductivity values at all temperatures. This oil was degassed by drawing a rough vacuum on the oil to remove any excess of dissolved gases. No significant amount of gas evolution was observed.

Figure 9 shows the results for the X-586 fluid. When this oil was tested "as received", a considerable number of bubbles were formed under the plastic film (which covered the fluid sample) as the fluid was heated. These bubbles were apparently the result of dissolved gases coming out of the oil. Since these bubbles could be acting as insulating gas layers, a sample of this fluid was degassed by evacuating the oil in a vacuum dessicator. A moderate amount of gas was expelled as evidenced by the bubbles which formed while the vacuum was being drawn. This degassed sample was then evaluated. The slope of the curve was the same, as shown in Fig. 9, but the thermal conductivity values were consistently higher.

Figure 10 shows the results for the X-707 fluid. Again, bubble formation was observed. When this fluid was degassed under vacuum and rerun, the thermal conductivity values were again consistently higher.

Figure 11 is the curve for the X-708 fluid. This fluid also showed considerable bubble formation. No test was run on this fluid after degassing.

Summary and Conclusions

Based on the results of these tests and on the results of previous tests which were done for the GE Silicone Products Department, there appears to be a slight increase in the thermal conductivity of silicone fluids as the fluids are heated from room temperature to about 125F, but this trend is reversed above 125 to 150F and the conductivity then decreases.

Within the limits of experimental error, all of the fluids which were evaluated in this work have the same thermal conductivity values at room temperature.

The X-707 and the X-708 fluids appear to have similar thermal conductivity characteristics over the temperature range from 75 to 350F, and both are better than the X-586 fluid. The new sample of SF 1093 is close to the X-707, but appears to show a drop in conductivity with running time. The X-707 does not appear to be quite as good as the SF 97(50) at temperatures up to 300F, but does not show as drastic a decrease in conductivity at higher temperatures. All of the X-fluids appeared to have considerable amounts of dissolved gases in the fluids. Either they dissolve more gases at lower temperatures than fluids such as the SF 97(50), or they give up dissolved gases more readily than some of the other silicone fluids when they are heated.

TABLE 1

Thermal Conductivity Values for Silicone Fluids

(Estimated from comparator readings and calibration curve)

Fluid	Temp. °F	Recorder reading- Microvolts	Milliwatts/cm.°K (a)	$\frac{Btu}{hr.\ ft.^{\circ}F}$ (b)
SF 97(50) (new)	75°	108	1.12	.064
	100	115	1.20	.069
	150	119	1.25	.072
	200	117	1.23	.071
	250	102	1.12	.065
	300	82	0.90	.052
	325	58	0.75	.043
SF 97(50) (ten cycles)	75	103	1.07	062
	100	110	1.15	.067
	150	113	1.17	.068
	200	105	1.10	.064
	250	90	0.95	.055
	300	67	0.80	.046
SF97 (50) (2K hours)	75	109	1.13	.065
	100	113	1.17	.068
	150	111	1.15	.067
	200	81	0.90	.052
	250	75	0.87	.050
	300	62	0.77	.045
	350	43	0.67	.039
SF 1093(50) (new)	75	110	1.15	.067
	100	116	1.2	.069
	150	119	1.25	.072
	200	110	1.15	.067
	250	87	0.95	.055
	300	67	0.80	.046
	350	32	0.63	.036
SF 1093 (ten cycles)	75	105	1.10	.064
	100	120	1.25	.072
	150	121	1.26	.073
	200	85	0.92	.053
	250	73	0.79	.052
	300	69	0.80	.047
	350	32	0.63	.036

(a) From Calibration Curve

(b) Conversion to Engineering Units

TABLE 1 (Concluded)

Fluid	Temp. °F	Recorder Reading - Microvolts	Milliwatts/cm.°K	Btu / hr. ft. °F
SF 1093 (2K hours)	75	104	1.1	.064
	100	107	1.13	.065
	150	103	1.1	.064
	200	92	1.0	.058
	250	75	0.88	.051
	300	53	0.72	.042
	350	23	0.57	.033
X-586 (as received)	75	103	1.07	.062
	100	112	1.16	.067
	150	94	1.02	.059
	200	76	0.85	.049
	250	57	0.74	.043
	300	37	0.65	.038
	325	28	0.62	.036
X-707 (as received)	75	109	1.11	.065
	100	113	1.17	.068
	150	107	1.10	.064
	200	94	1.02	.059
	250	79	0.22	.051
	300	60	0.77	.045
	325	47	0.69	.040
X-708 (as received)	75	108	1.11	.064
	100	121	1.25	.072
	150	122	1.27	.073
	200	98	1.03	.060
	250	68	0.81	.047
	300	54	0.73	.042
	325	39	0.65	.038

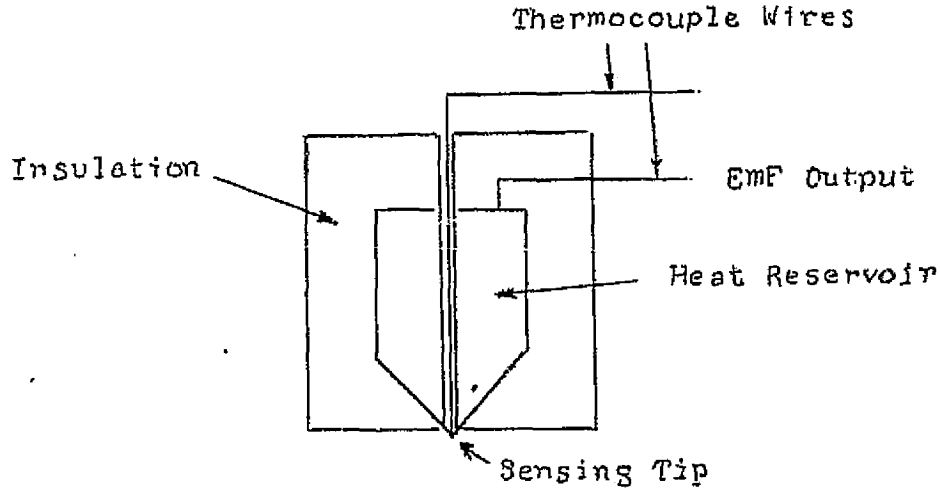

Figure 1. Schematic of Thermal Comparator Probe

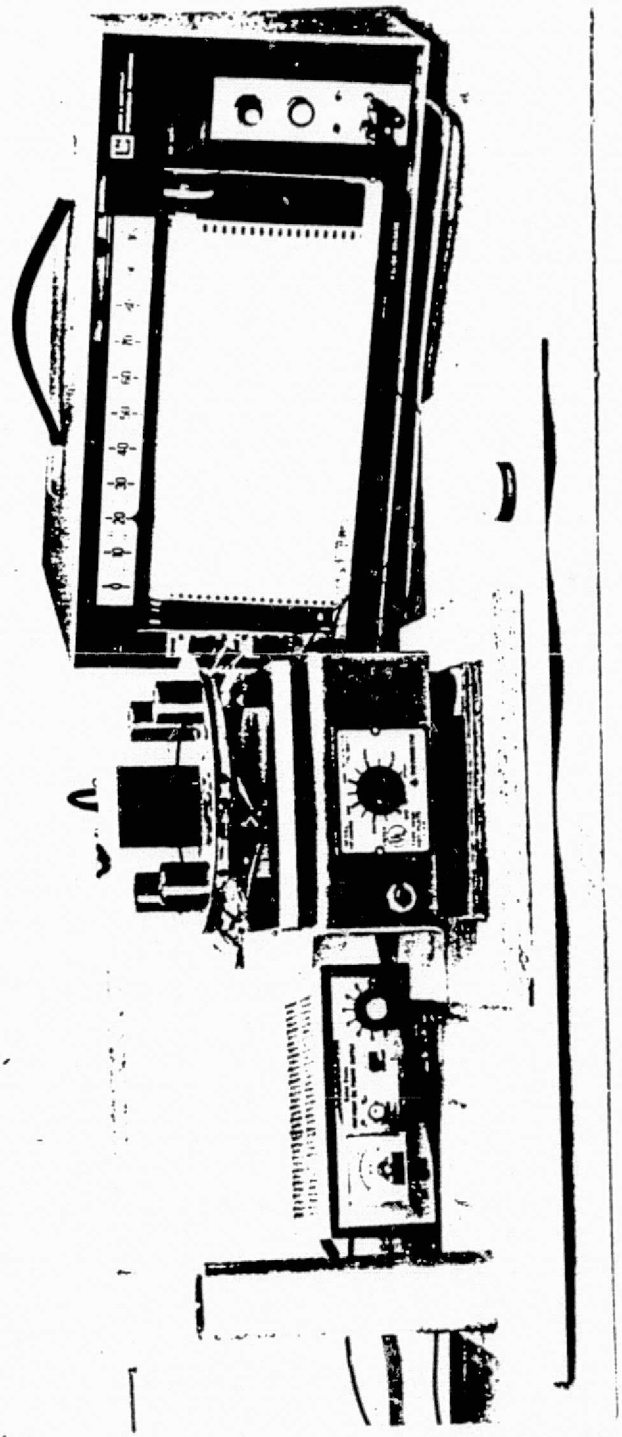

Figure 2 Photograph of Test Rig

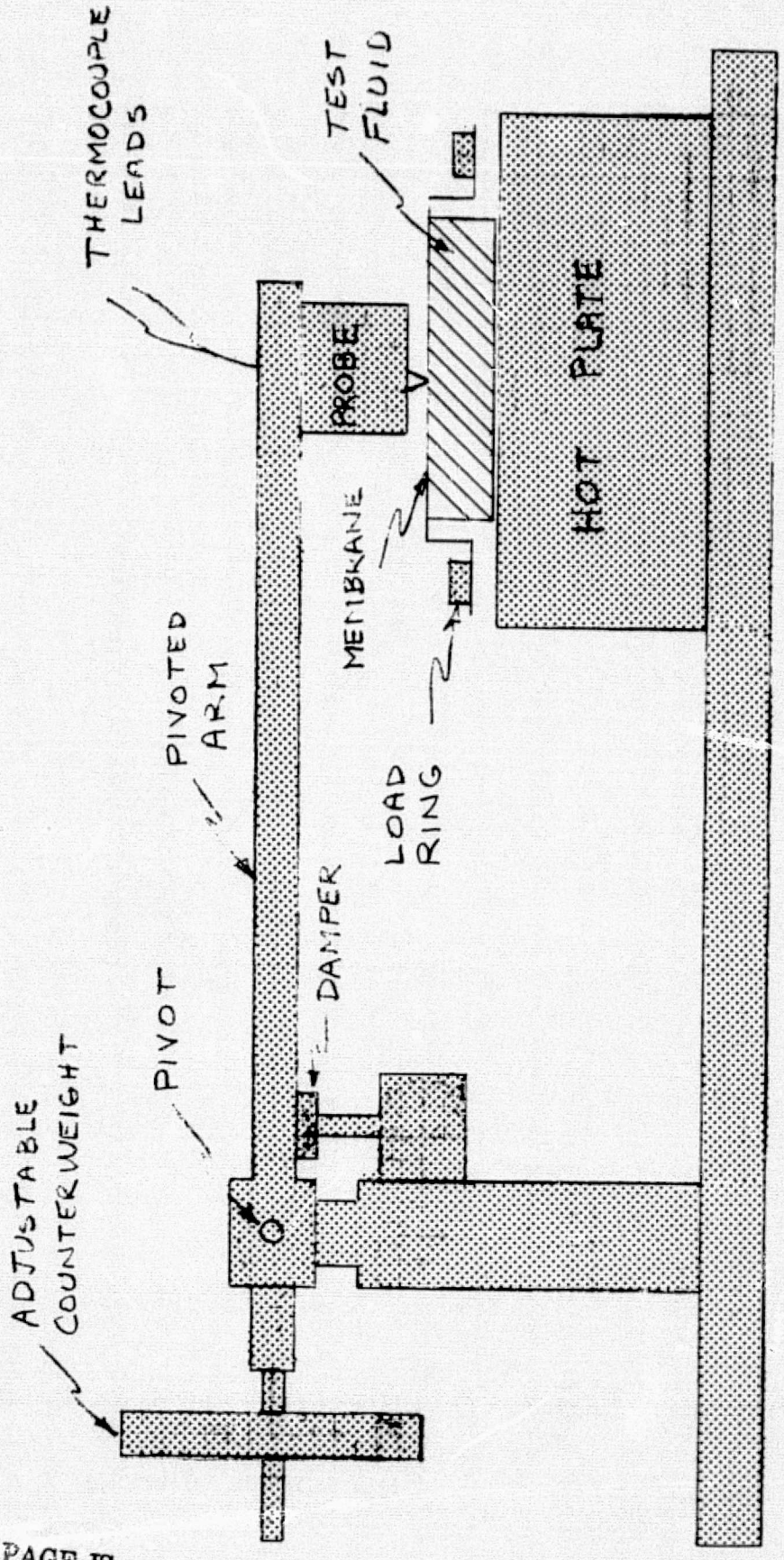

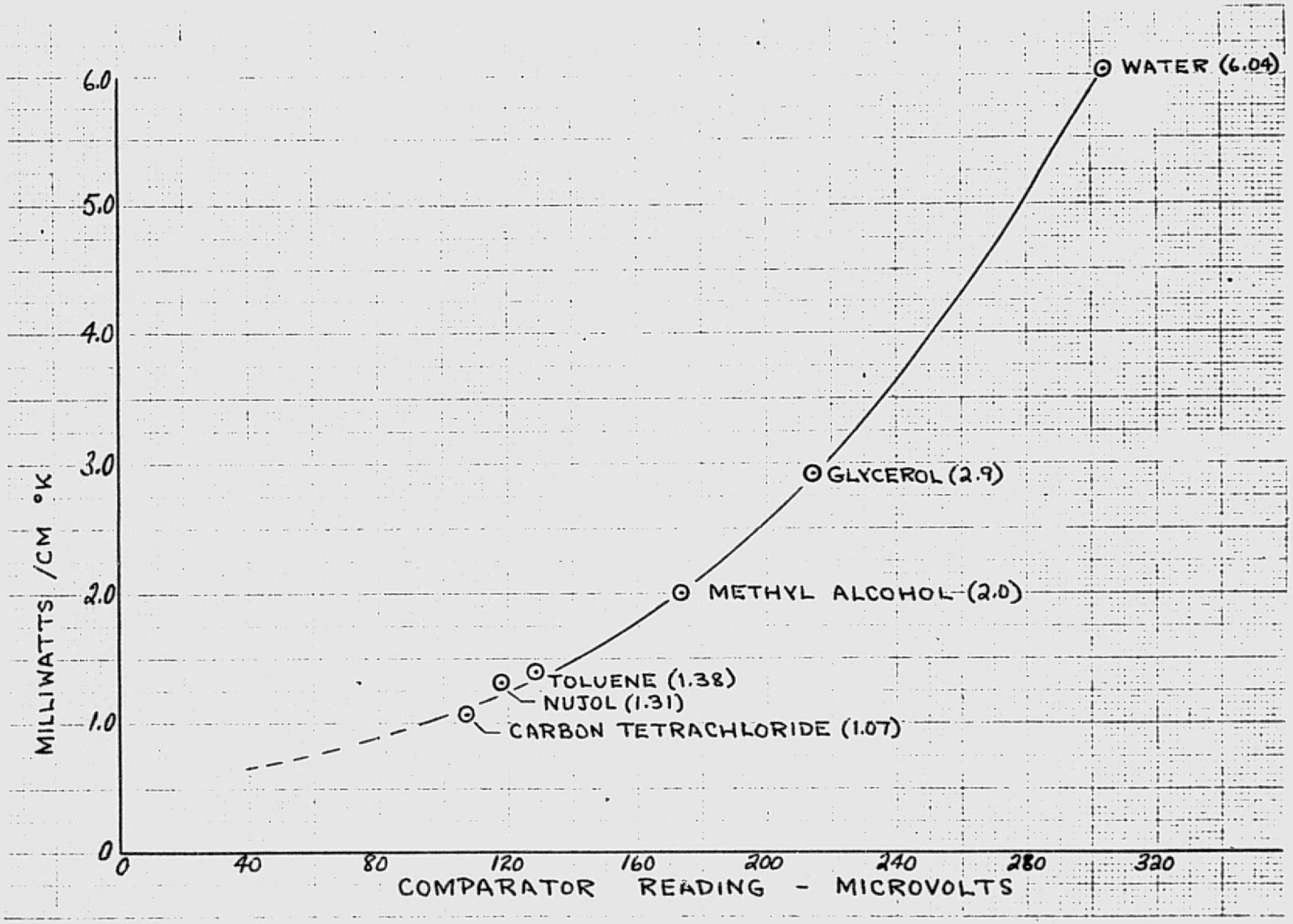

Fig. 4 Calibration Curve for Thermal Comparator. 1/16/'75.

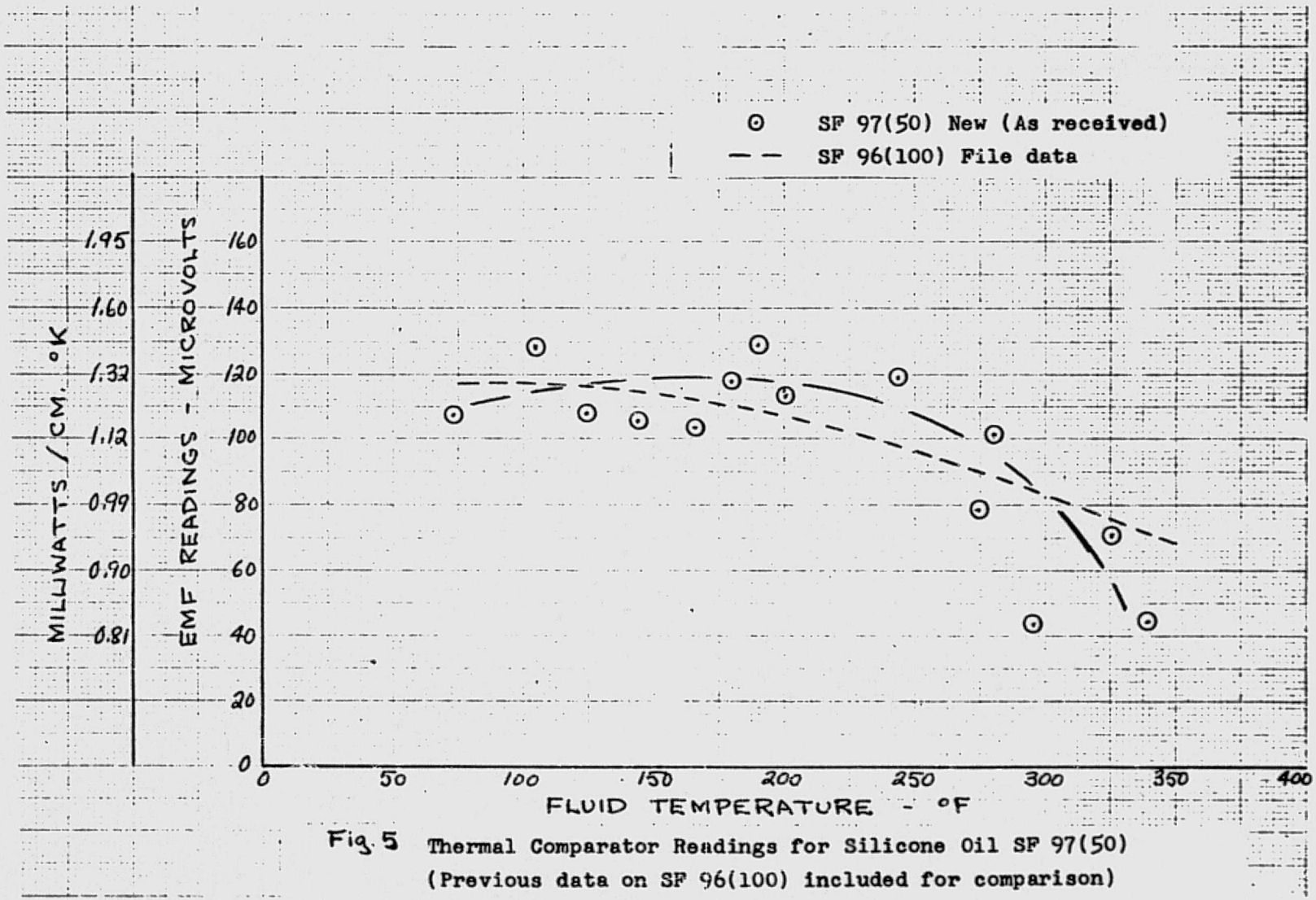

Fig. 5 Thermal Comparator Readings for Silicone Oil SF 97(50)
(Previous data on SF 96(100) included for comparison)

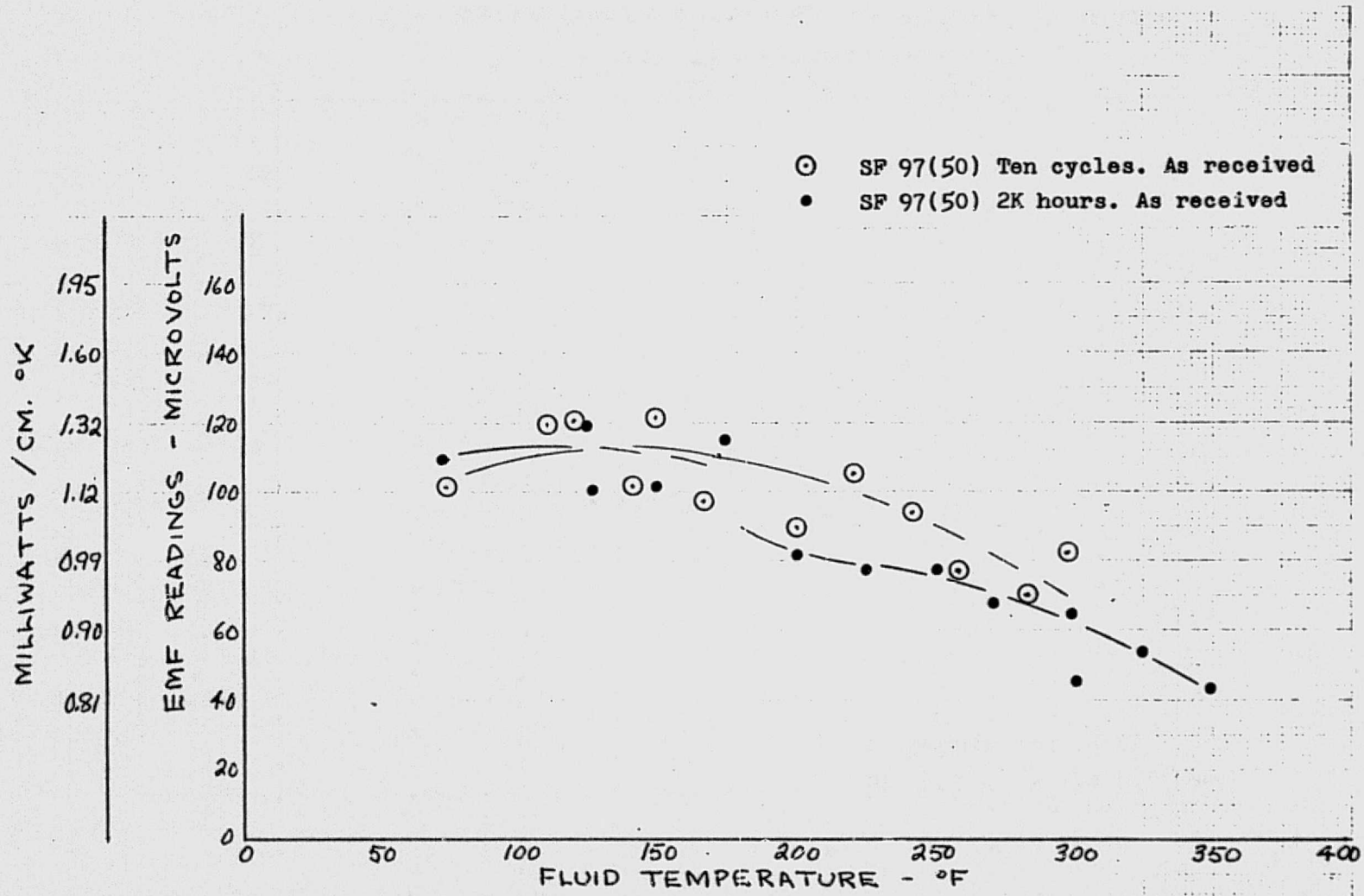

Fig. 6 Thermal Comparator Readings for Silicone Oil SF 97(50)

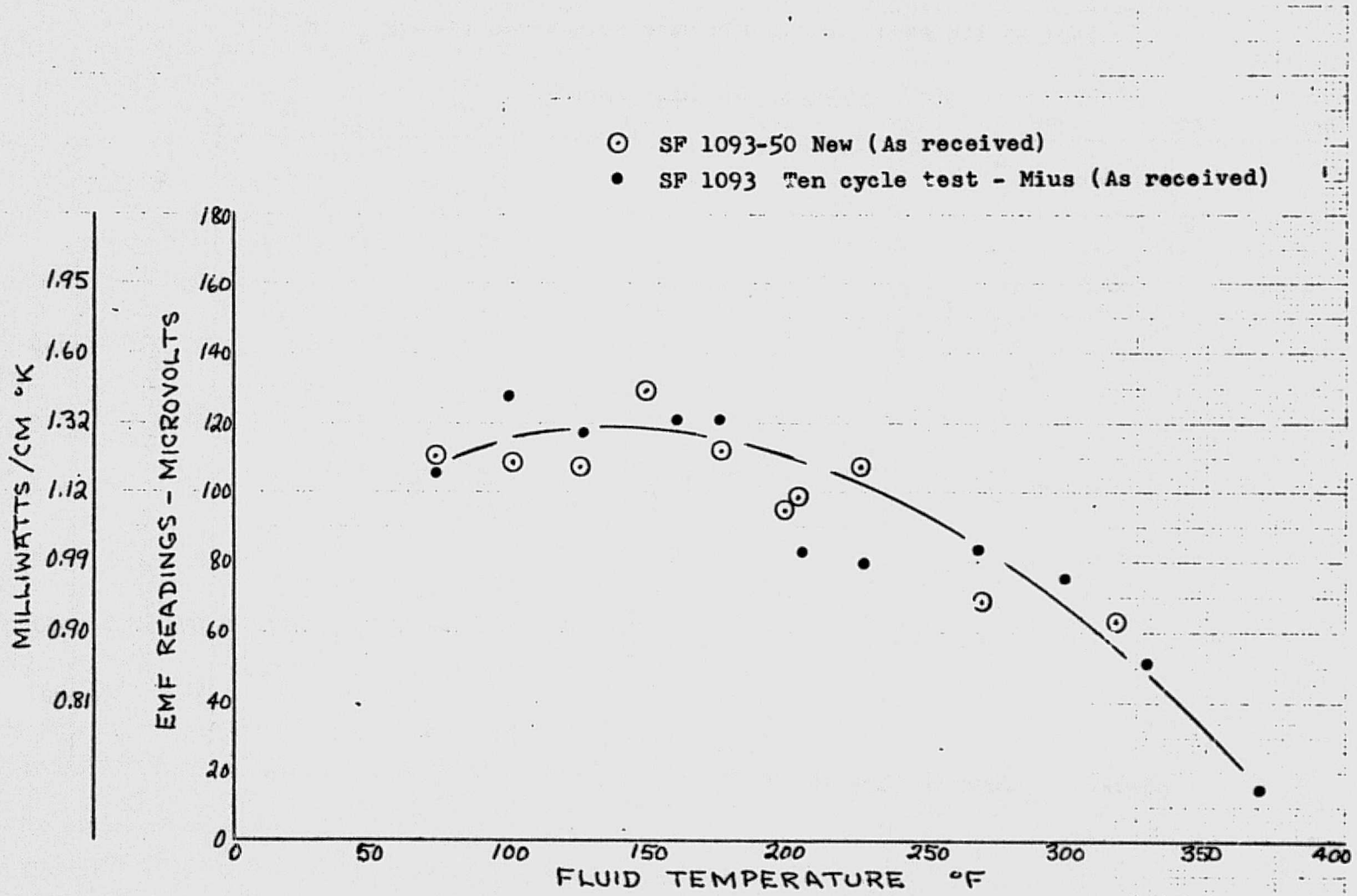

Fig. 7 Thermal Comparator Readings for Silicone oil SF 1093

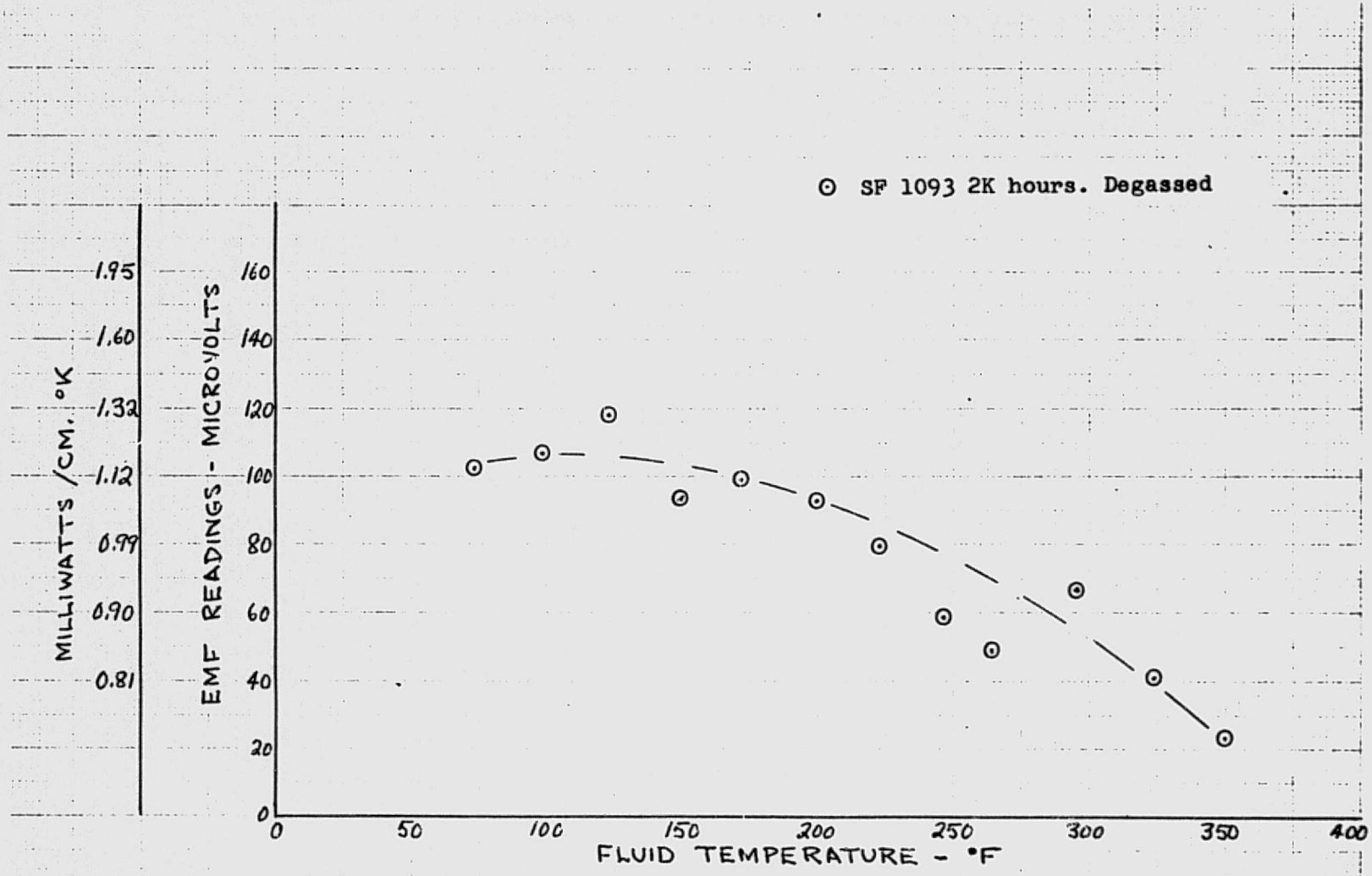

Fig. 8 Thermal Comparator Readings for Silicone Oil SF 1093

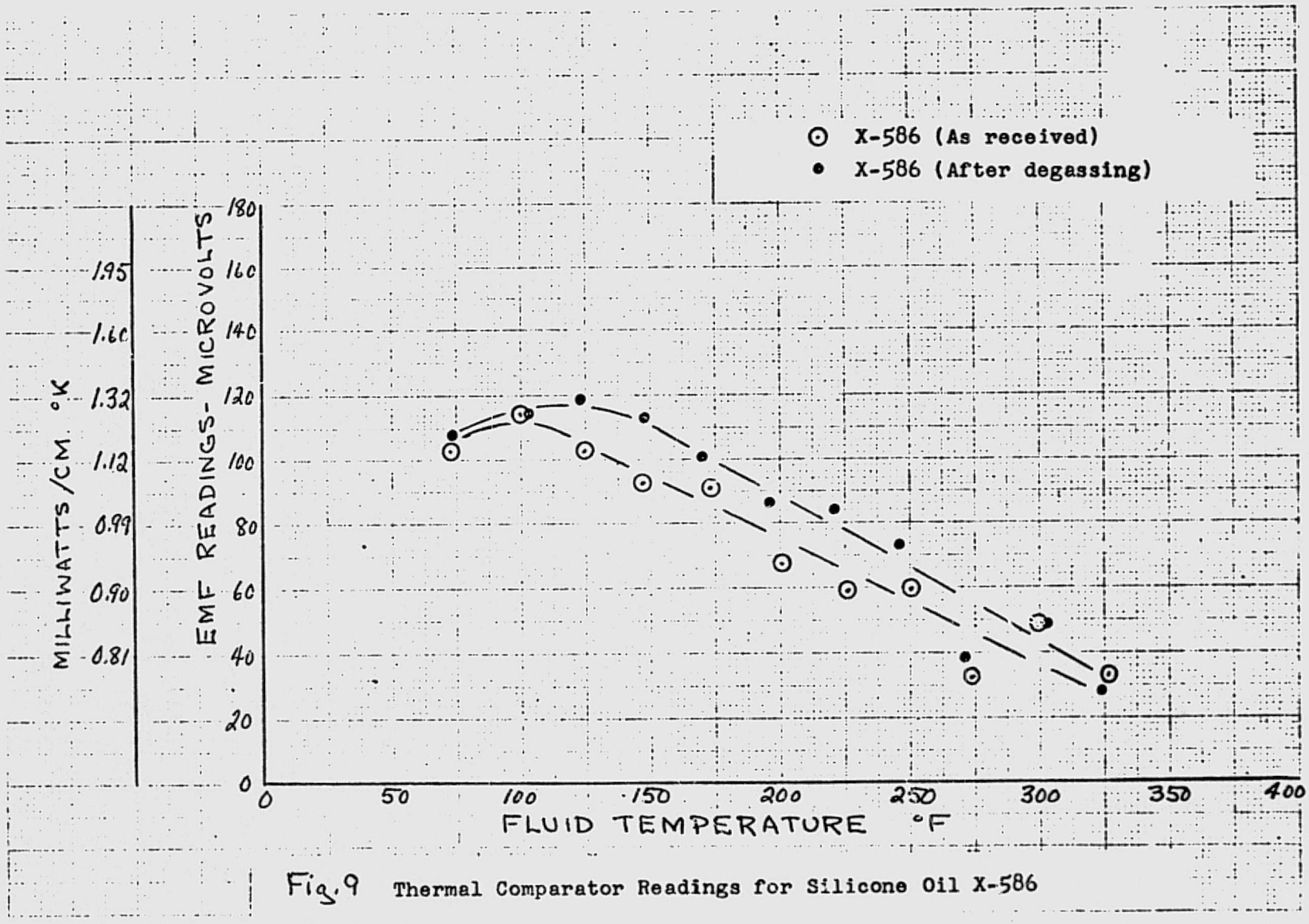

Fig. 9 Thermal Comparator Readings for Silicone Oil X-586

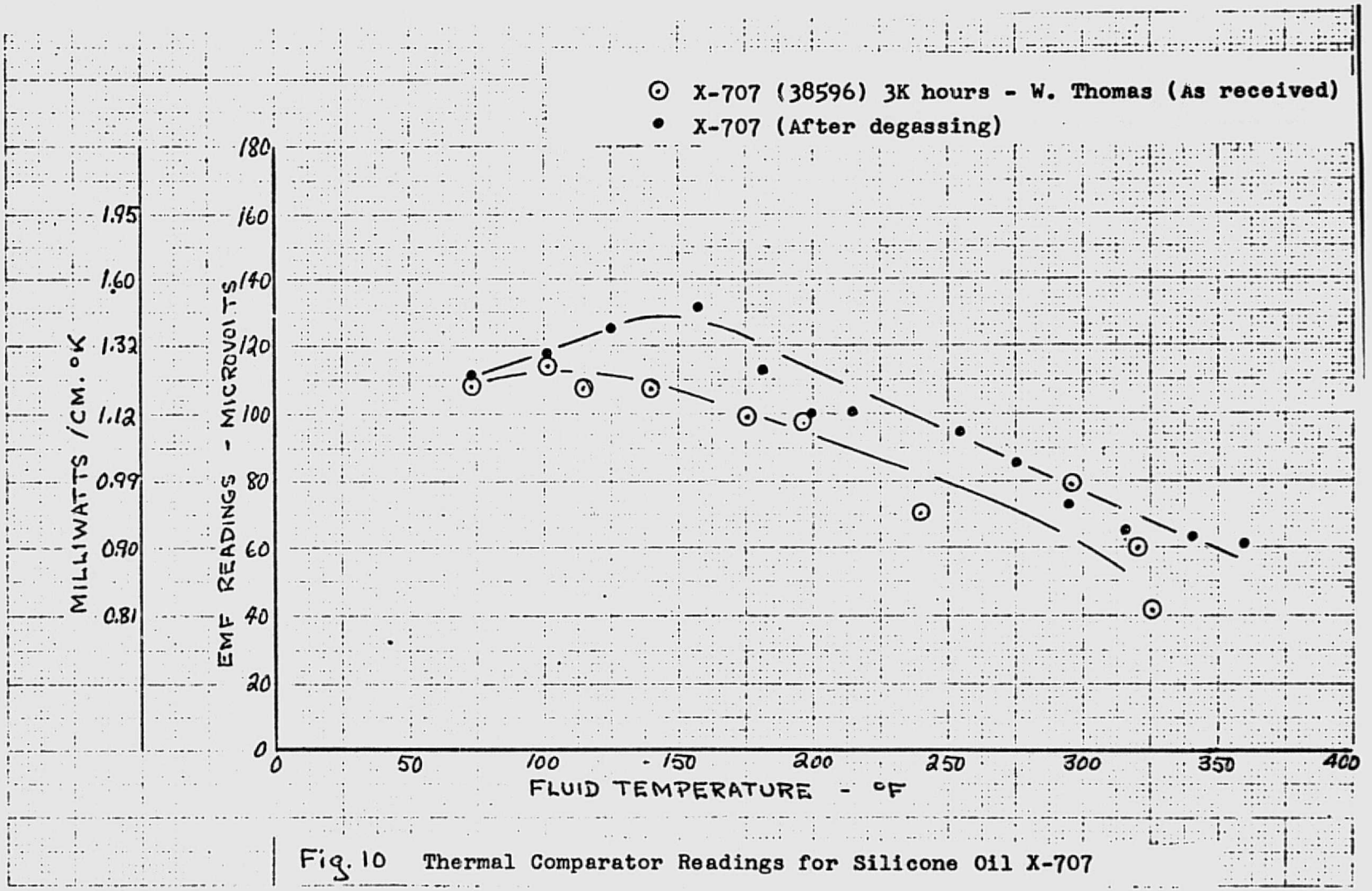

Fig. 10 Thermal Comparator Readings for Silicone Oil X-707

Fig F

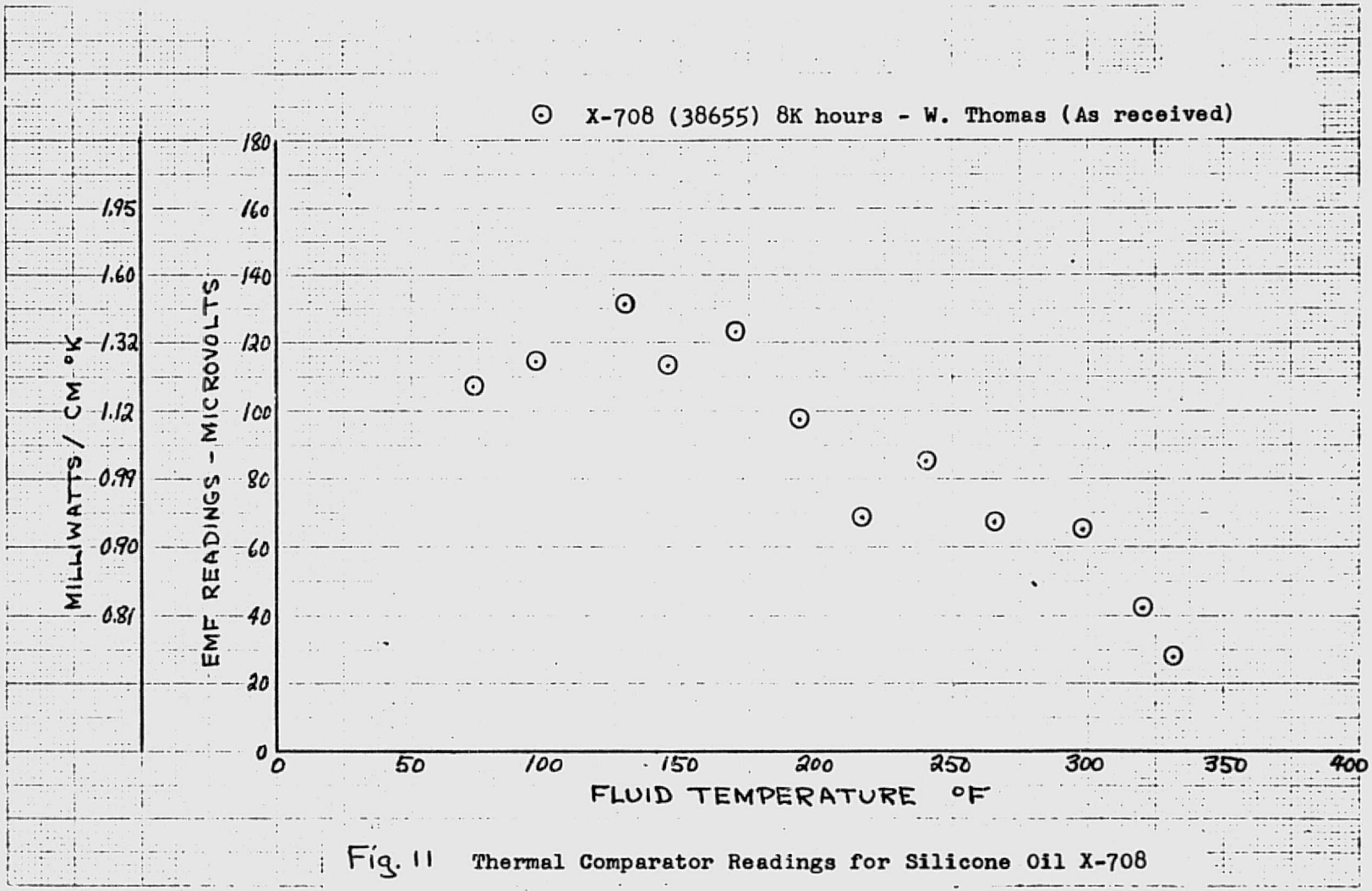

Fig. 11 Thermal Comparator Readings for Silicone Oil X-708